Functionalization of metal-organic frameworks for liquid membrane separations

YOU Hui

Japan Advanced Institute of Science and Technology

Doctoral Dissertation

Functionalization of metal-organic frameworks for liquid membrane separations

YOU Hui

Supervisor: Professor (Dr) Toshiaki Taniike

Graduate School of Advanced Science and Technology

Japan Advanced Institute of Science and Technology

[Materials Science]

March 2022

Abstract

Metal-organic frameworks (MOFs), which are emerging porous materials composed of metal ions/clusters and organic linkers, exhibit great advantages in membrane separations due to their well-defined and tunable pore structure. In particular, MOF-based composite membranes that combine the excellent separation capability of MOFs with the processability of polymers are promising for liquid separations. However, the separation performance of the present MOF-based composite membranes is usually limited by poor interfacial bonding between MOFs and polymers. Among many appealing characteristics of MOFs, their tailorable nature enables MOFs to impart desirable properties by surface modification, such as stability, hydrophilicity/hydrophobicity, and dispersibility. In this thesis, I aimed to overcome the limitations of MOF-based composite membranes for improving liquid separation performance by chemically engineering MOF surfaces (Fig. 1). Here, zeolitic imidazolate framework-8 (ZIF-8), one of the most stable MOFs, was employed as a scaffold and the main research results are as follows:

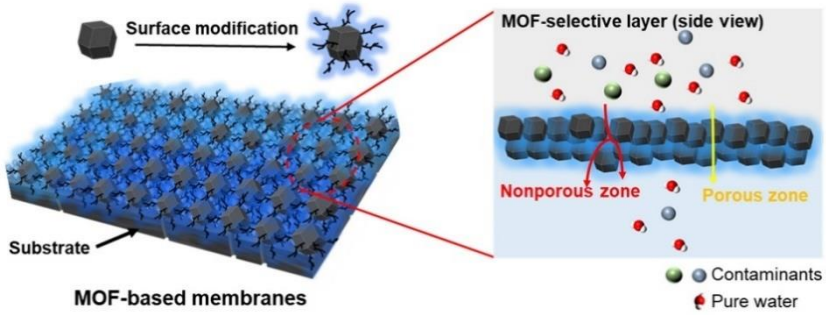

Fig. 1. Schematic illustration of MOF-based composite membranes for liquid separation.

Surfactant-stabilized oil-water emulsions (including oil-in-water and water-in-oil emulsions) are especially difficult contaminants to separate. In **Chapter 2**, membranes prepared by sequential deposition of ZIF-8 microparticles followed by nanoparticles on a regenerated cellulose substrate were applied for oil-water emulsion separation. In order to separate both oil-in-water and water-in-oil emulsions, hydrophobic modification of ZIF-8 was performed via ligand exchange reaction to switch the surface properties of the original particles from hydrophilic to hydrophobic. The unmodified-membranes were effective in separating oil-in-water emulsions due to their relative hydrophilicity, while the hydrophobic modification of ZIF-8 enabled membranes to separate water-in-oil emulsions successfully.

To separate species of a smaller size, in **Chapter 3**, I focused on ZIF-8-based thin-film nanocomposite (TFN) membranes for desalination, where surface modification was performed on ZIF-8 nanoparticles by polydopamine (PDA) coating, and the modified ZIF-8 nanoparticles were incorporated into polyamide as a selective layer supported by a polyethersulfone membrane. The PDA coating improved the dispersibility, chemical stability, and hydrophilicity of ZIF-8 nanoparticles, leading to good separation performances (permeability: 11.1 L m^{-2} h^{-1} bar^{-1}; Na_2SO_4 rejection: 95.1% with 20 wt% of PDA-coated ZIF-8 in the selective layer) for the membranes.

In general, increasing the MOF loading in MOF-based TFN membranes tends to increase permeability due to additional transport channels. However, this is accompanied by a deterioration in the selectivity because of MOF agglomeration and interfacial failure, which restricts the effectiveness of MOF loading. In **Chapter 4**, I proposed a breakthrough method to fabricate a ZIF-8-matrix nanocomposite membrane with ultrahigh ZIF-8 loading (70 wt%) by using polyethyleneimine-grafted ZIF-8 nanoparticles with film-forming ability as building blocks. Such design exhibited ultrahigh permeability (43.6 L m^{-2} h^{-1} bar^{-1}) while maintaining comparable selectivity (95%).

In conclusion, the surface engineering of MOF nanoparticles has provided a smart strategy to maximize the advantages of MOFs' nanochannels and alleviate their interfacial failure in designing MOF-based membranes for liquid separation.

Keywords: Membranes; metal-organic frameworks; liquid separation; interfacial bonding; surface modification.

Referee-in-chief: Professor Toshiaki Taniike
Japan Advanced Institute of Science and Technology

Referees: Professor Tatsuo Kaneko
Japan Advanced Institute of Science and Technology

Professor Noriyoshi Matsumi
Japan Advanced Institute of Science and Technology

Associate Professor Van Anh Ho
Japan Advanced Institute of Science and Technology

Associate Professor Wei Xia
China University of petroleum

Preface

The present thesis is submitted for the Degree of Doctor of Philosophy at the Japan Advanced Institute of Science and Technology, Japan. The thesis is a consolidation of the results of the research work on the topic "Functionalization of metal-organic frameworks for liquid membrane separations" and was implemented during April 2019–March 2022 under the supervision of Professor (Dr) Toshiaki Taniike at the Graduate School of Advanced Science and Technology, Japan Advanced Institute of Science and Technology.

Chapter 1 provides a general introduction to the research field and, accordingly, the objective of this thesis. **Chapter 2** reports surface wettability switching of a zeolitic imidazolate framework-deposited membrane for selective efficient oil/water emulsion separation. **Chapter 3** Introduces the advantages of polydopamine coating in the design of ZIF-8-filled thin-film nanocomposite (TFN) membranes for desalination. **Chapter 4** reports on the preparation of ZIF-8-matrix nanocomposite membranes for high-flux desalination. Finally, **Chapter 5** describes the general conclusions of this thesis. The work is original and no part of this thesis has been plagiarized.

YOU Hui

Graduate School of Advanced Science and Technology

Japan Advanced Institute of Science and Technology

March 2022

Acknowledgements

I would like to offer my deepest gratitude to all the people who have guided, supported, and encouraged me throughout my Ph.D. program.

First and foremost, my deep and sincere appreciation should go to my supervisor, Professor (Dr) Toshiaki Taniike, at the Japan Advanced Institute of Science and Technology (JAIST), who has given me great encouragement and instructions throughout the process of selecting the subject, doing the experiments, improving the outline, writing the thesis, and correcting the grammatical errors. His enlightening suggestions on each draft have inspired me with many enlightening ideas. The thesis could not be completed without his support.

Secondly, I am grateful to the China Scholarship Council (CSC) of the Ministry of Education, China, for financing my studies in JAIST. CSC benefits me greatly since it allows me to widen my horizons and change my thinking during my time in JAIST. A special thanks to everyone at the Research Fund for assisting and providing funds for the project.

I am also thankful to D. Eng. (Mrs.) Patchanee Chammingkwan in JAIST for her diligent guidance, useful comments during experimentation as well as discussion of results, and great efforts in revising my papers. In addition, I would also like to take this opportunity to thank Professor Dr Tatsuo Kaneko (second supervisor) and Professor Dr Noriyoshi Matsumi (minor research supervisor) at JAIST for their guidance and encouragement. I am also grateful to all of the Taniike laboratory membranes for their helpful comments, cooperation, and support.

I would like to appreciate all the support from JAIST and the Japanese government, especially during the most difficult time with COVID-19. Great thanks to all the JAIST staff for their care. Thanks to Ishikawa Prefecture for offering me a wonderful life for the past 3 years.

Last but not least, I would like to express my gratitude to my family, who have always been there for me, caring, supporting, and assisting me. Special thanks should go to my friends for their utmost care and moral support.

YOU Hui

Graduate School of Advanced Science and Technology

Japan Advanced Institute of Science and Technology

March 2022

Table of Contents

Chapter 1

General Introduction

1.1. Water scarcity and water treatment

Water is one of the most precious and non-renewable resources on the planet. Although water covers 72% of the Earth's surface, freshwater accounts for only 0.5% of that, and less than 1% of the world's freshwater is drinkable [1]. Due to population growth, industrialization, and climate change, water supplies are becoming dangerously scarce [2,3]. In the past decades, water consumption has increased fourfold [4], and the global population under water scarcity has increased from 0.24 billion to 3.8 billion [5]. In addition, around 4 billion tons of communal and industrial waste are generated every year [6], which causes severe water pollution, leading to a major concern about global freshwater scarcity.

Nowadays, providing adequate and fresh water is one of the primary objectives for sustainable development [7]. According to the Agenda of the United Nations for Sustainable Development, water resource recovery will be the top priority of water treatment in the coming decades [8]. For example, utilizing unconventional sources of water (e.g., brackish groundwater and seawater) and recycling wastewater will be essential. Indeed, various impurities and/or contaminants in the aforementioned water sources are the primary reasons why they are not classified as freshwater. According to the definition of the Safe Drinking Water Act, any physical, chemical, or biological matter in water can be a contaminant [9]. Common contaminants, such as oxyanions/cations, heavy metal ions, dyes, oils, pesticides, pharmaceuticals, and microorganisms, can have detrimental effects on source water, even at low concentrations [1]. Here, the development of sustainable and effective technologies for

the removal of impurities and/or contaminants is regarded as the key issue for providing clean and safe water [10].

Currently, a variety of technologies have been applied to produce freshwater in water treatment plants, such as adsorption [11], coagulation-flocculation [12], precipitation [13], sand filtration [14], etc. However, most of these conventional strategies are effective in removing macro pollutants, suspended solids, natural organic matter, dissolved iron and manganese, etc. [15], but cannot eliminate contaminants smaller in size. Furthermore, some of them also suffer from high energy consumption and the production of secondary pollutants [4]. Therefore, the development of effective, environmentally-friendly, and energy-efficient techniques for water treatment is highly desired.

1.2. Membrane technologies for liquid separation

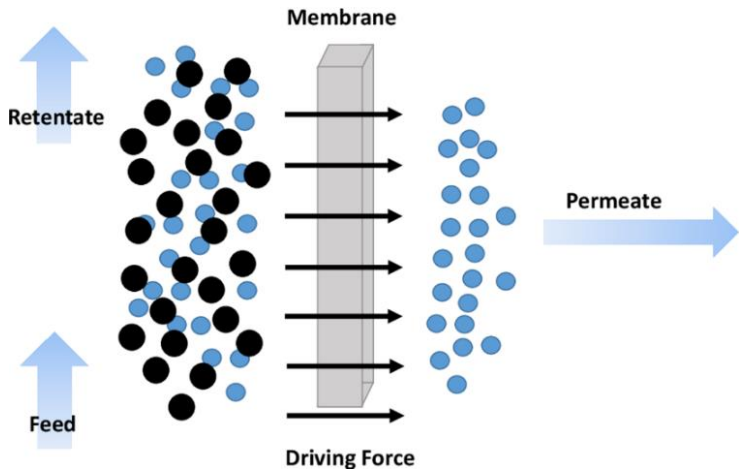

Fig. 1.1. Schematic illustration of membrane separation processes. Adapted from Ref. [16].

To date, membrane technologies have been widely investigated and regarded as promising strategies for liquid separation, including seawater desalination, wastewater

purification, food processing, pharmaceutical and chemical separations, etc. [1,17,18]. A membrane can be defined as: A thin physical interface that allows some species to pass through when subjected to external driving forces (as shown in Fig. 1.1) [19]. Compared with conventional strategies, membrane technologies possess distinct advantages, including high energy efficiency, easy scale-up, small capital investment, low carbon footprint, and so on [20].

1.2.1. Classification of membranes

According to different morphologies or structures (defined as cross-section), membranes can be divided into two types: isotropic (or symmetric) membranes and anisotropic (asymmetric) membranes, as shown in Fig. 1.2 [21].

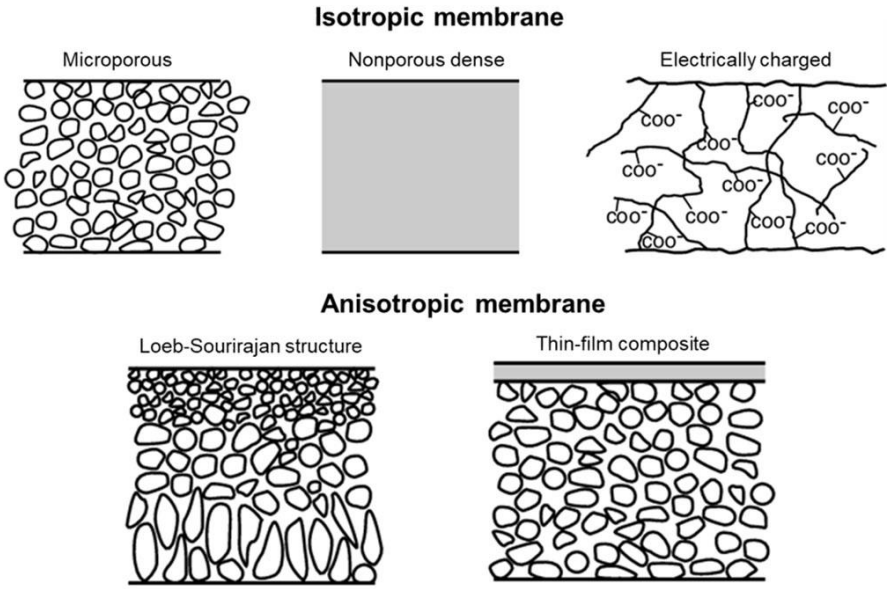

Fig. 1.2. Schematic illustration of isotropic (symmetric) membranes and anisotropic (asymmetric) membranes. Adapted from Ref. [21].

Isotropic (or symmetric) membranes

Isotropic membranes are homogeneous in both of their chemical composition and

structure. They can be subdivided into isotropic microporous membranes, nonporous or dense membranes, and electrically-charged membranes [21]. Microporous membranes exhibit a randomly voided structure with interconnected pores (pore size is in the range of 0.01–10 μm). An effective separation process is mainly based on the size of solutes and the pore size distribution of the membranes. Nonporous or dense membranes are composed of a dense film through which transport of species is driven by diffusion under a driving force such as concentration, pressure, or electrical potential gradient. As a result, the separation of various solutes in a mixture is governed by their relative transport rates. In the case of electrically-charged membranes, they can be either porous or dense, with positively or negatively charged ions on the membrane walls. The separation is determined by charge exclusion and ion concentrations.

Anisotropic (or asymmetric) membranes

Anisotropic membranes are chemically or/and structurally heterogeneous, which are mainly divided into Loeb-Sourirajan membranes (phase-separation membranes) and thin-film composite (TFC) membranes [19]. Loeb-Sourirajan membranes are developed via a phase inversion method using a single polymer [22], which are similar to isotropic microporous membranes, except that the porosity and pore sizes vary throughout the whole membrane. TFC membranes consist of a thin and dense layer of highly cross-linked polymer that is supported on a thicker microporous substrate, in which the thin and thicker layers function separately as a selective layer and a mechanical support.

1.2.2. Mass transport mechanism

The mass transport mechanism for liquid membrane separations can be divided into two types: the pore-flow model and the solution-diffusion model, as depicted in Fig. 1.3 [23–25]. In the pore-flow model, convective flow under pressure gradients dominates mass transport through the pores of membranes. Species are separated based on size-exclusion, which means that species with a size larger than the membranes' pores cannot pass through. In the case of the solution-diffusion model, species should first dissolve in membranes, followed by diffusing across the membrane along with the concentration gradient. Therefore, the separation of species is governed by their different solubilities and diffusion rates in membranes.

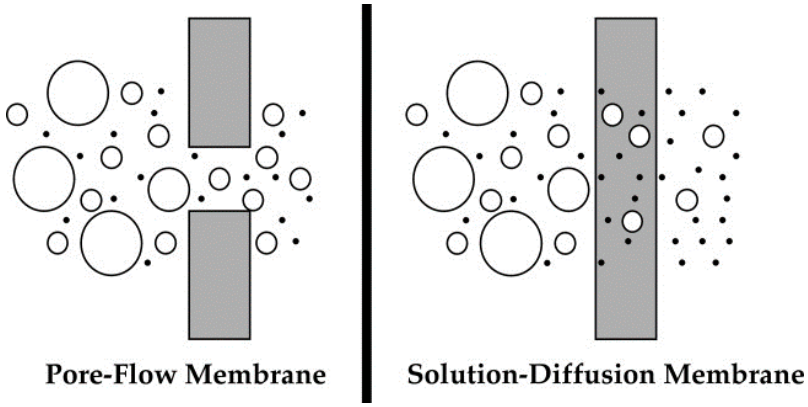

Fig. 1.3. Schematic illustrations for pore-flow and solution-diffusion membranes [23].

Diffusion is an inherently slow process. Fick's law of diffusion appropriately describes the solution-diffusion model, which states:

$$J_{\mathrm{i}} = -D_{\mathrm{i}} \frac{\mathrm{d}c_i}{\mathrm{d}x}, \tag{1.1}$$

where J_{i} and $\frac{\mathrm{d}c_i}{\mathrm{d}x}$ represent the transport rate and concentration gradient of component i, respectively. D_{i} is the diffusion coefficient, and the minus sign indicates that diffusion

is occurring down the concentration gradient. The pore-flow model, which is mainly driven by pressure, can be described by Darcy's law for a porous membrane:

$$J_{\mathrm{i}} = K' c_i \frac{\mathrm{d}p}{\mathrm{d}x}, \tag{1.2}$$

where $\frac{\mathrm{d}p}{\mathrm{d}x}$ and c_i are the pressure gradient and concentration of component *i* existing in the porous membrane, respectively. K' is a coefficient that represents the nature of the membrane. The permeance and relative size of the pores distinguish the pore-flow and solution-diffusion mechanisms. For membranes in which transport is dominated by the solution-diffusion mechanism, the transport channels in the membrane are free volume between polymer chains. On the other hand, for the pore-flow membranes, the channels are relatively large and fixed [21].

1.2.3. Pressure-driven membrane processes

Pressure-driven and thermally-driven processes are two main operation methods for liquid membrane separations [26,27], while pressure-driven membranes are frequently applied for water purification and desalination due to the advantages of milder operation conditions and lower energy usage. Based on the size of solutes that are rejected, pressure-driven membrane processes are divided into particle filtration, microfiltration (MF), ultrafiltration (UF), nanofiltration (NF), and reverse osmosis (RO) membranes, as summarized in Fig. 1.4 [1,19].

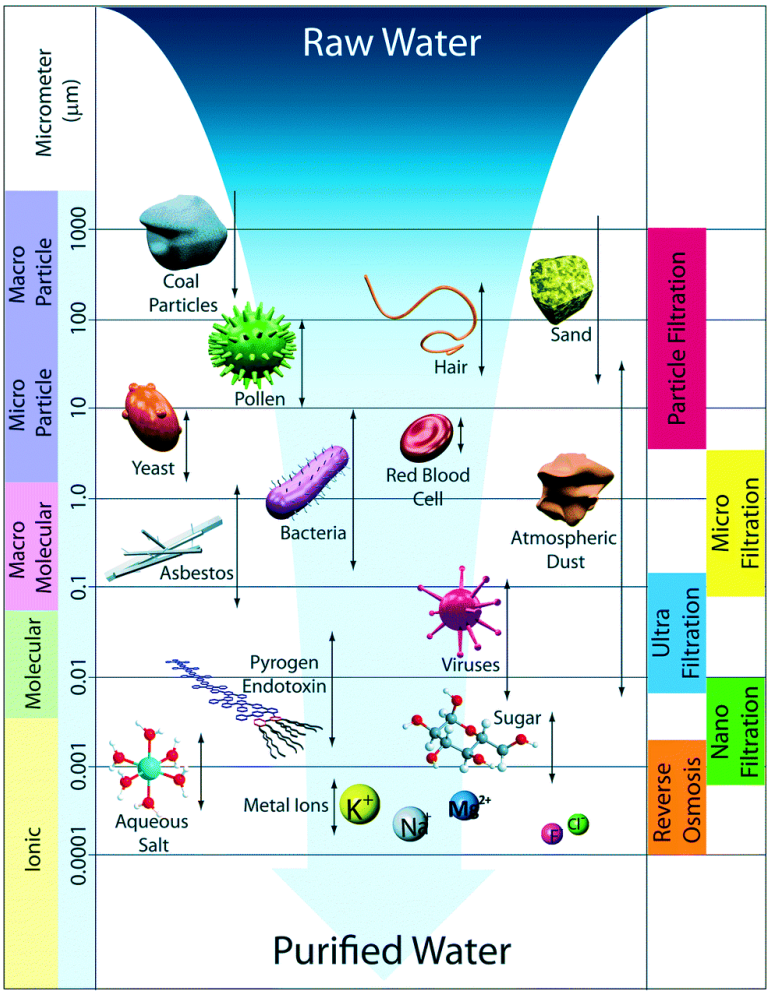

Fig. 1.4. Schematic diagram of the filtration spectrum for pressure-driven membrane processes. Adapted from Ref. [19].

MF and UF membranes follow a comparable process to that of particle filtration through membrane pores in which mass transport is based on size sieving. MF membranes with pore sizes of about 0.1–5 µm can reject suspended particles and various microbial pathogens. UF membranes are designed with smaller pores (approx. 0.01–0.1 µm), which are suitable for removing macromolecules, such as viruses and proteins [28]. Compared to MF and UF membranes, NF membranes exhibit much smaller pore sizes that can even reject solutes around 0.5–2 nm in diameter, which

includes most organic molecules, divalent salt ions, and viruses. Therefore, NF membranes are often applied to soften hard water [29]. The pore size of RO membranes is approximately 0.1–1 nm, which corresponds to the typical size of polymer free volume. Therefore, RO membranes are normally considered non-porous and are designed for desalination [30]. They can reject low molecular-weight solutes such as organic molecules and inorganic solutes (including metal ions, minerals, and even monovalent salt ions). The mechanism of mass transport by RO membranes is supposed to be governed by a solution-diffusion model through distributed free volume areas [31].

1.2.4. Nanofiltration membranes used for liquid separation

In between UF and RO, NF membranes with pore sizes of approximately 0.5–2 nm were first developed in the 1970s [32]. They exhibit advantages of low operation pressure, high flux, and high rejection towards multivalent ions, which have emerged as superior methods in liquid separation and purification for applications such as wastewater reclamation, desalting of dye solutions, water softening, pharmaceuticals, solvent purification in the oil industry, etc. [33–37]. The overall goal of NF membranes for liquid separation and purification is to establish a process with low energy consumption, small footprint, and high stability. The development of materials for NF membranes with good processability, high stability, low cost, and high separation performance is the key issue. In general, NF membranes can be made from organic, inorganic, or hybrid materials [38,39].

Organic membranes

Organic membranes explored for NF processes to date are almost entirely made of

polymeric materials, such as cellulose acetate, cellulose nitrates, polyethersulfone, polycarbonate, polyvinylidene, polysulfone, polyacrylonitrile, poly vinyl alcohol, polypropylene, polyamide, and so on [21,40–43], which make up the majority of commercial membranes due to their low price and high processability [44]. The majority of the early polymeric membranes were homogeneous with thicknesses greater than tens of micrometers, which hindered their application due to low permeability. The appearance of TFC membranes marked a significant breakthrough in polymeric membranes, where an ultrathin barrier layer was coated onto the top of a microporous substrate [45]. The first TFC membrane was made by float-casting a cellulose acetate ultrathin layer onto the water surface, then annealing and laminating it to a pre-formed microporous substrate of cellulose acetate [46]. With the development of a polysulfone substrate and a crosslinked aromatic polyamide selective layer, TFC membranes are gradually being commercialized [47]. The conventional NF TFC membranes can be described as Fig. 1.5 [48]. However, the permeability-selectivity tradeoff has become a bottleneck of polymeric membranes, in which increasing permeability leads to a decrease in selectivity and vice versa [1]. Furthermore, most polymeric materials are intrinsically hydrophobic, which can result in a high fouling tendency [49].

Inorganic membranes

Inorganic membranes are made of ceramic materials, such as Al_2O_3, TiO_2, ZnO, ZrO_2, SiO_2, or a mixture of the above materials [50,51]. Their mechanical robustness and thermal as well as chemical stability are superior to those of polymeric membranes. More importantly, inorganic membranes with regular channels can effectively address

the tradeoff problem in polymeric membranes [52]. Unfortunately, the ceramic membranes are fragile, which prevents them from being used in large-scale production. In recent years, inorganic membranes for NF processes have been created using advanced materials such as graphene [53] and carbon nanotubes [54]. The high cost of raw materials and manufacturing of such membranes, on the other hand, limits their industrial application [55,56].

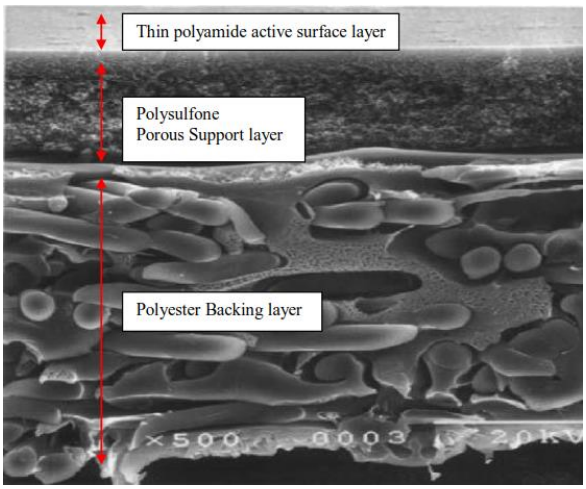

Fig. 1.5. Cross-sectional SEM images of a conventional NF TFC membrane [49].

Hybrid organic-inorganic membranes

Hybrid organic-inorganic membranes which incorporate inorganic fillers within polymer matrices have been developed with the purpose of combining the excellent stability of inorganic materials with the flexibility of polymer materials [56,57]. Furthermore, the polymer-inorganic filler interfaces can also provide additional molecular transfer pathways. As a result, hybrid membranes are expected to alleviate the tradeoff problem in polymeric membranes. Up to now, various fillers, such as zeolites [58], graphene oxide [59], carbon nanotubes [60], silica [61], etc., have been

investigated for the development of hybrid membranes with improved NF performance.

1.2.5. Challenges and trends for next-generation membranes

The development of next-generation membranes for liquid separation and purification is anticipated to be primarily focused on solving the permeability-selectivity tradeoff problem. High-permeability membranes can facilitate production as well as reduce the membrane area, whereas high selectivity ensures product purity. Additionally, the design of membrane materials with low-fouling properties and long-term stability is also vitally important for efficient operation.

In recent years, more and more advanced materials are being designed and developed, greatly expanding the types of membranes and their applications. Since porous graphene prepared by electron beam irradiation, oxygen plasma etching, ultraviolet light, and so on, has been explored for improved permeability in membrane separations [62], crystalline porous materials have attracted extensive attention. Porous materials with well-defined pore structures, controllable physio- as well as chemical properties, and ease of preparation are obviously desirable for efficient membrane separation. In this regard, metal-organic frameworks (MOFs), a group of porous materials composed of metal ions/nodes and organic ligands, are promising candidates as membrane materials. More details about MOF-based membranes for liquid separation are described in Section 1.3.

1.3. Metal-organic frameworks-based membranes

1.3.1. General introduction of metal-organic frameworks

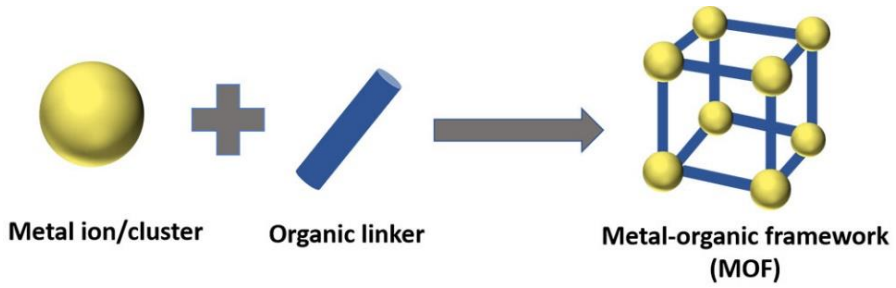

Fig. 1.6. Schematic illustration of the building blocks of MOFs.

MOFs are a kind of emerging porous materials that are composed by coordination between building units (metal ions/clusters) and organic linkers, as illustrated in Fig. 1.6 [63,64]. In 1990, Hoskins and Robson first introduced the concept of constructing 3-dimensional frameworks using metal ions/clusters and organic linkers [65]. Various MOF materials have been developed and received extensive attention, since the discovery of HKUST-1 [Hong Kong University of Science and Technology, $Cu_3(BTC)_2$, where BTC represents 1,3,5-benzenetricarboxylate] [66] and MOF-5 [or IRMOF-1, $Zn_4O(BDC)_3$, where BDC represents 1,4-benzenedicarboxylate] [67]. Fig. 1.7 displays some reported MOF structures [68]. Nowadays, research on MOF materials is not only limited to the development of different types of MOFs, but also involves their applications. It is well established that MOFs exhibit many desirable properties, such as well-defined pore size, controlled porosity, structural tailorability, and high crystallinity, which have shown great potential in catalysis, molecular capture, energy storage, separation, information encryption, and so on [69–73].

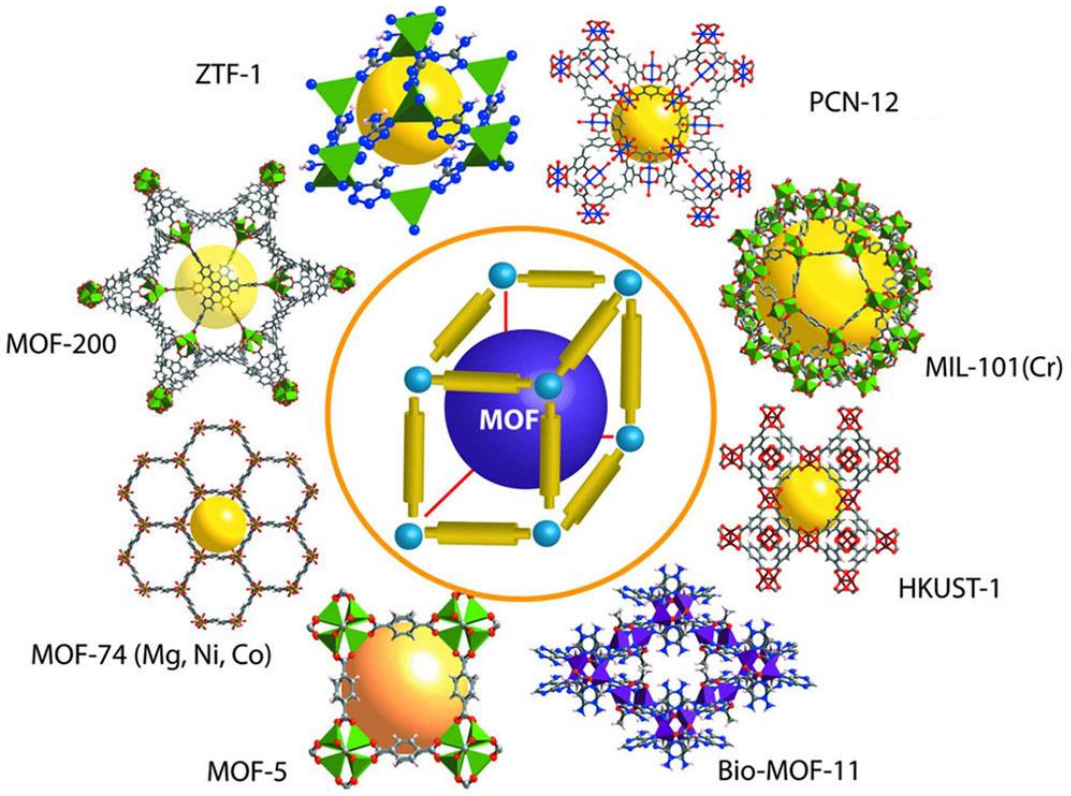

Fig. 1.7. Representation of some reported MOF structures. Reproduced from Ref. [69].

1.3.2. Types of MOF-based membranes for liquid separation

In the light of the advantages of the well-defined pore structure, uniform as well as tunable pore size, and adjustable surface property, MOFs have been considered as appealing candidates for separation [74]. In recent years, MOF-based membranes have been diversely investigated for liquid separation. There have been developed three main forms of MOF-based membranes: Continuous MOF membranes, MOF-based mixed matrix membranes (MMMs), and MOF-based thin-film nanocomposite (TFN) membranes [75], as illustrated in Fig. 1.8. The latter two forms can also be regarded as variants of MOF-based composite membranes.

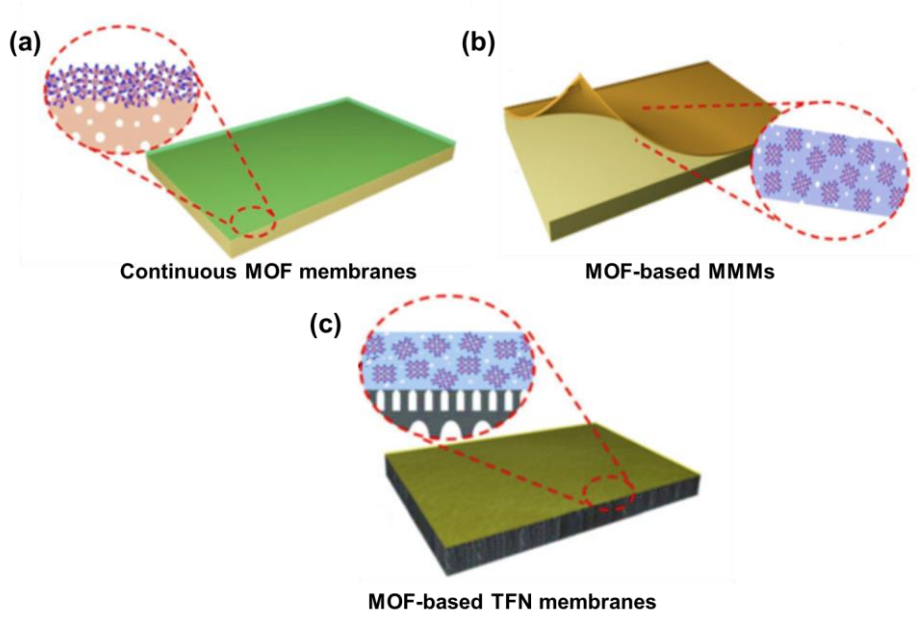

Fig. 1.8. Schematic illustration of three main forms of MOF-based membranes. a) Continuous MOF membranes, b) MOF-based MMMs, and c) MOF-based TFN membranes. Adapted from Ref. Adapted from Ref. [75].

1.3.2.1. Continuous MOF membranes

Continuous MOF membranes are formed by in-situ growth of MOF crystals on the top of a microporous substrate, as illustrated in Fig. 1.8a [76]. In other words, the selective layer of such membranes is composed of a pure and uninterrupted MOF layer. In this case, the pores of MOFs are the sole transport channels for species through membranes. Therefore, continuous MOF membranes should theoretically exhibit near-optimal selectivity for liquid separations. An impressive case is shown in Fig. 1.9, where a continuous MOF membrane was prepared by in-situ growth of Zr-MOF (UiO-66, Universitetet i Oslo) crystals on an alumina hollow fiber for desalination [77]. The resulting membrane demonstrated excellent rejection of multivalent ions (99.3% for

Al^{3+}, 98.0% for Mg^{2+}, and 86.3% for Ca^{2+}), as well as good permeability (0.28 L m^{-2} h^{-1} bar^{-1} μm). Although continuous MOF membranes are ideal for liquid separations, they are prone to gain boundary and pinhole defects that can seriously impair separation performance [78]. Furthermore, continuous MOF membranes are brittle due to the nature of crystal.

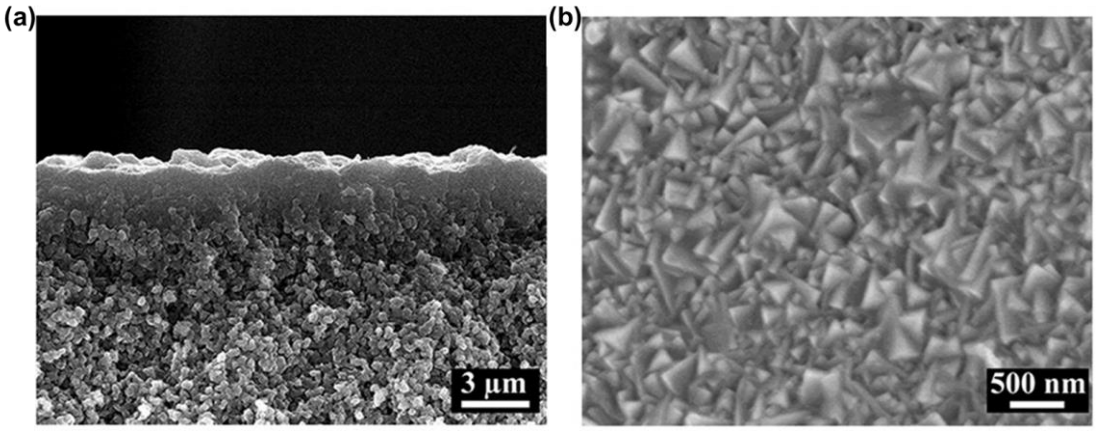

Fig.1.9. SEM images of the continuous UiO-66 membranes [78].

1.3.2.2. MOF-based composite membranes

MOF-based composite membranes are fabricated by incorporating MOF micro- or nanoparticles as fillers into polymers, which aim at overcoming the permeability-selectivity tradeoff in polymeric membranes while improving the thermal stability and mechanical properties of the membranes [79,80]. MOF-based MMMs and TFN membranes are two major forms of MOF-based composite membranes.

MOF-based mixed matrix membranes

MMMs are composite membranes prepared by incorporating inorganic or inorganic/organic hybrid fillers (as the dispersed phase) into a polymeric matrix (as the

continuous phase), as illustrated in Fig. 1.8b [71,81]. MOF-based MMMs mean the dispersed phase consists of MOF particles [75]. Unlike continuous MOF membranes, which require a supporting substrate, MOF-based MMMs can be manufactured as free-standing membranes. For example, Basu et al. reported for the first time MOF-based MMMs for liquid phase separation, which were prepared by incorporating a series of MOF fillers such as Cu_3BTC_2, MIL-47 (MIL, Matériaux de l'Institut Lavoisier), MIL-53 (Al), and ZIF-8 (ZIF, zeolitic imidazolate framework), as shown in Fig. 1.10, into polydimethylsiloxane (PDMS). The permeability of the resulting membranes, however, was comparable to that of the raw PDMS membrane (0.54 L m^{-2} h^{-1} bar^{-1}) [82].

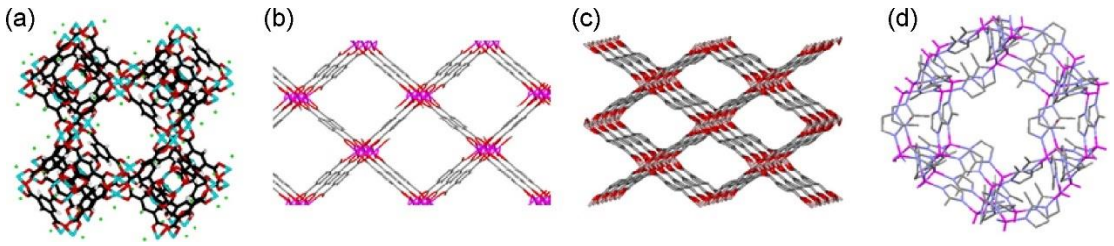

Fig. 1.10. The structures of MOFs: a) $Cu_3(BTC)_2$, b) MIL-47, c) MIL-53 (Al), and d) ZIF-8.

Due to the non-porous nature of many polymeric matrices, MOF-based MMMs should show lower permeability as compared to continuous MOF membranes. This limitation is supposed to be solved by increasing the fraction of MOFs within a membrane. However, the increase in the MOF loading also caused poor dispersion and agglomeration of MOF particles, which resulted in void defects in membranes. In order to improve the integration of MOFs and polymers, a better molecular-level understanding of the surface of MOFs is required.

MOF-based thin-film nanocomposite membranes

The concept of TFN membranes, as illustrated in Fig. 1.8c, was first proposed by Jeong et al. [83]. They are usually prepared by incorporating nanofillers into an ultrathin crosslinked aromatic polyamide selective layer that is supported by a microporous substrate. Membrane performance can be improved by modulating the chemical properties and structure of the selective layer through the embedment of appropriate nanofillers. In 2013, for the first time, Sorribas et al. fabricated TFN membranes for organic solvent nanofiltration by using MOF nanoparticles as fillers [84]. MOF nanoparticles including ZIF-8, MIL-101 (Cr), MIL-53 (Al) and NH_2-MIL-53 (Al) with different hydrophilicity were prepared and respectively embedded into the crosslinked aromatic polyamide selective layer via interfacial polymerization. The resulting membranes were used for the separation of polystyrene oligomers from methanol (as shown in Fig. 1.11). Among them, the embedment of MIL-101 (Cr) nanoparticles increased the permeability from 1.5 to 3.9 L m^{-2} h^{-1} bar^{-1} without decreasing the selectivity. The porous structure of MIL-101 (Cr) facilitated the transport of methanol, leading to enhanced permeability. In addition, the polyamide layer surrounding the MOF nanoparticles was thought to be responsible for the high rejection. The excellent compatibility of the MOF and polyamide matrix resulted in the absence of non-selective voids. Presently, publications on MOF-based TFN membranes for liquid separation have been increasing, in most of which MOF-based TFN membranes performed satisfactorily as compared to TFC membranes. In order to further improve separation performance, key issues are increasing the MOF loading, improving the dispersion of

MOF nanoparticles, and enhancing the compatibility between MOFs and the matrix.

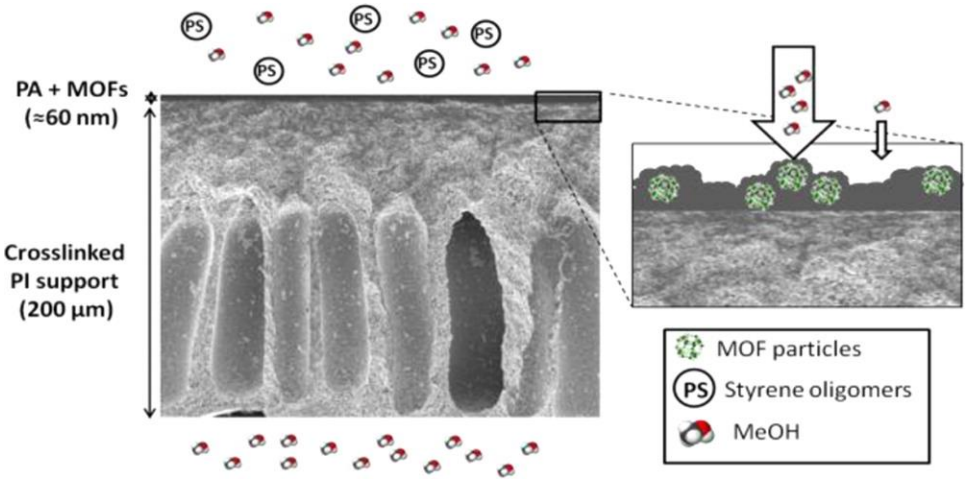

Fig. 1.11. Schematic illustration of MOF-based TFN membranes used for separation of polystyrene oligomers from methanol. Adapted from Ref. [84].

1.3.3. Key issues and challenges for MOF-based composite membranes in liquid separation

MOF-based composite membranes are promising for liquid separation because of the integrating advantages of polymers and MOF particles. To a great extent, their separation performance is influenced by the properties and structures of MOF particles. From the perspective of rational design, an ideal MOF-based composite membrane should possess high separation capacity, long-term operation stability, and be easy to fabricate. The stability, hydrophilicity/hydrophobicity, and dispersibility of MOFs should be considered for the preparation of MOF-based composite membranes for liquid separation.

Stability

For MOF-based composite membranes that are applied in water separation and

purification, the stability of MOFs against water, especially under water, is one of the most important factors. MOFs can be considered to be water-stable if there is no collapse of frameworks or structural degradation in the presence of water. In general, MOF structures with significant steric hindrance or strong coordination bonds are not susceptible to attack by water molecules [85]. Based on this, a consolidated database for water-stable MOFs has been created. For instance, a series of iron-based MOFs [MIL-101 (Fe)] and chromium-based MOFs [MIL-101 (Cr)] with excellent water stability have been developed by Ferey et al. [86]. The high valence of Fe^{3+} and Cr^{3+} facilitates high connectivity to organic ligands. Consequently, MIL-101 (Fe, Cr) is resistant to water molecules. ZIF-8, consisting of Zn^{2+} connected by imidazolate linkers, is another water-stable MOF established by Yaghi and his coworkers, which was demonstrated to be stable in alkaline solutions, refluxing organic solvents, and boiled water without losing crystallinity [87]. This remarkable water resistance could be attributed to the strong coordination bonds and the surface structure of ZIF-8.

Hydrophilicity/hydrophobicity

The hydrophilicity/hydrophobicity of MOFs is determined by the existence of open metal sites and ligands. Their rational selection in MOF-based membranes for liquid separation depends on the nature of the compounds to be separated. Hydrophilic MOFs are generally used to remove organics from water. For example, ZIF-71, synthesized from zinc acetate and 4,5-dichloroimidazole, exhibits intrinsic hydrophobicity. Dong et al. prepared a hydrophobic ZIF-71 membrane using a reactive seeding method supported on a ZnO porous substrate. The resulting membrane showed permselectivity

for dimethyl carbonate (DMC) over methanol and for alcohols over water in pervaporation separation of DMC-methanol and alcohol-water mixtures, respectively [88]. In contrast, hydrophobic MOFs can show negative effects on performances, e.g., water permeability, selectivity, and antifouling properties when they are used in MOF-based membranes for water purification and separation. For example, high hydrophilicity and an appropriate porous structure of MOFs are required for both high flux and selectivity of MOF-based composite membranes in the dye desalination process [89]. When MOF-based composite membranes are prepared via interfacial polymerization, the hydrophilicity of MOFs may result in weak entrapment into the selective layer, which leads to loss of MOFs. In this sense, improving the hydrophilicity of MOFs is critical for optimizing the performance of MOF-based composite membranes in water separation and purification.

Dispersibility

The dispersion of MOF particles in polymers has a great influence on the separation performance of MOF-based composite membranes. When MOF nanoparticles are embedded into polymers during the membrane preparation process, they are prone to aggregate due to the high surface energy, especially at a high MOF loading, which may result in non-selective defects, leading to a deterioration of performance in liquid separation [75]. On the other hand, the poor dispersion hinders the maximum loading of MOF particles in composite membranes, thus limiting the enhancement of permeability. Surface modification of MOFs has been proven to be a good strategy for improving their dispersibility. MOFs allow for the incorporation of a variety of

functionalities, which facilitates the dispersion of MOFs in the membranes. For example, amine groups were introduced on the surface of MIL-101 to afford NH_2-MIL-101/chitosan NF membranes. Due to the increase in positive charges after the introduction of the amino group, NH_2-MIL-101 dispersed better in chitosan, which resulted in an improved removal of multivalent cations [90].

1.4. Objective of the thesis

The limitations of membranes for liquid separation, such as permeability-selectivity tradeoff and fouling, can be addressed to an extent by integrating polymers with nanoporous materials. MOFs, a kind of emerging crystalline porous material, show high potential in separation processes because their highly tunable pore structure, chemical functionality, and flexibility make them superior to traditional porous materials such as carbon-based materials and zeolites. Although significant progress has been made in recent years, the challenges of developing MOF-based composite membranes for liquid separation must be overcome before practical applications. As mentioned above, due to the deterioration of water-sensitive MOF materials, the long-term stability of MOF-based composite membranes remains a concern. For different purposes of separation, modulation of the hydrophilicity/hydrophobicity of MOFs is also required. Agglomeration of MOF particles in the polymeric matrix leads to the formation of non-selective voids that further impede membrane performance.

Among the many appealing characteristics of MOFs, their modular nature makes them ideal for chemical manipulations aimed at tuning functionality. The objective of the thesis is to solve the above problems for the preparation of high-performance MOF-

based liquid separation membranes by engineering MOF surfaces. In the thesis, ZIF-8, one of the relative hydro-stable MOFs, was chosen as a scaffold for the preparation of MOF-based membranes. To be more specific, three research items have been carried out, and they are summarized in **Chapters 2–4**.

In **Chapter 2**, hydrophobic modification of ZIF-8 nanoparticles was conducted to switch the wettability of ZIF-8 from relative hydrophilic to hydrophobic. This chapter aimed to adopt ZIF-8-deposited membranes for both water-in-oil and oil-in-water emulsion separation.

In **Chapter 3**, a ZIF-8 TFN membrane was prepared for desalination by using ZIF-8 nanoparticles as fillers. The purpose of this chapter was to balance the permeability-selectivity tradeoff and reduce fouling of membranes by improving the hydrophilicity of ZIF-8 and its dispersibility in water via modifying the surface with polydopamine (PDA).

Chapter 4 focuses on the fabrication of ZIF-8-matrix nanocomposite membranes for the purpose of enhancing permeability while maintaining selectivity for desalination. To achieve this, a hydrophilic polymer was grafted on the external surface of ZIF-8, which can be used as building blocks to construct a high ZIF-8 loading selective layer.

Chapter 5 summarizes and concludes the thesis.

1.5. References

[1] W.J. Koros, C. Zhang, Materials for next-generation molecularly selective synthetic membranes, Nat. Mater. 16 (2017) 289–297.

[2] C.J. Vörösmarty, P. Green, J. Salisbury, R.B. Lammers, Global water resources: vulnerability from climate change and population growth, Science 289 (2000) 284–288.

[3] A. Rolston, Social changes affect water quality too, Nature 536 (2016) 396–396.

[4] R.M. Rego, G. Kuriya, M.D. Kurkuri, M. Kigga, MOF based engineered materials in water remediation: recent trends, J. Hazard. Mater. 403 (2021) 123605.

[5] M. Kummu, J.H.A. Guillaume, H. Moel, S. Eisner, M. Flörke, M. Porkka, S. Siebert, T.I.E. Veldkamp, P.J. Ward, The world's road to water scarcity: shortage and stress in the 20th century and pathways towards sustainability, Sci. Rep. 6 (2016) 1–16.

[6] S.A. Bhat, S. Singh, J. Singh, S. Kunar, Bhawana, A.P. Vig, Bioremediation and detoxification of industrial wastes by earthworms: vermicompost as powerful crop nutrient in sustainable agriculture, Bioresour. Technol. 252 (2018) 172–179.

[7] UN General Assembly, Resolution adopted by the General Assembly on 11 September, (2015) New York, Accessed, Nov 2017. http://www.un.org/ga/search/view_doc.asp?symbol=A/RES/70/1&Lang=E.

[8] T. Tong, M. Elimelech, The global rise of zero liquid discharge for wastewater management: drivers, technologies, and future directions, Environ. Sci. Technol. 50 (2016) 6846–6855.

[9] M. Mon, R. Bruno, J. Ferrando-Soria, D. Armentano, E. Pardo, Metal-organic framework technologies for water remediation: towards a sustainable ecosystem, J. Mater. Chem. A 6 (2018) 4912–4947.

[10] R.P Schwarzenbach., B.I. Escher, K. Fenner, T.B. Hofstetter, C.A. Johnson, U.V. Gunten, B. Wehrli, The challenge of micropollutants in aquatic systems, Science 313 (2006) 1072–1077.

[11] R.M. Hegde, R.M. Rego, K.M. Potla, M.D. Kurkuria, M. Kiggaa, Bio-inspired materials for defluoridation of water: a review, Chemosphere 253(2020) 126657.

[12] R. Li, L. Zhang, P. Wang, Rational design of nanomaterials for water treatment, Nanoscale 7 (2015) 17167–17194.

[13] A.K. Tolkou, M. Mitrakas, I.A. Katsoyiannis, M. Ernst, A.I. Zouboulis, Fluoride removal from water by composite Al/Fe/Si/Mg pre-polymerized coagulants: characterization and application, Chemosphere 231(2019) 528–537.

[14] W.L. Ang, A.W. Mohammad, N. Hilal, C.P. Leo, A review on the applicability of integrated/hybrid membrane processes in water treatment and desalination plants, Desalination 362 (2015) 2–18.

[15] A. Gil, L.A. Galeano, M.Á. Vicente, Applications of advanced oxidation processes (AOPs) in drinking water treatment, Springer International Publishing, 2019.

[16] L. Wang, PVDF Membranes with Stable, Ultrathin graphene oxide (GO) functional coatings for antifouling oil/water separation under cross-flow condition, University of South Carolina, 2016.

[17] Z. Zhang, L. Wen, L. Jiang, Bioinspired smart asymmetric nanochannel membranes, Chem. Soc. Rev. 47 (2018) 322–356.

[18] X.Q. Cheng, Z.X. Wang, X. Jiang, T. Li, C.H. Lau, Z. Guo, J. Ma, L. Shao, Towards sustainable ultrafast molecular-separation membranes: from conventional polymers to emerging materials, Prog. Mater. Sci. 92 (2018) 258–283.

[19] A. Lee, J.W. Elam, S.B. Darling, Membrane materials for water purification: design, development, and application, Environ. Sci.: Water Res. Technol. 2 (2016) 17–42.

[20] C. Zhang, B.H. Wu, M.Q. Ma, Z. Wang, Z.K. Xu, Ultrathin metal/covalent-organic framework membranes towards ultimate separation, Chem. Soc. Rev. 48 (2019) 3811–3841.

[21] R.W. Baker, Membrane technology and applications, John Wiley & Sons, 2012.

[22] E.D. Howe, Sea water conversion, Advances in Hydroscience 3 (2013).

[23] G.M. Geise, H.S. Lee, D.J. Miller, B.D. Freeman, J.E. McGrath, D.R. Paul, Water purification by membranes: the role of polymer science, J. Polym. Sci., Part B: Polym. Phys. 48 (2010) 1685–1718.

[24] H. Yasuda, A. Peterlin, Diffusive and bulk flow transport in polymers, J. Appl. Polym. Sci. 17 (1973) 433–442.

[25] J.G. Wijmans, R.W. Baker, The solution-diffusion model: a review, J. Membr. Sci. 107 (1995) 1–21.

[26] A. Criscuoli, A. Figoli, Pressure-driven and thermally-driven membrane

operations for the treatment of arsenic-contaminated waters: a comparison, J. Hazard. Mater. 370 (2019) 147–155.

[27] F. Macedonio, E. Drioli, Pressure-driven membrane operations and membrane distillation technology integration for water purification, Desalination 223 (2008) 396–409.

[28] E. Arkhangelsky, A. Duek, V. Gitis, Maximal pore size in UF membranes, J. Membr. Sci. 394 (2012) 89–97.

[29] N. Hilal, H. Al-Zoubi, N.A. Darwish, A.W. Mohamma, M. Abu Arabi, A comprehensive review of nanofiltration membranes: treatment, pretreatment, modelling, and atomic force microscopy, Desalination 170 (2004), 281–308.

[30] G.M. Geise, D.R. Paul, B.D. Freeman, Fundamental water and salt transport properties of polymeric materials, Prog. Mater. Sci. 39 (2014) 1–42.

[31] B. Van der Bruggen, C. Vandecasteele, Distillation vs. membrane filtration: Overview of process evolutions in seawater desalination, Desalination 143 (2002) 207–218.

[32] P. Eriksson, Nanofiltration extends the range of membrane filtration, Environ. Prog. 7 (1988) 58–62.

[33] B. Van der Bruggen, M. Mänttäri, M. Nyström, Drawbacks of applying nanofiltration and how to avoid them: a review, Sep. Purif. Technol. 63 (2008) 251–263.

[34] M. Homayoonfal, A. Akbari, M.R. Mehrnia, Preparation of polysulfone nanofiltration membranes by UV-assisted grafting polymerization for water

softening, Desalination 263 (2010) 217–225.

[35] L.D. Nghiem, A.I. Schäfer, M. Elimelech, Role of electrostatic interactions in the retention of pharmaceutically active contaminants by a loose nanofiltration membrane, J. Membr. Sci. 286 (2006) 52–59.

[36] S. Yu, M. Liu, M. Ma, M. Qi, Z. Lü, C. Gao, Impacts of membrane properties on reactive dye removal from dye/salt mixtures by asymmetric cellulose acetate and composite polyamide nanofiltration membranes, J. Membr. Sci. 350 (2010) 83–91.

[37] S. Darvishmanesh, T. Robberecht, P. Luis, J. Degrève, B. Van der Bruggen, Performance of nanofiltration membranes for solvent purification in the oil industry, J. Am. Oil Chem. Soc. 88 (2011) 1255–1261.

[38] Z. Wang, A. Wu, L.C. Ciacchi, G.Wei, Recent advances in nanoporous membranes for water purification, Nanomaterials 8 (2018) 65.

[39] N.G. Doménech, F. Purcell-Milton, Y.K. Gun'ko, Recent progress and future prospects in development of advanced materials for nanofiltration, Mater. Today Commun. 23 (2020) 100888.

[40] T. Shibutani, T. Kitaura, Y. Ohmukai, T. Maruyama, S. Nakatsuka, T. Watabe, H. Matsuyama, Membrane fouling properties of hollow fiber membranes prepared from cellulose acetate derivatives, J. Membr. Sci. 376 (2011) 102–109.

[41] A.L. Ahmad, A.A. Abdulkarim, B.S. Ooi, S. Ismail, Recent development in additives modifications of polyethersulfone membrane for flux enhancement, Chem. Eng. J. 223 (2013) 246–267.

[42] H.M. Park, K.Y. Jee, Y.T. Lee Preparation and characterization of a thin-film composite reverse osmosis membrane using a polysulfone membrane including metal-organic frameworks, J. Membr. Sci. 541 (2017) 510–518.

[43] H.R. Lohokare, M.R. Muthu, G.P. Agarwal, U.K. Kharul, Effective arsenic removal using polyacrylonitrile-based ultrafiltration (UF) membrane, J. Membr. Sci. 320 (2008) 159–166.

[44] M. Bassyouni, M.H. Abdel-Aziz, M.S. Zoromba, S.M.S.Abdel-Hamid, E. Drioli, A review of polymeric nanocomposite membranes for water purification, J. Ind. Eng. Chem. 73 (2019) 19–46.

[45] R.J. Petersen, Composite reverse osmosis and nanofiltration membranes, J. Membr. Sci. 83 (1993) 81–150.

[46] F.S. Francis, Fabrication and evaluation of new ultra-thin reverse osmosis membranes, National Technical Information Services, 1966.

[47] L.T. Rozelle, J.E. Cadotte, R.D. Corneliussen, E.E. Erickson, Final report on development of new reverse osmosis membrane, 1968.

[48] S. Kaur, S. Sundarrajan, D. Rana, T. Matsuura, S. Ramakrishna, Influence of electrospun fiber size on the separation efficiency of thin film nanofiltration composite membrane, J. Membr. Sci. 392 (2012) 101–111.

[49] P. Hadi, M. Yang, H. Ma, X. Huang, H. Walker, B.S. Hsiao, Biofouling-resistant nanocellulose layer in hierarchical polymeric membranes: synthesis, characterization and performance, J. Membr. Sci. 579 (2019) 162–171.

[50] A.J. Burggraaf, L. Cot, Fundamentals of inorganic membrane science and

technology, Elsevier, 1996.

[51] B. Van der Bruggen, C. Vandecasteele, T.V. Gestel, W. Doyen, R. Leysen, A review of pressure-driven membrane processes in wastewater treatment and drinking water production, Environ. Prog. 22 (2003) 46–56.

[52] A.K. Pabby, S.S.H. Rizvi, A.M.S. Requena, Handbook of membrane separations: chemical, pharmaceutical, food, and biotechnological applications, CRC press, 2008.

[53] H. Liu, H. Wang, X. Zhang, Facile fabrication of freestanding ultrathin reduced graphene oxide membranes for water purification, Adv. Mater. 27 (2015) 249–254.

[54] M.S. Rahaman, C.D. Vecitis, M. Elimelech, Electrochemical carbon-nanotube filter performance toward virus removal and inactivation in the presence of natural organic matter, Environ. Sci. Technol. 46 (2012) 1556–1564.

[55] B. Van der Bruggen, K. Jeonghwan, Nanofiltration of aqueous solutions: recent developments and progresses, Advanced Materials for Membrane Preparation, 2012.

[56] K.P. Lee, T.C. Arnot, D. Mattia, A review of reverse osmosis membrane materials for desalination-development to date and future potential, J. Membr. Sci. 370 (2011) 1–22.

[57] J. Yin, B. Deng, Polymer-matrix nanocomposite membranes for water treatment, J. Membr. Sci. 479 (2015) 256–275.

[58] X. Qiao, T.S. Chung, R. Rajagopalan, Zeolite filled P84 co-polyimide membranes

for dehydration of isopropanol through pervaporation process, Chem. Eng. Sci. 61 (2006) 6816–6825.

[59] K. Cao, Z. Jiang, J. Zhao, C. Zhao, C. Gao, F. Pan, B. Wang, X. Cao, J. Yang, Enhanced water permeation through sodium alginate membranes by incorporating graphene oxides, J. Membr. Sci. 469 (2014) 272–283.

[60] J.H. Choi, J. Jegal, W.N. Kim, H.S. Choi, Incorporation of multiwalled carbon nanotubes into poly (vinyl alcohol) membranes for use in the pervaporation of water/ethanol mixtures, J. Appl. Polym. Sci. 111 (2009) 2186–2193.

[61] Q. Zhao, J. Qian, C. Zhu, Q. An, T. Xu, Q. Zheng, Y. Song, A novel method for fabricating polyelectrolyte complex/inorganic nanohybrid membranes with high isopropanol dehydration performance, J. Membr. Sci. 345 (2009), 233–241.

[62] L.H. Le, D.X. Trinh, N.B. Trung, T.P.N. Tran, T. Taniike, Fabrication of assembled membrane from malonate-functionalized graphene and evaluation of its permeation performance, Carbon 114 (2017) 519–525.

[63] H.C. Zhou, S. Kitagawa, Metal-organic frameworks (MOFs), Chem. Soc. Rev. 43 (2014) 5415–5418.

[64] M. Eddaoudi, J. Kim, N. Rosi, D. Vodak, J. Wachter, M. O'keeffe, O.M. Yaghi, Systematic design of pore size and functionality in isoreticular MOFs and their application in methane storage, Science 295 (2002) 469–472.

[65] B.F. Hoskins, R. Robson, Design and construction of a new class of scaffolding-like materials comprising infinite polymeric frameworks of 3D-linked molecular rods. A reappraisal of the zinc cyanide and cadmium cyanide structures and the

synthesis and structure of the diamond-related frameworks [$N(CH_3)_4$] [CuIZnII $(CN)_4$] and CuI [4,4',4'',4'''-tetracyanotetraphenylmethane] BF_4. $xC_6H_5NO_2$[J]. J. Am. Chem. Soc. 112 (1990) 1546–1554.

[66] S.S.Y. Chui, S.M.F. Lo, J.P.H. Charmant, A.G. Orpen, I.D. Williams, A chemically functionalizable nanoporous material $[Cu_3(TMA)_2 (H_2O)_3]_n$, Science 283 (1999) 1148–1150.

[67] H. Li, M. Eddaoudi, M. O'Keeffe, O.M. Yaghi, Design and synthesis of an exceptionally stable and highly porous metal-organic framework, Nature 402 (1999) 276–279.

[68] C. Dey, T. Kundu, B.P. Biswal, A. Mallick, R. Banerjee, Crystalline metal-organic frameworks (MOFs): synthesis, structure and function, Acta Crystallogr., Sect. B: Struct. Sci 70 (2014) 3–10.

[69] W. Li, Y. Zhang, Q. Li, G. Zhang, Metal-organic framework composite membranes: synthesis and separation applications, Chem. Eng. Sci. 135 (2015) 232–257.

[70] H. Furukawa, K.E. Cordova, M. O'Keeffe, O.M. Yaghi, The chemistry and applications of metal-organic frameworks, Science 341 (2013) 1230444.

[71] M.S. Denny, J.C. Moreton, L. Benz, S.M. Cohen, Metal-organic frameworks for membrane-based separations, Nat. Rev. Mater. 1 (2016) 1–17.

[72] C. Zhang, B. Wang, W. Li, S. Huang, L. Kong, Z. Li, L. Li, Conversion of invisible metal-organic frameworks to luminescent perovskite nanocrystals for confidential information encryption and decryption, Nat. Commun. 8 (2017) 1–9.

[73] Y.S. Kang, Y. Lu, K. Chen, Y. Zhao, P. Wang, W.Y. Sun, Metal-organic frameworks with catalytic centers: from synthesis to catalytic application, Coord. Chem. Rev. 378 (2019) 262–280.

[74] J. Liu, C. Wöll, Surface-supported metal-organic framework thin films: fabrication methods, applications, and challenges, Chem. Soc. Rev. 46 (2017) 5730–5770.

[75] X. Li, Y. Liu, J. Wang, J. Gascon, J. Li, B. Van der Bruggen, Metal-organic frameworks-based membranes for liquid separation, Chem. Soc. Rev. 46 (2017) 7124–7144.

[76] Q. Zhang, Y. Cui, G. Qian, Goal-directed design of metal-organic frameworks for liquid-phase adsorption and separation, Coord. Chem. Rev. 378 (2019) 310–332.

[77] X. Liu, N.K. Demir, Z. Wu, K. Li, Highly water-stable zirconium metal-organic framework UiO-66 membranes supported on alumina hollow fibers for desalination, J. Am. Chem. Soc. 137 (2015) 6999–7002.

[78] H.B. Park, J. Kamcev, L.M. Robeson, M. Elimelech, B.D. Freeman, Maximizing the right stuff: the trade-off between membrane permeability and selectivity, Science 356 (2017) eaab0530.

[79] T.Y. Liu, H.G. Yuan, Y.Y. Liu, D. Ren, Y.C. Su, X. Wang, Metal-organic framework nanocomposite thin films with interfacial bindings and self-standing robustness for high water flux and enhanced ion selectivity, ACS nano 12 (2018) 9253–9265.

[80] Y. Zhang, X. Feng, S. Yuan, J. Zhou, B. Wang, Challenges and recent advances in

MOF-polymer composite membranes for gas separation, Inorg. Chem. Front. 3 (2016) 896–909.

[81] J. Dechnik, J. Gascon, C.J. Doonan, C. Janiak, C.J. Sumby, Mixed-matrix membranes, Angew. Chem. Int. Ed. 56 (2017) 9292–9310.

[82] S. Basu, M. Maes, A. Cano-Odena, L. Alaerts, D.E. De Vos, I.F.J. Vankelecom, Solvent resistant nanofiltration (SRNF) membranes based on metal-organic frameworks, J. Membr. Sci. 344 (2009) 190–198.

[83] B. Jeong, E.M.V. Hoek, Y. Yan, A. Subramani, X. Huang, G. Hurwitz, A.K. Ghosh, A. Jaworar, Interfacial polymerization of thin film nanocomposites: a new concept for reverse osmosis membranes, J. Membr. Sci. 294 (2007) 1–7.

[84] S. Sorribas, P. Gorgojo, C. Téllez, J. Coronas, A.G. Livingston, High flux thin film nanocomposite membranes based on metal-organic frameworks for organic solvent nanofiltration, J. Am. Chem. Soc. 135 (2013) 15201–15208.

[85] N. Qadir, S.A.M. Said, H.M. Bahaidarah, Structural stability of metal organic frameworks in aqueous media-controlling factors and methods to improve hydrostability and hydrothermal cyclic stability, Microporous and Mesoporous Mater. 201 (2015) 61–90.

[86] G. Férey, C. Mellot-Draznieks, C. Serre, F. Millange, J. Dutour, S. Surbléand, I. Margiolaki, A chromium terephthalate-based solid with unusually large pore volumes and surface area, Science 309 (2005) 2040–2042.

[87] K.S. Park, Z. Ni, A.P. Côté, J.Y. Choi, R. Huang, F.J. Uribe-Romo, H.K. Chae, M. O'Keeffe, O.M. Yaghi, Exceptional chemical and thermal stability of zeolitic

imidazolate frameworks, Proc. Natl. Acad. Sci. U.S.A. 103 (2006) 10186–10191.

[88] X. Dong, Y.S. Lin, Synthesis of an organophilic ZIF-71 membrane for pervaporation solvent separation, Chem. Commun. 49 (2013) 1196–1198.

[89] H. Ruan, C. Guo, H. Yu, J. Shen, C. Gao, A. Sotto, B. Van der Bruggen, Fabrication of a MIL-53 (Al) nanocomposite membrane and potential application in desalination of dye solutions, Ind. Eng. Chem. Res. 55 (2016) 12099–12110.

[90] X.H. Ma, Z. Yang, Z.K. Yao, Z.L. Xu, C.Y. Tang, A facile preparation of novel positively charged MOF/chitosan nanofiltration membranes, J. Membr. Sci. 525 (2017) 269–276.

Chapter 2

Surface wettability switching of a zeolitic imidazolate framework-deposited membrane for selective and efficient oil/water emulsion separation

Abstract

Oil/water emulsion separation, especially for surfactant-stabilized emulsions, remains a major challenge for environmental protection. Due to low energy consumption and good separation performance, membrane separation technology based on special wettable materials is promising for oil/water emulsion separation. In this chapter, zeolitic imidazolate framework-8 (ZIF-8) membranes were prepared by vacuum deposition of ZIF-8 particles of different sizes on a regenerated cellulose support. Microparticles gave a better performance as compared to nanoparticles in terms of the permeate flux, while the presence of large interparticle voids adversely affected the rejection efficiency. Such a detriment could be overcome by a sequential deposition of microparticles followed by nanoparticles to form a dense selective layer for oil/water emulsion separation. Hydrophobic modification of pre-formed ZIF-8 particles switched the surface wettability of ZIF-8 deposited membranes from hydrophilic to hydrophobic, offering versatility of the deposited membrane for both oil-in-water and water-in-oil emulsion filtration.

2.1. Introduction

Industrial oily waste water and frequent oil spills have highlighted the urgent demand for effective oil/water treatments due to irrecoverable damage to the ecosystem [1–3]. Various methods have been used or proposed for oil/water separation, such as in-situ burning, gravity separation, flotation, coalescence, thermo/chemical demulsification, and electrolytic demulsification [4–8]. However, they face individual disadvantages in terms of separation or process efficiency. In the past decade, membrane separation technologies have attracted great attention to tackle energy and environmental challenges [9–13]. In particular, they emerge as an effective method for oil/water separation due to low energy consumption, minimal land usage, ease of operation, and good separation performance [14].

To achieve effective oil/water separation in a membrane separation process, it is essential to maintain one phase (water or oil) preferentially on a membrane. Since water and oils are basically immiscible, attempts have been made to develop special wettable materials, “oil-removing” and “water-removing” materials, that exhibit opposite affinity towards oils and water, respectively [15–18]. In 2004, Jiang and coworkers reported an “oil-removing” PTFE-coated stainless-steel mesh [15]. The craterlike structure created by micro- and nanoscale assemblies of PTFE made the coated mesh superhydrophobic. At the same time, the rough surface increased an oleophilic property of PTFE to make the coated mesh equipped with both superhydrophobic and superoleophilic properties for the first time. In a subsequent publication, the same group reported a kind of “water removing” material by depositing a hydrophilic

polyacrylamide hydrogel onto a stainless-steel mesh surface for successful separation of oil/water mixtures [16]. When water was trapped in nanostructured hydrogel, the oil/water/solid composite interface exhibited underwater superoleophobic properties to prevent the coated mesh from fouling by oil. Gao et al. prepared a superhydrophobic poly (lactic acid) membrane via a one-step phase separation method, which was used to control the release of oil-soluble drugs [19]. You et al. reported a superhydrophilic/underwater superhydrophobic glass fabric for the removal of the oil from an oil/water mixture by coating it with a konjac glucomannan hydrogel through a dip-coating method [20]. Zhang et al. fabricated a $Cu(OH)_2$ nanowire-haired Cu mesh by oxidizing the Cu mesh using an $(NH_4)_2S_2O_8$ solution [21]. Such a structure can trap water on the surface, thus preventing oil from permeating across the mesh. In this way, various inorganic and organic materials with special surface wettability have been reported for separating oil/water mixtures [20,22–24]. On the other hand, most of these efforts have focused on immiscible oil/water mixtures, and membrane separation of oil/water emulsions (both oil-in-water and water-in-oil emulsions), especially surfactant-stabilized emulsions with a droplet size below 20 μm, has not been sufficiently addressed.

Metal-organic frameworks (MOFs), a kind of emerging crystalline porous material constructed by metal clusters and organic ligands, have been considered as a promising candidate for adsorption and separation applications due to their tunable pore structure, designability, as well as tenability [25–27]. Compared with zeolites, activated carbon, and other porous materials, MOFs exhibit significant advantages in the modulation of

pore architectures and properties [28,29]. Among known MOFs, zeolitic imidazolate frameworks (ZIFs), particularly ZIF-8, have been dominantly used in the existing reports for oil/water separation [30–34]. Benefiting from their exceptional water stability and highly tunable surface wettability, membranes with special wettability from hydrophobic/oleophilic to hydrophilic/oleophobic were explored for efficient oil/water separation. For example, Ma et al. deposited pre-synthesized ZIF-8 crystals on a stainless-steel mesh with the aid of a polymer binder [30]. These crystals were exploited as seed crystals for the secondary growth of ZIF-8 to make a denser ZIF-8 mesh. They showed that pre-wetting of the ZIF-8 meshes induced underwater oleophobic properties to allow efficient separation of light and heavy oils from water. Xu et al. prepared ZIF-8 seed crystals on an electrospun PVDF/ZnO membrane [31]. The growth of the seed crystals in the subsequent process afforded a PVDF-g-ZIF-8 membrane with a hierarchical fiber structure and an enhanced oil wettability. Xie et al. immobilized Zn^{2+} ions on a surface of a polydopamine-coated regenerated cellulose membrane [32]. Self-assembly of Zn^{2+} ions and the organic ligand generated ZIF-8 crystals on a membrane surface. The membrane exhibited underwater superoleophobic and underoil hydrophobic properties.

As reviewed above, most past efforts have adopted seed-induced crystallization [30,31,33] and in-situ growth [32,34] methods to integrate ZIF-8 into membranes to induce special wettable surfaces. Recently, a facile method to fabricate MOF membranes was reported, which is based on a vacuum deposition of pre-synthesized MOF nanoparticles to form a semi-continuous selective layer on a membrane support

[12,13]. The method is appealing in a sense that the tuning of nanoparticle morphology as a building block and the construction of an optimized selective layer can be carried out separately, which is infeasible in the other methods. By controlling the particle size distribution of deposited MOF nanoparticles, a highly permeable, selective, and fouling-resistant UiO-66 membrane for methylene blue nanofiltration was reported [13].

In this chapter, ZIF-8 membranes were fabricated for oil/water emulsion separation. By depositing ZIF-8 particles on a regenerated cellulose membrane via vacuum filtration, a selective layer for oil/water emulsion separation was formed in a simple preparation step. The sequential deposition of microparticles followed by nanoparticles greatly enhanced the packing of the selective layer to maintain high rejection efficiency even at high operation pressure. Besides, hydrophobic modification of the pre-formed ZIF-8 particles was performed to switch the surface wettability of ZIF-8 membranes from hydrophilic to hydrophobic. Based on these strategies, I would like to deliver promising aspects of the ZIF-8-deposited membranes for both oil-in-water and water-in-oil emulsion separation.

2.2. Experimental section

2.2.1. Materials

All reagents and solvents are commercially available. They were used as received without further purification. Zinc nitrate hexahydrate ($Zn(NO_3)_2 \cdot 6H_2O$, > 98%) and d_4-acetic acid (> 99.5%) were purchased from Sigma-Aldrich. 2-Methylimidazole (MIM, > 98%), 5,6-dimethylbenzimidazole (DMBIM, > 98%), triethylamine (> 99%), Tween 60, and Span 80 were obtained from TCI Chemical Industry Co., Ltd. Methanol and toluene

were purchased from Wako Chemical Industries Ltd. Poreless TiO_2 nanoparticles (TTO-55A) with a particle size of 30–50 nm were purchased from Ishihara Sangyo Kaisha, Ltd. A regenerated cellulose (RC) membrane (RC58, 47 mm dia., 0.2 μm pore size, Whatman) was selected as a support membrane due to its high-quality microporous structure and wide chemical compatibility.

2.2.2. Synthesis of ZIF-8

Synthesis of ZIF-8 microparticles

ZIF-8 microparticles (denoted as ZIF-8_1) were synthesized according to a previously reported procedure [28]. 0.97 mmol of $Zn(NO_3)_2{\cdot}6H_2O$ in 10 mL of deionized (DI) water was added to a solution of MIM (55.3 mmol in 70 mL of DI water), and stirred for 5 min at room temperature. The solution mixture was transferred into a Teflon-lined autoclave for the hydrothermal treatment at 120 °C for 6 h. The solid product was collected by centrifugation, repetitively washed with methanol for 5 times, and dried at 40 °C under vacuum for 12 h.

Synthesis of ZIF-8 nanoparticles

ZIF-8 nanoparticles (denoted as ZIF-8_2) were prepared by a precipitation method in methanol [35]. A solution of $Zn(NO_3)_2{\cdot}6H_2O$ (4.94 mmol in 100 mL of methanol) was rapidly poured into a solution of MIM (39.52 mmol in 100 mL of methanol) under vigorous stirring. The mixture slowly became turbid. After stirring for 1 h at room temperature, the solid product was collected by centrifugation, repetitively washed with methanol for 5 times, and then dried at 40 °C under vacuum for 12 h.

2.2.3. Hydrophobic modification of ZIF-8

Hydrophobic modification of ZIF-8 particles was carried out via a solvent-assisted ligand exchange (SALE) reaction (Scheme 2.1) according to the procedure reported by Yang et al. [36]. Briefly, 0.50 g of ZIF-8 and 3.42 mmol of DMBIM were mixed in 80 mL of methanol, followed by the addition of 4.94 mmol of triethylamine. The mixture was sonicated for 1 h, and then heated at 60 °C for 24 h under stirring. The modified particles were washed with methanol, collected by centrifugation, and dried at room temperature. The samples were denoted as ZIF-8_1-DMBIM and ZIF-8_2-DMBIM for modified ZIF-8_1 and ZIF-8_2, respectively.

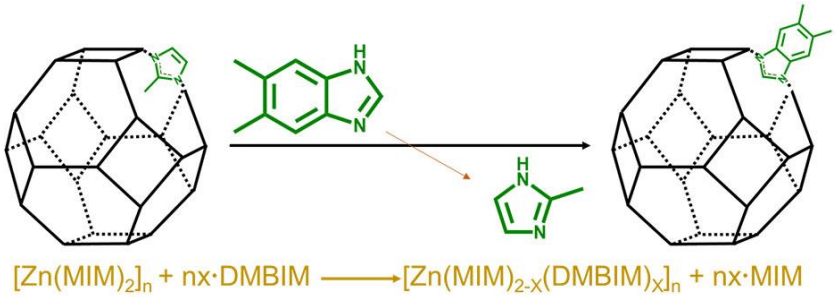

Scheme 2.1. Hydrophobic modification of ZIF-8 via a SALE reaction [36].

2.2.4. Characterization

The chemical structure of ZIF-8 before and after hydrophobic modification was analyzed using a Fourier transform infrared spectrometer equipped with an attenuated total reflection accessory (FTIR-ATR, 100, Perkin Elmer). ^{1}HNMR measurements were performed using a Bruker 400 MHz spectrometer. *Ca.* 3 mg of ZIF-8 particles was fully digested in a 99.5% solution of d_4-acetic acid. ^{1}HNMR spectra were calibrated by the methyl proton residue of d_4-acetic acid. The crystalline structure was analyzed by X-

ray diffraction spectroscopy (XRD, Rigaku SmartLab) using Cu Kα radiation at a scan step of 0.5° per min in the range of 5–45°. N_2 adsorption/desorption experiments were conducted at 77 K using a BELSORP-mini II instrument (BEL JAPAN, Inc.). The specific surface area and the pore volume were determined by the Brunauer-Emmet-Teller (BET) and Horvath-Kawazoe methods, respectively. The morphology of ZIF-8 particles was observed by scanning electron microscopy (SEM, Hitachi S-4100) operated at an accelerating voltage of 20 kV, and by transmission electron microscopy (TEM, Hitachi H-7100) operated at an accelerated voltage of 100 kV. The particle size was acquired from the analysis of TEM images using Image J software. Water contact angle (WCA) measurements were carried out on a ZIF-8 pellet prepared by compression of ZIF-8 particles using a 15 mm mold. 5.0 μL of DI water was dropped onto the surface of the pellet using a syringe. Then, WCAs were recorded on a contact angle goniometer (JY-PHB, Chende Jinhe, China) at room temperature.

2.2.5. Preparation of ZIF-8 composite membranes

The composite membranes were prepared by depositing ZIF-8 particles on an RC membrane by a vacuum filtration. ZIF-8 particles were dispersed in 10 mL of methanol and sonicated for 1 h prior to the deposition. Suction filtration was performed at a differential pressure of 50 mbar for 5 min, and subsequently at 100 mbar for 5 min. The deposited membrane was washed with 10 mL of methanol for 3 times. Three types of ZIF-8 membranes with the ZIF-8_1:ZIF-8_2 weight ratios of 100:0 (M1), 40:60 (M2), and 0:100 (M3) were prepared by fixing the total amount of ZIF-8 at 5.0 mg. For the preparation of M2, ZIF-8_1 microparticles were firstly deposited on the RC support,

followed by the deposition of ZIF-8_2 nanoparticles. ZIF-8-DMBIM membranes were prepared using the same procedure at the ZIF-8_1-DMBIM:ZIF-8_2-DMBIM weight ratios of 100:0 (D1), 40:60 (D2), and 0:100 (D3). For the sake of comparison, the TiO_2 composite membrane was also prepared using the same procedure, except poreless TiO_2 nanoparticles were used instead of ZIF-8 particles.

2.2.6. Oil/water emulsion separation

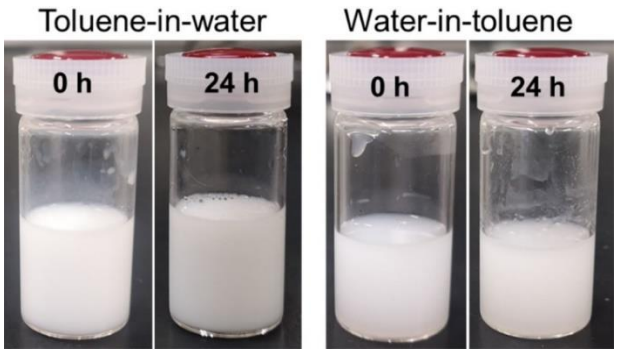

Fig. 2.1. Appearances of surfactant-stabilized toluene-in-water and water-in-toluene emulsions after keeping for 24 h under static conditions.

Oil-in-water and water-in-oil emulsions were prepared using toluene as the oil phase. In both of the emulsions, the volume ratio between the dispersed phase and the dispersion medium was fixed at 10:90. 10 mg of Tween 60 (HLB = 14.9) or Span 80 (HLB = 4.3) was added per 100 mL of the emulsion to stabilize the oil-in-water or water-in-oil emulsion, respectively. For both of the cases, the mixtures slowly turned oyster white during stirring for 5 h and subsequent sonication for 3 h. Optical microscope images of the emulsions were taken using a polarizing optical microscope (POM, OLYMPUS DP12). According to the micrographs, the droplet size of the dispersed phase was less than 20 μm. These droplets were stable for more than 24 h

under static conditions (Fig. 2.1). To avoid demulsification, the emulsions were sonicated for 2 h prior to use.

The oil/water emulsion filtration experiments were performed using a dead-end vacuum filtration system with an effective membrane area of 9.61 cm^2. The permeate flux (L m^{-2} h^{-1} bar^{-1}) was calculated according to Equation (2.1):

$$\text{Flux} = \frac{V}{A\,t\,\Delta P} \quad (2.1),$$

where V (L) is the volume of the permeate, A (m^2) is the effective membrane area, t (h) is the filtration time, and ΔP (bar) is the differential pressure. After a standard pretreatment procedure, the oil/water emulsion filtration was conducted at different differential pressures (100, 200 and 300 mbar). The rejection of the oil/water emulsion was calculated using Equation (2.2):

$$\text{Rejection (\%)} = \left(1-\frac{C_p}{C_0}\right) \times 100 \quad (2.2),$$

where C_p and C_0 are the concentrations of water (or oil) in the permeate and feed, respectively. The concentration of toluene in the oil-in-water emulsion was analyzed by UV-Vis spectrometry (Jasco V670, Japan). In detail, the filtrate was dissolved in cyclohexane. The intensity of the absorption peak of toluene at 261 nm was converted into the concentration based on the pre-determined standard curve. The water content in the water-in-oil emulsion was measured using a Karl Fischer coulombmeter (Metrohm 899). After the filtration experiment, the membrane was repetitively washed with ethanol for the recyclability test.

2.3. Results and discussion

2.3.1. Synthesis of ZIF-8 and their hydrophobic modification

The morphology of as-synthesized ZIF-8_1 and ZIF-8_2 particles was observed by SEM (Fig. 2.2a,b) and TEM (Fig. 2.2e,f). Both of the samples exhibited a typical ZIF-8 morphology: Rhombic dodecahedron with truncated corners. The average particle sizes of ZIF-8_1 and ZIF-8_2 acquired from the TEM images were 1.37 ± 0.22 μm and 41.97 ± 3.57 nm, respectively. In Fig. 2.3, the XRD patterns of ZIF-8_1 and ZIF-8_2 showed characteristic peaks at 2θ = 7.32°, 10.45°, 12.77°, 14.69°, 16.50°, and 18.12°, which respectively correspond to the (011), (002), (112), (022), (013), and (222) crystal faces of ZIF-8 [35,37]. These results confirmed the successful synthesis of ZIF-8 micro- and nanoparticles. Hydrophobic modification based on SALE reaction was carried out for both of the ZIF-8_1 and ZIF-8_2 particles to introduce a hydrophobic DMBIM ligand to the outer shell (Scheme 2.1). Figs 2.2 and 2.3 show that the modification hardly altered the morphology and crystalline structure of the original particles.

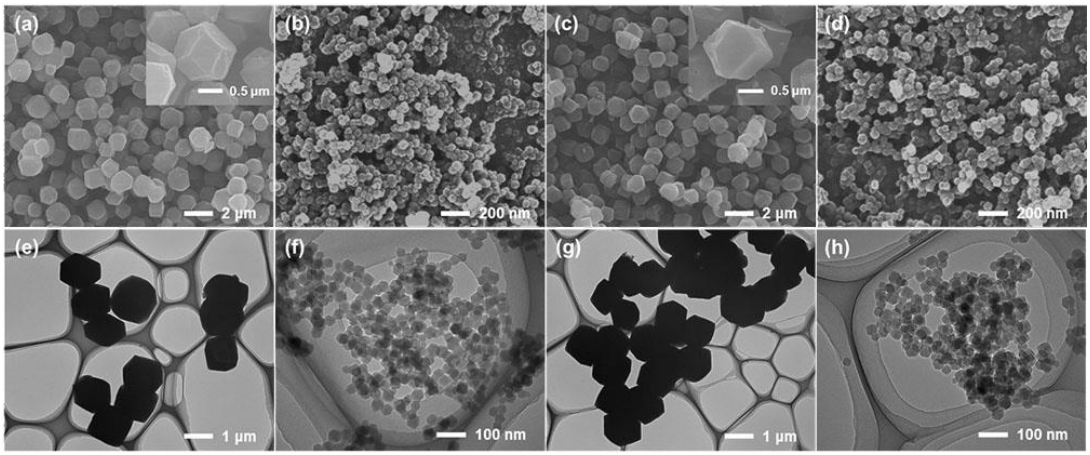

Fig. 2.2. SEM (top) and TEM (bottom) images of ZIF-8 particles: a,e) ZIF-8_1, b,f) ZIF-8_2, c,g) ZIF-8_1-DMBIM, and d,h) ZIF-8_2-DMBIM.

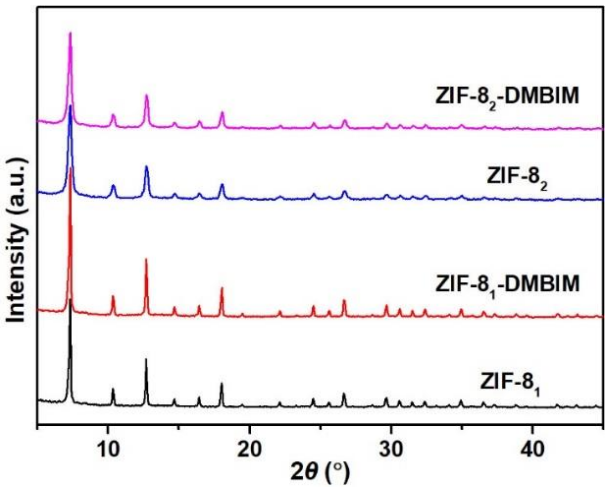

Fig. 2.3. XRD patterns of ZIF-8 particles.

Fig. 2.4 shows N_2 adsorption/desorption isotherms of the ZIF-8 particles. ZIF-8_1 and ZIF-8_2 displayed a similar isotherm of Type I, which is characteristic for microporous materials [38]. The sharp increase in the N_2 uptake at a very low relative pressure ($P/P_0 < 0.01$) is attributed to the micropore filling [27,39]. The subsequent plateau is a sign of complete filling of the micropores. On the other hand, ZIF-8_2 exhibited an increase in the N_2 uptake over $P/P_0 = 0.4$ with the appearance of a hysteresis loop. This corresponds to the presence of mesopores as interparticle voids among nanoparticles. The BET surface area and the micropore volume of ZIF-8_2 were found to be slightly higher than those of ZIF-8_1 (Table 2.1). A higher surface area for ZIF-8_2 is plausibly originated from the inclusion of the external surface area of nanoparticles, while the higher micropore volume is due to the contribution of small interparticle voids. After the modification with DMBIM, slight reductions in the BET surface area and the micropore volume were observed for both of the ZIF-8_1-DMBIM and ZIF-8_2-DMBIM particles.

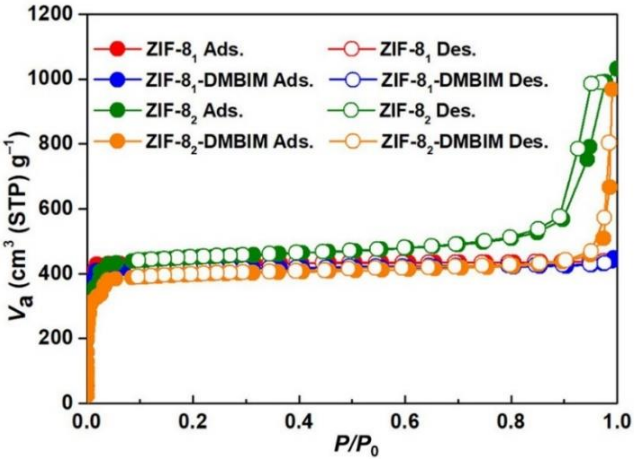

Fig. 2.4. N_2 adsorption/desorption isotherms of ZIF-8 particles.

Table 2.1. BET surface areas and pore volumes of ZIF-8 particles.

Sample	Surface area[a] (m^2 g^{-1})	V_{micro}[b] (cm^3 g^{-1})
ZIF-8_1	1742.7	0.627
ZIF-8_1-DMBIM	1673.5	0.595
ZIF-8_2	1805.4	0.670
ZIF-8_2-DMBIM	1591.0	0.591

[a]Determined by the BET method; [b]Micropore volume determined by the Horvath-Kawazoe method.

The chemical structure of ZIF-8 before and after the modification with DMBIM was investigated by FTIR. As shown in Fig. 2.5, ZIF-8_1 and ZIF-8_2 exhibited identical spectra. After the modification, new peaks appeared at 813 cm^{-1} and 855 cm^{-1} for both of ZIF-8_1-DMBIM and ZIF-8_2-DMBIM. These peaks correspond to the out-of-plane deformation of the aromatic C–H bonds of DMBIM [38,40]. Considerable red shifts of these peaks as compared to those of pure DMBIM suggested the deprotonation of DMBIM and the subsequent coordination of imidazole nitrogen to zinc ions. The

disappearance of a broad band at 3095 cm^{-1} (N–H stretching vibrations) provided further evidence [41]. ^{1}HNMR was performed to further confirm the successful modification (Fig. 2.6). Upon the SALE reaction, the two equivalent methyl groups of DMBIM were observed at δ ~ 2.41 ppm.

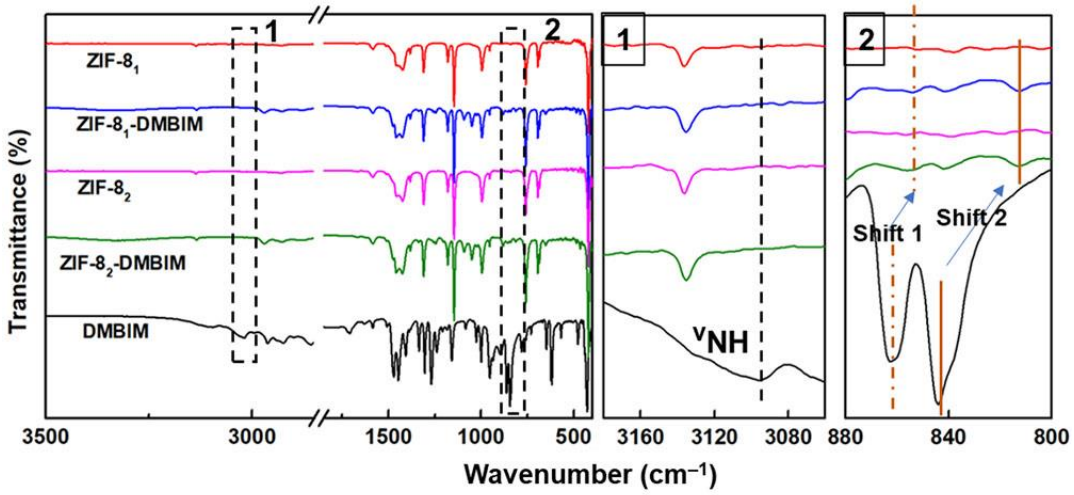

Fig. 2.5. FTIR-ATR spectra of ZIF-8 particles.

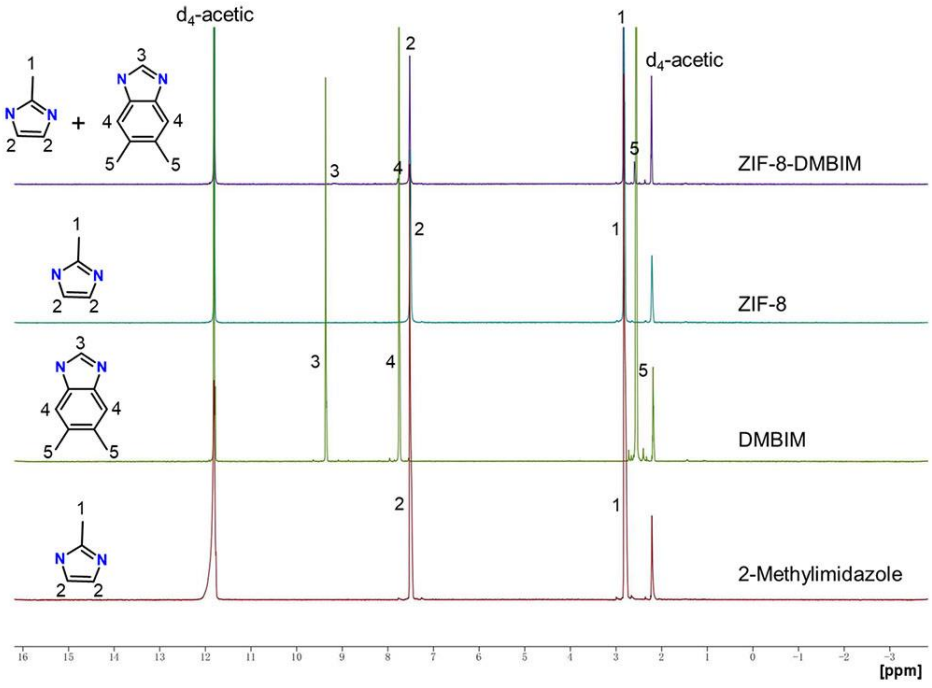

Fig. 2.6. ^{1}H NMR spectra of 2-methylimidazole, DMBIM, ZIF-8, and ZIF-8-DMBIM. A 6.2% (M_{DMBIM}/ (M_{DMBIM} + M_{MIM})) ligand exchange molar ratio was identified based on the signal integration of ^{1}HNMR.

2.3.2. Surface wettability of ZIF-8 and modified ZIF-8 particles

In general, a hydrophilic surface has a WCA of < 90°, while a hydrophobic surface has a WCA of > 90°. A surface with a water or oil contact angle of > 150° is usually considered superhydrophobic or superoleophobic, respectively [40,42]. WCA measurements were carried out to address the changes in wettability before and after the modification with DMBIM. As shown in Fig. 2.7, the ZIF-8_1 and ZIF-8_2 particles showed WCAs of 47.9 ± 1.3° and 55.8 ± 1.5°, respectively. In fact, ZIF-8 is intrinsically a hydrophobic material. The hydrophilicity of ZIF-8 originates from the coordinatively unsaturated metal ions and the presence of −NH groups on the outer surface [43,44]. After the modification, WCAs increased to 132.5° ± 2.0° for ZIF-8_1-DMBIM and 141.7° ± 2.5° for ZIF-8_2-DMBIM. The increase in the WCA arose from the replacement of 2-methylimidazole with more hydrophobic dimethylbenzimidazole. A larger WCA for ZIF-8_2-DMBIM as compared to ZIF-8_1-DMBIM likely came from the nanostructure of the sample surface. The WCAs were also acquired for ZIF-8 membranes (Fig. 2.8). The observed WCAs were indeed very similar to those for the particles.

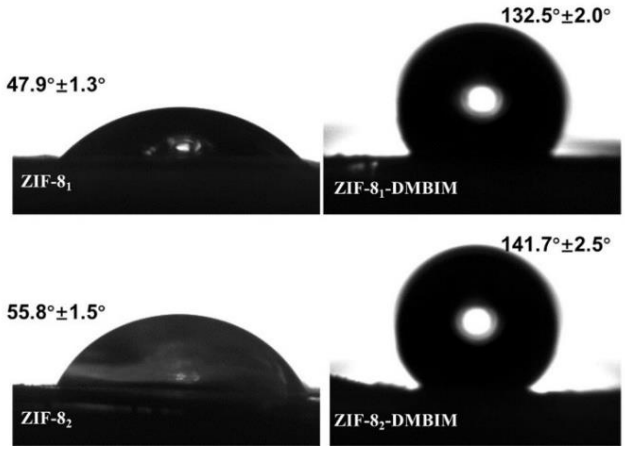

Fig. 2.7. Water contact angles of ZIF-8 particles: ZIF-8_1 (47.9° ± 1.3°, top left), ZIF-8_1-DMBIM (132.5° ± 2.0°, top right), ZIF-8_2 (55.8° ± 1.5°, bottom left) and ZIF-8_2-DMBIM (141.7° ± 2.5°, bottom right).

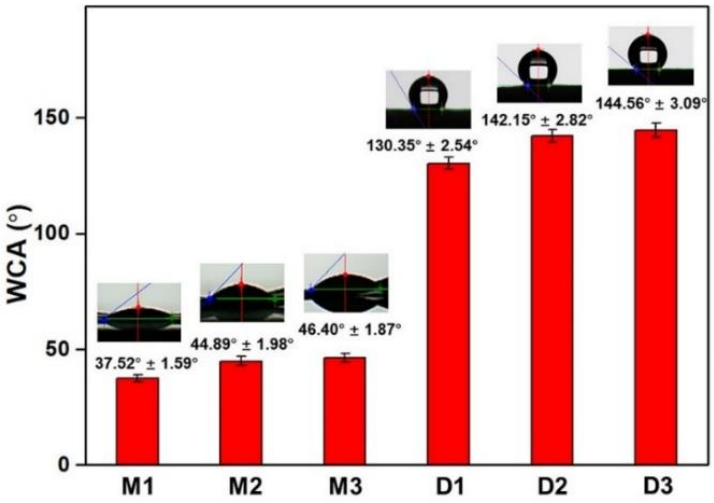

Fig. 2.8. Water contact angles of membranes.

2.3.3. Oil/water emulsion separation

Based on the hydrophilicity of the ZIF-8 particles and the hydrophobicity of the ZIF-8-DMBIM particles, ZIF-8 and ZIF-8-DMBIM membranes (M1 and D1) were first fabricated using the corresponding microparticles for separating oil-in-water and

water-in-oil emulsions, respectively. An oil/water emulsion separation experiment was performed to evaluate the separation performance using a dead-end filtration setup. For separating an oil-in-water emulsion, water is expected to pass through the ZIF-8 membrane, whereas the oil phase (toluene) remains on the membrane surface. The opposite is expected for water-in-oil emulsion separation using the ZIF-8-DMBIM membrane.

Fig. 2.9 shows the appearance of the feed and permeate after oil-in-water separation and water-in-oil separation at the differential pressure of 100 mbar. In both of the cases, the collected permeates (Fig. 2.9, right) were transparent as compared to the original milky white feed emulsions (Fig. 2.9, left). In optical microscope images, a numerous number of dispersed droplets were clearly seen in the feeds. The droplets were distributed mostly in the size range of 3–15 μm for both of the toluene-in-water and water-in-toluene emulsions (Fig.2.9). After separation, no droplets were observed in the collected permeates, indicating successful separation of emulsions based on the ZIF-8 and ZIF-8-DMBIM membranes.

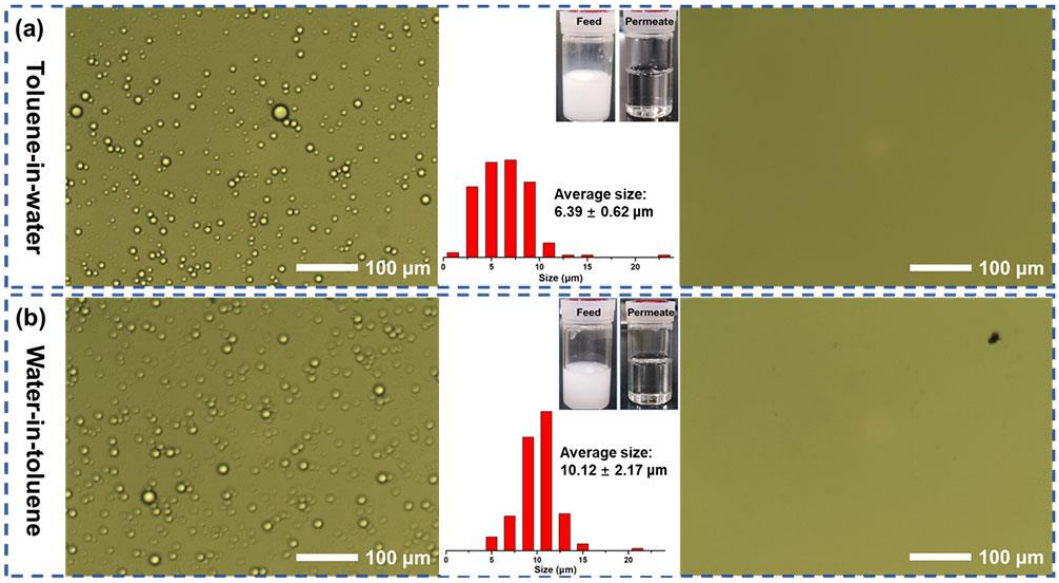

Fig. 2.9. Appearance of feeds (left) and permeates (right) in a) oil-in-water emulsion separation using a ZIF-8 membrane, and b) water-in-oil emulsion separation using a ZIF-8-DMBIM membrane. The membranes were prepared by depositing 5.0 mg of the corresponding microparticles (ZIF-8_1 and ZIF-8_1-DMBIM) on a RC membrane. The size distributions of the droplets in the feeds are also shown.

On the other hand, the ZIF-8 membranes failed to separate the water-in-oil emulsion, and a similarly poor performance was observed for the ZIF-8-DMBIM membranes in oil-in-water emulsion separation (Fig. 2.10). Such a selective separation is explained by solid surface wettability. For the hydrophilic ZIF-8 membrane, oil-in-water emulsion droplets was demulsified once touching the membrane [45]. Due to the hydrophilicity of ZIF-8 membrane, the water phase can spread out on the membrane surface before penetrating through the membrane pores. The formation of the water layer also helps to prevent oil droplets from approaching the membrane surface [46]. The mechanism of water-in-oil emulsion separation is similar [47]. With the

hydrophobic modification, the WCA became significantly larger, thus switching the affinity of the selective layer from water to the oil phase. With the hydrophobic modification, the WCA became significantly larger, thus switching the affinity of the selective layer from water to the oil phase.

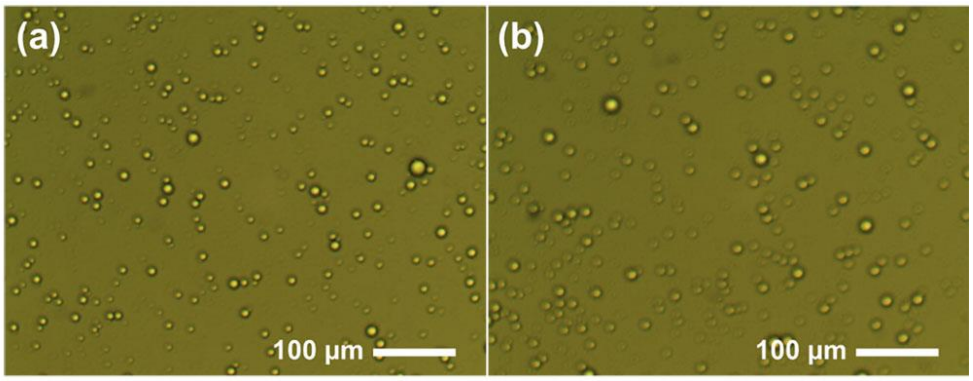

Fig. 2.10. Optical microscope images of permeates: a) after water-in-toluene emulsion separation using a ZIF-8 membrane, and b) after toluene-in-water emulsion separation using a ZIF-8-DMBIM membrane.

In order to maximize the separation performance in terms of the balance between the flux and the rejection, the influences of the particle size and its distribution were investigated on the selective layer formation. For this, ZIF-8 membranes with the weight ratio of ZIF-8_1:ZIF-8_2 = 100:0 (M1), 40:60 (M2), and 0:100 (M3) were prepared for oil-in-water separation. In the same way, ZIF-8-DMBIM membranes with the weight ratio of ZIF-8_1-DMBIM:ZIF-8_2-DMBIM = 100:0 (D1), 40:60 (D2), and 0:100 (D3) were prepared for water-in-oil separation. SEM images in Fig. 2.11 show that the particle size of ZIF-8 greatly affected the packing and roughness of the selective layer. The RC membrane showed a highly porous structure (Fig. 2.11a,e), which became

invisible after the particle deposition. For M1 and D1 (prepared from the microparticles), micron-sized channels arising from interparticle voids can be clearly observed (Fig. 2.11b,f). These voids were greatly reduced when the nanoparticles were deposited (M3 and D3 in Fig. 2.11d,h). However, the membranes prepared from a single type of particles possessed corrugated surfaces, reflecting the rough surface of the support membrane. When micro- and nanoparticles were sequentially deposited, (M2 and D2), the membrane surfaces became significantly smoother (Fig. 2.11c,g). It is plausible that microparticles firstly filled the porous structure of the RC membrane, and nanoparticles subsequently filled interparticle voids among the microparticles to create a denser and smoother layer on the topmost surface of the membrane. The formation of the selective layer by the deposition of micro- and nanoparticles is illustrated in Fig. 2.11i.

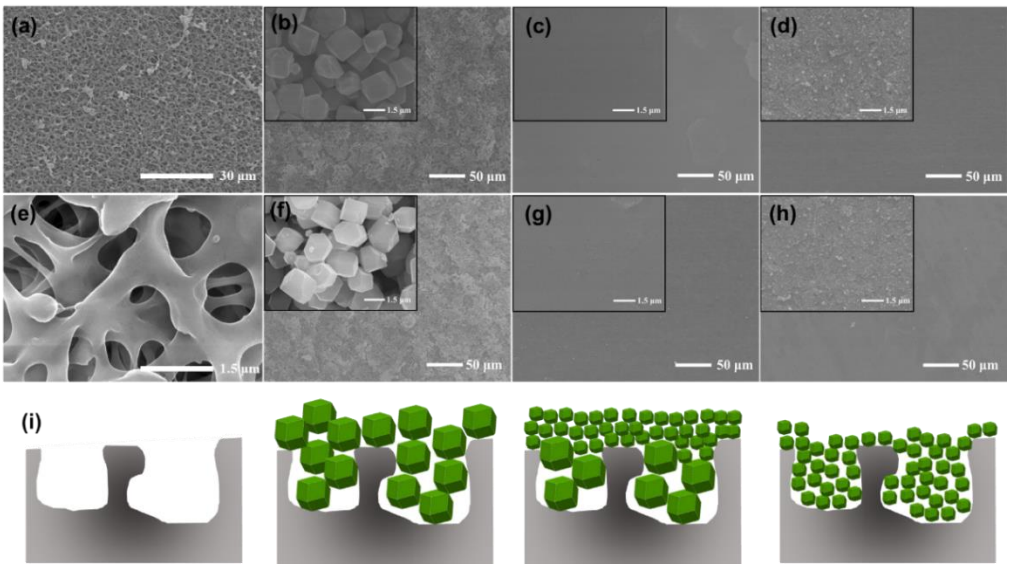

Fig. 2.11. Top view SEM images: a,e) RC support membrane, b,c,d) ZIF-8 membranes (M1, M2, and M3, respectively), and f,g,h) ZIF-8-DMIBM membranes (D1, D2, and

D3, respectively). Illustrations in i) show the formation of the selective layer by deposition of micro- and nanoparticles onto the support membrane.

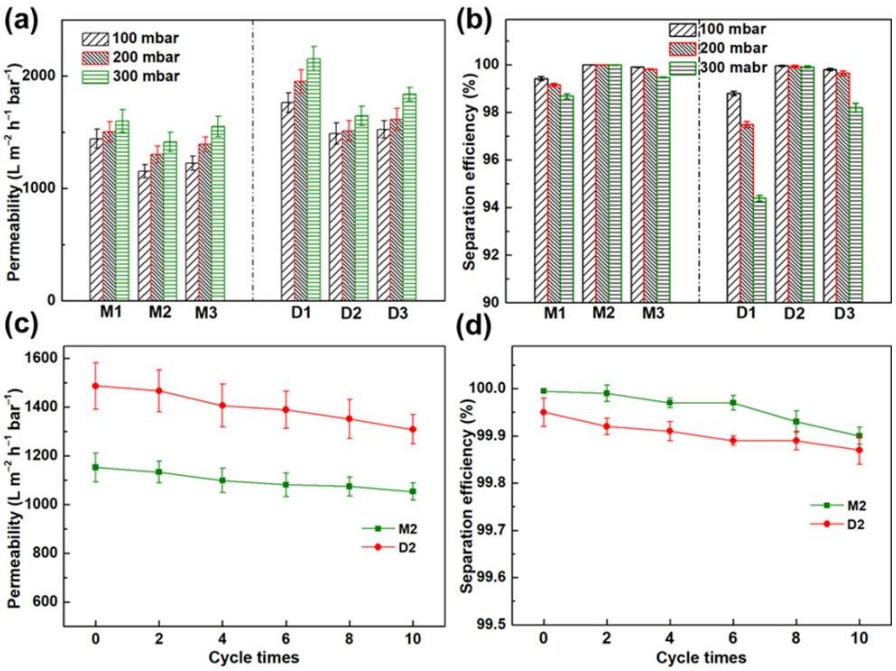

Fig. 2.12. Separation performance of ZIF-8 membranes for oil-in-water separation and that of ZIF-8-DMBIM membranes for water-in-oil separation: a,b) permeability and separation efficiency. c,d) represent the results of recyclability tests for M2 and D2 membranes at the pressure of 100 mbar.

Fig. 2.12a,b display the separation performance of the ZIF-8 membranes for oil-in-water separation, and that of the ZIF-8-DMBIM membranes for water-in-oil separation under the differential pressure of 100, 200 and 300 mbar. Irrespective of the pressure, the permeation flux followed the order of M1 > M3 > M2 and D1 > D3 > D2, while the separation efficiency followed the order of M2 > M3 > M1 and D2 > D3 > D1. Clearly, the use of microparticles is advantageous over nanoparticles in terms of

the permeation flux, but this compensates the separation efficiency due to the presence of larger interparticle voids. The flux values increased along with the differential pressure for all the membranes. However, the response of the separation efficiency on the differential pressure was found to be different according to the construction of the selective layers. When one type of particles was used, the separation efficiency monotonously dropped along with the pressure. Such the decrement became more evident for the microparticles (M1 and D1). As the transmembrane pressure increases, droplets approach the membrane surface. The critical pressure to force the droplets penetrate into the membrane pores is dependent on the sizes of the droplets and pores. Hence, the decrease in the separation efficiency at a higher pressure is linked with the dimension of interparticle voids. Contrary to the above case, the separation efficiency was not decreased along with the pressure when micro- and nanoparticles were sequentially deposited (M2 and D2). The separation efficiency was 99.99% for M2, and 99.91% for D2. Such the pressure-invariant separation efficiency suggested that the selective layer in these membranes could be regarded as continuous within the applied transmembrane pressure. The separation performance with a good balance between flux and separation efficiency is highly desirable for oil/water emulsion separation. Evidently, the sequential deposition of microparticles followed by nanoparticles improved the packing of the selective layer, so as to allow the operation at a higher pressure for high permeate flux without sacrificing the separation efficiency. The recyclability of the M2 and D2 membranes was also examined (Fig. 2.12c,d). After ten cycles of repetitive filtration, the separation efficiency retained above 99.9% for M2

and above 99.8% for D2.

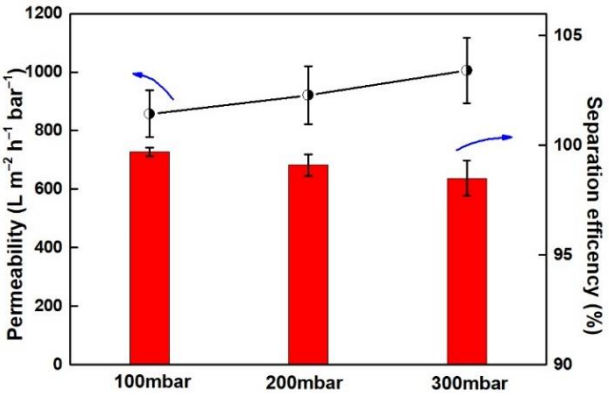

Fig. 2.13. Separation performance of a TiO_2-deposited membrane in toluene-in-water emulsion separation.

In the ZIF-8-deposited membrane system, there are two types of channels for mass transportation: structural porosity of the ZIF-8 framework and interparticle voids. In order to clarify the main transportation pathway, poreless TiO_2 nanoparticles were deposited on the RC membrane using the same procedure. The TiO_2 membrane differs from the ZIF-8 membranes in a sense that only interparticle voids are available for mass transportation. Due to the hydrophilic properties of TiO_2, the performance of the TiO_2 membrane was evaluated in oil-in-water separation. At 300 mbar, the permeability of 1005 ± 112 L m^{-2} h^{-1} bar^{-1} with the separation efficiency of 98.5 ± 0.8% were obtained (Fig. 2.13). Significantly higher permeability for the ZIF-8 membranes as compared to that of the TiO_2 membrane suggested that both of the structural porosity and interparticle voids are involved in mass transportation. Table 2.2 summarizes the oil/water emulsion separation performance for different types of ZIF-8 membranes reported in literature. It is clear that the deposition-type membranes are superior in

terms of the balance between the permeability and separation efficiency (i.e. the productivity) for both of oil-in-water and water-in-oil separation.

Table 2.2. Comparison of oil/water emulsion separation performance.

Membrane	Fabrication method	Droplet size	Permeability ($L\ m^{-2}\ h^{-1}\ bar^{-1}$)	Separation efficiency (%)	Ref.
ZIF-8	Deposition	3–15 μm	1411.8	> 99.99	This work
ZIF-8-DMBIM	Deposition	3–15 μm	1643.1	99.95	This work
PVDF-g-ZIF-8	Seed method	0.5–1 μm	1.11	92.93%	[31]
Co-PDMS@ZIF-8 -coated MWCNT	Seed method	n.d.	170	99.97	[44]
RC@PDA/ZIF-8	In-situ growth method	10 μm	446.4	99%	[32]
$Cu(OH)_2$@ZIF-8	In-situ growth method	2–10 μm	90000	97.2%	[34]
Cotton/ZIF-8 @PDMS	In-situ growth method	0.2–0.8 μm	n.d.	95%	[48]

2.4. Conclusions

In **Chapter 2**, ZIF-8 micro- and nanoparticles were synthesized and used to prepare composite membranes for oil/water emulsion separation. Hydrophobic modification of ZIF-8 via a solvent-assisted ligand exchange reaction between 2-methylimidazole and dimethylbenzimidazole switched the surface properties of the original particles from hydrophilic to be hydrophobic. By depositing hydrophilic ZIF-8 or hydrophobic ZIF-8-DMBIM particles onto a regenerated cellulose support, efficient and selective separation of oil-in-water or water-in-oil emulsions was achieved. The utilization of microparticles led to higher permeability as compared to nanoparticles. On the other hand, the presence of large interparticle voids exhibited a detriment in the rejection efficiency, especially at a higher transmembrane pressure. Such the detriment could be

overcome by a sequential deposition of microparticles followed by nanoparticles: the nanoparticles filled the interparticle voids among the microparticles to create a dense and smooth layer. The membranes exhibited excellent permeability of 1411.8–1643.1 L m^{-2} h^{-1} bar^{-1} with more than 99.9% separation efficiency in both of oil-in-water and water-in-oil emulsion separation. In general, membranes with good productivity and recyclability were achieved for both separation of oil-in-water and water-in-oil emulsions in this chapter. A facile, scalable sequential deposition method was performed to quickly optimize the selective layer, which resulting an optimum balance between flux and separation efficiency.

2.5. References

[1] L. Guterman, Exxon Valdez turns 20, Science 323 (2009) 1558–1559.

[2] M.A. Shannon, P.W. Bohn, M. Elimelech, J.G. Georgiadis, B.J. Mariñas, A.M. Mayes, Science and technology for water purification in the coming decades, Nature 452 (2008) 301−310.

[3] K. Li, J. Ju, Z. Xue, J. Ma, L. Feng, S. Gao, L. Jiang, Structured cone arrays for continuous and effective collection of micron-sized oil droplets from water, Nat. Commun. 4 (2013) 1–7.

[4] M. Cheryan, N. Rajagopalan, Membrane processing of oily streams. Wastewater treatment and waste reduction, J. Membr. Sci. 151 (1998) 13–28.

[5] G. Kwon, A.K. Kota, Y. Li, A. Sohani, J.M. Mabry, A. Tuteja, On-demand separation of oil-water mixtures, Adv. Mater. 24 (2012) 3666–3671.

[6] J.C. Prados, G. Gutiérrez, J.M. Benito, Economic sustainability and environmental protection in mediterranean countries through clean manufacturing methods, Springer, 2013.

[7] H. Saboorian-Jooybari, M. Dejam, Z. Chen, Heavy oil polymer flooding from laboratory core floods to pilot tests and field applications: half-century studies, J. Pet. Sci. Eng. 142 (2016) 85–100.

[8] B.K. Körbahti, K. Artut, Electrochemical oil/water demulsification and purification of bilge water using Pt/Ir electrodes, Desalination 258 (2010) 219–228.

[9] A. Knebel, B. Geppert, K. Volgmann, D.I. Kolokolov, A.G. Stepanov, J.

Twiefel, P. Heitjans, D. Volkmer, J. Caro, Defibrillation of soft porous metal-organic frameworks with electric fields, Science 358 (2017) 347–351.

[10] L. Chen, G. Shi, J. Shen, B. Peng, B. Zhang, Y. Wang, Y. Wang, F. Bian, J. Wang, D. Li, Z. Qian, G. Xu, G. Liu, J. Zeng, L. Zhang, Y. Yang, G. Zhou, M. Wu, W. Jin, J. Li, H. Fang, Ion sieving in graphene oxide membranes via cationic control of interlayer spacing, Nature 550 (2017) 380–383.

[11] W.J. Koros, C. Zhang, Materials for next-generation molecularly selective synthetic membranes, Nat. Mater. 16 (2017) 289–297.

[12] D.X. Trinh, T.P.N. Tran, T. Taniike, Fabrication of new composite membrane filled with UiO-66 nanoparticles and its application to nanofiltration, Sep. Purif. Technol. 177 (2017) 249–256.

[13] G.Y. Shangkum, P. Chammingkwan, D.X. Trinh, T. Taniike, Design of a semi-continuous selective layer based on deposition of UiO-66 nanoparticles for nanofiltration, Membranes 8 (2018) 129.

[14] Y. Yu, H. Chen, Y. Liu, S.J.C. Vincent, Z. Lai, Selective separation of oil and water with mesh membranes by capillarity, Adv. Colloid Interface Sci. 235 (2016) 46–55.

[15] L. Feng, Z. Zhang, Z. Mai, Y. Ma, B. Liu, L. Jiang, D. Zhu, A super-hydrophobic and super-oleophilic coating mesh film for the separation of oil and water, Angew. Chem., Int. Ed. Engl. 116 (2004) 2046–2048.

[16] Z. Xue, S. Wang, L. Lin, L. Chen, M. Liu, L. Feng, L. Jiang, A novel superhydrophilic and underwater superoleophobic hydrogel-coated mesh for

oil/water separation, Adv. Mater. 23 (2011) 4270–4273.

[17] Q. Ma, H. Cheng, A.G. Fane, R. Wang, H. Zhang, Recent development of advanced materials with special wettability for selective oil/water separation, Small 12 (2016) 2186–2202.

[18] J. Chen, H. You, L. Xu, T. Li, X. Jiang, C. Li, Facile synthesis of a two-tier hierarchical structured superhydrophobic-superoleophilic melamine sponge for rapid and efficient oil/water separation, J. Colloid Interface Sci. 506 (2017) 659–668.

[19] A. Gao, F. Liu, Z. Xiong, Q. Yang, Tunable adhesion of superoleophilic/superhydrophobic poly (lactic acid) membrane for controlled-release of oil soluble drugs, J. Colloid Interface Sci. 505 (2017) 49–58.

[20] J. Lin, F. Lin, R. Liu, P. Li, S. Fang, W. Ye, S. Zhao, Scalable fabrication of robust superhydrophobic membranes by one-step spray-coating for gravitational water-in-oil emulsion separation, Sep. Purif. Technol. 231 (2020) 115898.

[21] F. Zhang, W. Zhang, Z. Shi, D. Wang, J. Jin, L. Jiang, Nanowire-haired inorganic membranes with superhydrophilicity and underwater ultralow adhesive superoleophobicity for high-efficiency oil/water separation, Adv. Mater. 25 (2013) 4192–4198.

[22] X. Zheng, Z. Guo, D. Tian, X. Zhang, W. Li, L. Jiang, Underwater self-cleaning scaly fabric membrane for oily water separation, ACS Appl. Mater. Interfaces 7 (2015) 4336–4343.

[23] H. You, Y. Jin, J. Chen, C. Li, Direct coating of a DKGM hydrogel on glass fabric for multifunctional oil-water separation in harsh environments, Chem. Eng. J. 334 (2018) 2273–2282.

[24] Q. Wen, J. Di, L. Jiang, J. Yu, R. Xu, Zeolite-coated mesh film for efficient oil-water separation, Chem. Sci. 4 (2013) 591–595.

[25] X. Li, Y. Liu, J. Wang, J. Gascon, J, Li, B. Van der Bruggen, Metal-organic frameworks-based membranes for liquid separation, Chem. Soc. Rev. 46 (2017) 7124–7144.

[26] S. Qiu, M. Xue, G. Zhu, Metal-organic framework membranes: From synthesis to separation application, Chem. Soc. Rev. 43 (2014) 6116–6140.

[27] P. Chammingkwan, G.Y. Shangkum, L.T.T. Mai, P. Mohan, A. Thakur, T. Wada, T. Taniike, Modulator-free approach towards missing-cluster defect formation in Zr-based UiO-66, RSC Adv. 10 (2020) 28180–28185.

[28] Y. Pan, D. Heryadi, F. Zhou, L. Zhao, G. Lestari, H. Su, Z. Lai, Tuning the crystal morphology and size of zeolitic imidazolate framework-8 in aqueous solution by surfactants, CrystEngComm 13 (2011) 6937–6940.

[29] W. Zhang, Y. Hu, J. Ge, H. Jiang, S. Yu, A facile and general coating approach to moisture/water-resistant metal-organic frameworks with intact porosity, J. Am. Chem. Soc. 136 (2014) 16978–16981.

[30] Q. Ma, G. Li, X. Liu, Z. Wang, Z. Song, H. Wang, Zeolitic imidazolate framework-8 film coated stainless steel meshes for highly efficient oil/water separation, Chem. Commun. 54 (2018) 5530–5533.

[31] S. Xu, L. Ren, Q. Zhou, H. Bai, J. Li, J. Shao, Facile ZIF-8 functionalized hierarchical micronanofiber membrane for high-efficiency separation of water-in-oil emulsions, J. Appl. Polym. Sci. 135 (2018) 46462.

[32] A. Xie, J. Cui, J. Yang, Y. Chen, J. Lang, C. Li, Y. Yan, J. Dai, Dual superlyophobic zeolitic imidazolate framework-8 modified membrane for controllable oil/water emulsion separation, Sep. Purif. Technol. 236 (2020) 116273.

[33] M. Song, Y. Zhao, S. Mu, C. Jiang, Z. Li, P. Yang, Q. Fang, M. Xue, S. Qiu, A stable ZIF-8-coated mesh membrane with micro-/nano architectures produced by a facile fabrication method for high-efficiency oil-water separation, Sci. China Mater. 62 (2019) 536–544.

[34] Q. Li, W. Deng, C. Li, Q. Sun, F. Huang, Y. Zhao, S. Li, High-flux oil/water separation with interfacial capillary effect in switchable superwetting $Cu(OH)_2$@ZIF-8 nanowire membranes, ACS Appl. Mater. Interfaces 10 (2018) 40265–40273.

[35] J. Cravillon, S. Münzer, S.J. Lohmeier, A. Feldhoff, K. Huber, M. Wiebcke, Rapid room-temperature synthesis and characterization of nanocrystals of a prototypical zeolitic imidazolate framework, Chem. Mater. 21 (2009) 1410–1412.

[36] X. Liu, Y. Li, Y. Ban, Y. Peng, H. Jin, H. Bux, L. Xu, J. Caro, W. Yang, Improvement of hydrothermal stability of zeolitic imidazolate frameworks, Chem. Commun. 49 (2013) 9140–9142.

[37] S. Li, Z. Chen, Y. Yang, Z. Si, P. Li, P. Qin, T. Tan, Improving the pervaporation performance of PDMS membranes for *n*-butanol by incorporating silane-modified ZIF-8 particles, Sep. Purif. Technol. 215 (2019) 163–172.

[38] Z. Li, W. Sun, C. Chen, Q. Guo, X. Li, M. Gu, N. Feng, J. Ding, H. Wan, G. Guan, Deep eutectic solvents appended to UiO-66 type metal organic frameworks: preserved open metal sites and extra adsorption sites for CO_2 capture, Appl. Surf. Sci. 480 (2019) 770–778.

[39] K.S.W. Sing, The use of gas adsorption for the characterization of porous solids, Colloids and Surf. 38 (1989) 113–124.

[40] F. Jiao, P.G. Bruce, Two-and Three-Dimensional Mesoporous Iron Oxides with Microporous Walls, Angew. Chem., Int. Ed. Engl. 116 (2004) 6084–6087.

[41] H. Zhang, J. James, M. Zhao, Y. Yao, Y. Zhang, B. Zhang, Y.S. Lin, Improving hydrostability of ZIF-8 membranes via surface ligand exchange, J. Membr. Sci. 532 (2017) 1–8.

[42] K. Jayaramulu, F. Geyer, A. Schneemann, Š. Kment, M. Otyepka, R. Zboril, D. Vollmer, R.A. Fischer, Hydrophobic Metal-Organic Frameworks, Adv. Mater. 31 (2019) 1900820.

[43] K. Zhang, R.P. Lively, C. Zhang, R.R. Chance, W.J. Koros, D.S. Sholl, S. Nair, Exploring the framework hydrophobicity and flexibility of ZIF-8: From biofuel recovery to hydrocarbon separations, J. Phys. Chem. Lett. 4 (2013) 3618–3622.

[44] Y. Yang, Z. Guo, W. Huang, S. Zhang, J. Huang, H. Yang, Y. Zhou, W. Xu, S. Gu, Fabrication of multifunctional textiles with durable antibacterial property and efficient oil-water separation via in situ growth of zeolitic imidazolate framework-8 (ZIF-8) on cotton fabric, Appl. Surf. Sci. 503 (2020) 144079.

[45] L.Y. A. Lin, Y.C. Chen, S. Phattarapattamawong, Efficient demulsification of oil-in-water emulsions using a zeolitic imidazolate framework: adsorptive removal of oil droplets from water, J. Colloid Interface Sci. 478 (2016) 97–106.

[46] H. Li, Y. Yin, L. Zhu, Y. Xiong, X. Li, T. Guo, W. Xing, Q. Xue, A hierarchical structured steel mesh decorated with metal organic framework/graphene oxide for high-efficient oil/water separation, J. Hazard. Mater. 373 (2019) 725–732.

[47] W. Zhang, Z. Shi, F. Zhang, X. Liu, J. Jin, L. Jiang, Superhydrophobic and superoleophilic PVDF membranes for effective separation of water-in-oil emulsions with high flux, Adv. Mater. 25 (2013) 2071–2076.

[48] H. Ye, D. Chen, N. Li, Q. Xu, H. Li, J. He, J. Lu, Durable and robust self-healing superhydrophobic Co-PDMS@ZIF-8-Coated MWCNT films for extremely efficient emulsion separation, ACS Appl. Mater. Interfaces 11 (2019) 38313–38320.

Chapter 3

Advantages of polydopamine coating in the design of ZIF-8-filled thin-film nanocomposite (TFN) membranes for desalination

Abstract

In this chapter, zeolitic imidazolate framework-8 (ZIF-8) nanoparticles coated with polydopamine (PDA) were synthesized and used to prepare thin-film nanocomposite (TFN) membranes for desalination. Structures, properties, and desalination performances of the membranes were systematically compared with those of membranes containing unmodified ZIF-8 nanoparticles or not containing ZIF-8, revealing the significance of the PDA coating on the overall performance of the TFN membranes. The PDA coating provided ZIF-8 nanoparticles with dispersibility in water and resistance to hydrochloric acid as a by-product of interfacial polymerization, which allowed them to be uniformly dispersed in the selective layer without agglomeration and deterioration of the crystalline structure. These are very important for the improvement of the permeability and stability of TFN membranes while maintaining the selectivity. In addition, the PDA coating inhibited the direct contact of ZIF-8 with an organic foulant, which dramatically enhanced the fouling resistance of the membranes.

3.1. Introduction

A global water shortage caused by rapid population growth and industrial development in the last decade has motivated the development of more efficient water treatment processes, especially for saline water, which occupies more than 97% of the water on Earth. Compared to other conventional technologies, such as evaporation and distillation, membrane-based technologies offer more efficient as well as more eco-friendly alternatives to water desalination and purification [1,2]. In particular, reverse osmosis filtration and nanofiltration account for the main desalination capacity, where thin-film composite (TFC) membranes are the most widely used membranes. In general, TFC membranes are prepared by forming an ultrathin barrier layer, which is also called a selective layer and typically made of a polymer, on a microporous support membrane. Since the first TFC membrane in the 1960s, a great deal of effort has been devoted to finding an optimum combination of a molecular structure and a synthetic process for the selective layer [3]. Currently, the *de facto* standard for TFC membranes is the crosslinked fully aromatic polyamide (PA) TFC membrane prepared by interfacial polymerization of *m*-phenylenediamine (MPD) and trimesoyl chloride (TMC) [4], which affords a highly crosslinked, uniform, and crumpled selective layer advantageous for selective permeation and mechanical strength [5]. The increasing fresh water shortage demands further improvements in the membrane performance, whereby enhancing the membrane permeability by overcoming a tradeoff with selectivity is the most important challenge [6].

One promising strategy is the incorporation of nanomaterials into the selective

layer, and such membranes are collectively called thin-film nanocomposite (TFN) membranes [7–11]. Hoek and his coworkers [12] were the first to propose the concept of TFN membranes. They found that the incorporation of NaA zeolite nanoparticles into a selective layer of crosslinked aromatic PA evidently increased the permeability of the membrane without deteriorating the salt retention. After that, a variety of nanomaterials have been added with the aim of improving the permeability, primarily based on creating additional pathways, and secondarily based on improved hydrophilicity and/or optimized membrane structures [13–16]. The additional pathways must be size-selective: the addition of nanoporous materials with well-defined channels is preferred over only controlling the morphology of interfacial voids between the polymer and non-porous nanomaterials. Therefore, the first step towards high performing TFN membranes is to select nanomaterials that are stable under water and possess channels of an appropriate size for rejecting hydrated salt ions (e.g., Na^+ 0.72 nm, K^+ 0.66 nm, Mg^{2+} 0.86 nm, Cl^- 0.66 nm, SO_4^{2-} 1.00 nm in diameter) [17]. The dispersion of the nanomaterials and their interfacial connection with the polymer are also important issues as agglomeration and loose interfaces lead to the formation of non-selective voids [18].

Metal-organic frameworks (MOFs) represent a relatively new class of inorganic-organic hybrid porous materials consisting of metal clusters and organic ligands [19]. Compared to zeolites, MOFs have higher design flexibility due to the presence of organic ligands. This is a very important feature in terms of optimizing the chemical environment of channels as well as the dispersibility and compatibility of the inclusions.

Compared to covalent organic frameworks, MOFs tend to be more stable in water and more hydrophilic, i.e., more water-permeable, due to the metal clusters. Owing to these advantages, various TFN membranes with MOFs as nano-sized inclusions in the selective layer have been reported [20–23]. For example, Park et al. reported a polysulfone-supported TFN membrane prepared by the incorporation of HKUST-1 nanoparticles for desalination [22]. The permeability of the TFN membrane increased with the amount of HKUST nanoparticles (up to a certain incorporation amount). Kadhom et al. prepared TFN membranes using nanoparticles of UiO-66 and MIL-125 [23]. The incorporation of 0.15% w/v of UiO-66 and 0.3% w/v of MIL-125 led to an improvement in the water permeability by ca. 20% or 36%, respectively. Ideally, MOFs should provide additional size-selective channels for the selective layer to improve the permeability without deteriorating the selectivity. However, in reality, the ideal behavior is hardly achieved due to the void formation caused by the agglomeration of nanoparticles and/or interface failure, which sets the upper limit of the MOF loading in the selective layer, i.e., upper limit of the performance improvement.

Polydopamine (PDA) coating is one of the most versatile approaches in the last decade for surface functionalization and compatibilization [24]. As a bioinspired synthetic polymer, PDA can be easily obtained by self-assembly and oxidative polymerization of dopamine under slightly basic conditions (pH~8.5). Analogous to mussel adhesive proteins, PDA can form a biocompatible coating by strongly adhering to many kinds of materials. Moreover, the abundance of amino and catechol groups allows PDA to react and/or strongly interact with other polymers, making it an effective

compatibilizer [25,26]. Recently, PDA has been used to improve the compatibility of ZIF-8 in a mixed matrix membrane for gas separation [27], where the interfacial bonding between ZIF-8 nanoparticles and a polyimide matrix was significantly improved by the PDA coating. The resultant membrane indeed exhibited excellent performance in separating H_2/CH_4 and H_2/N_2. Importantly, the PDA coating did not cause pore blockage, which would hinder the solute diffusion to the pore entrance [28]. With these advantages, PDA coating of MOFs is considered to be promising for the development of TFN membranes for desalination.

In this chapter, I investigated the effect of PDA coating on the desalination performance of zeolitic imidazolate framework-8 (ZIF-8)-based TFN membranes. ZIF-8 is one of the most widely employed MOFs for desalination [29] due to its appropriate pore size and high stability in water. A molecular dynamics simulation showed fast water transport through ZIF-8 at high salt rejection [30]. PDA coating was applied to synthesize ZIF-8 nanoparticles. The obtained nanoparticles were incorporated into the selective layer made of crosslinked aromatic PA during interfacial polymerization. Unlike unmodified ZIF-8, the PDA-modified ZIF-8 nanoparticles increased the permeability more than twofold without significant loss of selectivity in the desalination of brackish water.

3.2. Experimental section

3.2.1. Materials

All reagents and solvents were commercially available and used as received. Zinc nitrate hexahydrate ($Zn(NO_3)_2 \cdot 6H_2O$, > 98%), tris(hydroxymethyl)aminomethane (tris-

base, ≥ 99.9%), dopamine hydrochloride (≥ 99.5%), and humic acid (HA, a technical grade) were purchased from Sigma-Aldrich. 2-Methylimidazole (> 98%), trimesoyl chloride (TMC, > 98%), *m*-phenylenediamine (MPD, > 98%), and triethylamine (TEA, > 99%) were obtained from TCI Chemical Industry Co., Ltd. Sodium sulfate (Na_2SO_4, > 99%), sodium chloride (NaCl, > 99%), methanol, *n*-hexane, and hydrochloric acid (HCl, ACS reagent, 37%) were purchased from Wako Chemical Industries Ltd. A polyether sulfone (PES) membrane (dia. = 47 mm, pore size = 0.22 μm) was purchased from Merck Millipore Ltd. Deionized (DI) water was used throughout the experiments.

3.2.2. Synthesis and modification of ZIF-8 nanoparticles

ZIF-8 nanoparticles were synthesized according to a previously reported protocol [31]. Briefly, a solution of $Zn(NO_3)_2 \cdot 6H_2O$ (9.87 mmol in 200 mL of methanol) was mixed with a solution of 2-methylimidazole (79.04 mmol in 200 mL of methanol) under stirring at room temperature for 1 h. The resultant precipitate was collected by centrifugation, repetitively rinsed with methanol for 5 times, and dried at 40 °C under vacuum for 12 h.

The PDA coating was performed based on self-polymerization of dopamine [29], as illustrated in Scheme 3.1. 0.5 g of ZIF-8 nanoparticles was dispersed in 50 mL of methanol by sonication for 2 h. 50 mL of a 10 mM tris-HCl buffer solution (pH~8.5) and 50 mg of dopamine hydrochloride were added to the dispersion. The mixture was stirred at room temperature for 5 h. The product was collected by centrifugation, repetitively washed with methanol, and dried at 40 °C under vacuum for 12 h. Thereafter, the PDA-coated ZIF-8 sample is denoted as cZIF-8.

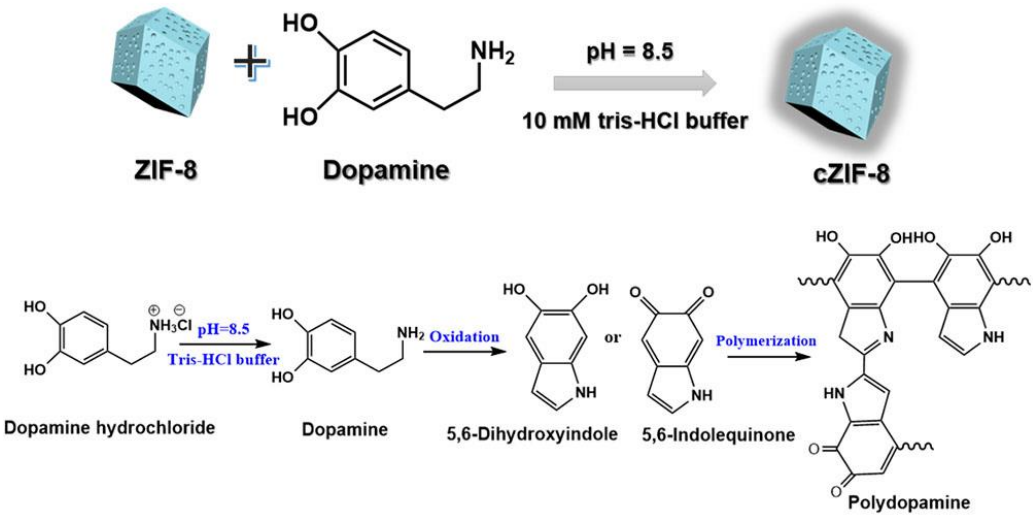

Scheme 3.1. PDA coating on ZIF-8 nanoparticles.

3.2.3. Membrane preparation

A TFC membrane was prepared by forming a selective layer of crosslinked aromatic PA on the PES substrate through interfacial polymerization. 2.0 mL of an aqueous solution containing 2.0% w/v MPD and 4.0% w/v TEA was gently dropped onto a PES membrane fixed on a holder, where TEA was used as an acid-binding agent to accelerate the interfacial polymerization process [9]. The membrane was completely immersed and superficially dried in a ventilated environment for about 20 min. Subsequently, a hexane solution of 0.15% w/v TMC was spread on the membrane. After 1 min, the excess solution was gently removed, and the membrane was kept in an oven at 60 °C for 10 min to carry out the post-polymerization. Finally, the membrane was rinsed thoroughly with hexane and stored in DI water until use. The prepared membrane is denoted as PA-TFC.

The preparation method of TFN membranes was the same as that of the TFC

membranes except that ZIF-8 nanoparticles were dispersed in the aqueous solution of MPD via ultrasonication. TFN membranes with different ZIF-8 loadings were prepared: those with 5, 10, 20, and 40 wt% of cZIF-8 and ZIF-8 nanoparticles, respectively. The weight fractions were calculated based on the weight of the PA selective layer. The prepared TFN membranes are denoted as PA/cZIF-8-TFN and PA/ZIF-8-TFN.

3.2.4. Characterization

Fourier transform infrared (FT-IR) spectra of ZIF-8 and cZIF-8 nanoparticles were acquired on a Perkin-Elmer Spectrum 100 FT-IR spectrometer with a resolution of 4 cm^{-1}. The nanoparticles were mixed with KBr and pressed into a disc for the measurement. X-ray diffraction (XRD) measurements were performed using a Rigaku SmartLab diffractometer at a scanning speed of 0.5° per min in the range of 5–45° using Cu Kα radiation. Thermo-gravimetric analysis (TGA, ThermoPlus EVO II, Rigaku) was used to determine the amount of PDA coating. A sample was heated from 30 °C to 900 °C at a heating rate of 10 °C/min under dry air flow. Nitrogen adsorption/desorption measurements at 77 K were performed on a BELSORP-mini II system (BEL JAPAN, Inc.). The specific surface area and pore volume were determined by the Brunauer-Emmet-Teller (BET) and Horvath-Kawazoe (HK) methods, respectively. The morphology of nanoparticles was observed by transmission electron microscopy (TEM, Hitachi H-7100) operated at an accelerated voltage of 100 kV. The particle size was determined from the analysis of TEM images using ImageJ software.

The formation of the selective layer was confirmed by attenuated total reflectance Fourier transform infrared spectroscopy (ATR-IR, Spectrum 100, Pekin Elmer). The

surface and cross-sectional morphologies of membranes were observed using scanning electron microscopy (SEM, Hitachi S-4100) operated at an accelerating voltage of 20 kV. The water contact angle (WCA) of membranes was analyzed using a contact angle goniometer (SImage AUTO 100, Excimer) at room temperature.

3.2.5. Membrane performance evaluation

The performance of the TFC and TFN membranes was evaluated using a dead-end filtration apparatus with an effective area of 7.1 cm^2 (as illustrated in Fig. 3.1). The membrane was appropriately cut and placed on the filtration holder. Before the filtration experiment, the membrane was pressurized at 4 bar for 1 h to stabilize the filtration system. Afterwards, pure water was introduced and the water fluxes under different pressures (1, 1.5, 2, 2.5, 3, and 3.5 bar) were measured. The water flux (J, L m^{-2} h^{-1}, abbreviated as LMH), was calculated according to Eq. (3.1):

$$J = \frac{V}{A \cdot \Delta t}, \tag{3.1}$$

where V (L) is the volume of the permeate, A (m^2) is the effective area of the membrane, and Δt (h) is the filtration time. The water permeability (P, LMH bar^{-1}) was calculated using Eq. (3.2):

$$P = \frac{J}{\Delta p}, \tag{3.2}$$

where Δp (bar) is the transmembrane pressure. The desalination performance of the membrane was evaluated at a differential pressure of 2 bar using aqueous solutions of NaCl and Na_2SO_4 at a concentration of 1000 ppm. The permeability was obtained according to Eq. (3.2). The rejection (%) was calculated according to Eq. (3.3):

$$\text{Rejection} = \left(1 - \frac{C_p}{C_0}\right) \times 100 \quad (3.3),$$

where C_p and C_0 are the concentrations of salts in the permeate and feed, respectively. The concentration of salts was analyzed using an electrical conductivity meter (FEP30, Mettler Toledo).

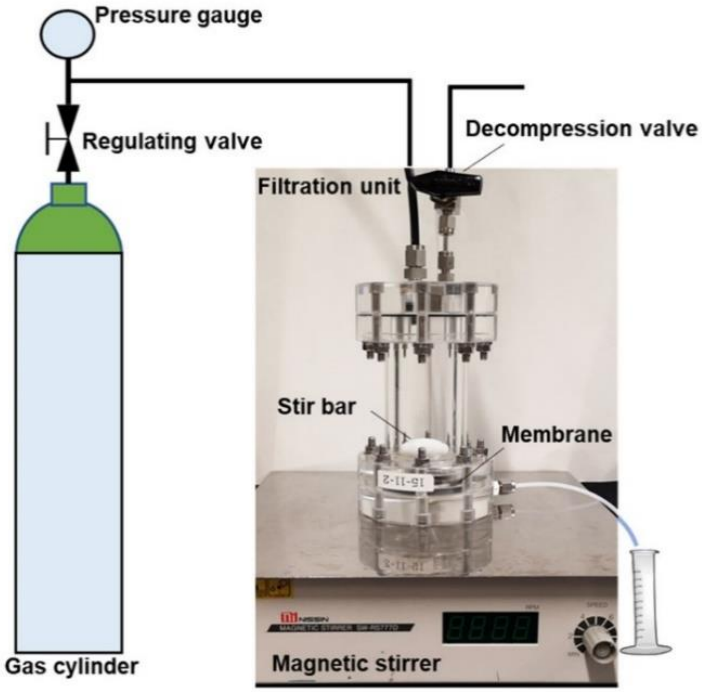

Fig. 3.1. Employed filtration setup.

Since HA is recognized as a major contaminant in the desalination process [32], an aqueous solution of HA (200 ppm) was employed to investigate the antifouling properties of the membranes. The experimental procedure is as follows. First, a membrane was pre-conditioned with DI water at a differential pressure of 2 bar for 30 min to obtain a stable water flux, J_0 (L m^{-2} h^{-1}). Then, the membrane was subjected to the filtration of the HA solution at a differential pressure of 2 bar for 30 min, followed by filtration of DI water at the same differential pressure for 30 min after rinsing with

water. The same cycle was repeated another two times, and the antifouling properties were evaluated through the total fouling ratio (F_r, %), the flux recovery ratio (F_{rr}, %), the reversible fouling ratio (R_r, %), and the irreversible fouling ratio (R_{ir}, %), defined as follows:

$$F_r = \left(1 - \frac{J_1}{J_0}\right) \times 100, \quad (3.4),$$

$$F_{rr} = \left(\frac{J_R}{J_0}\right) \times 100, \quad (3.5),$$

$$R_r = \left(\frac{J_R - J_1}{J_0}\right) \times 100, \quad (3.6),$$

$$R_{ir} = \left(\frac{J_0 - J_R}{J_0}\right) \times 100, \quad (3.7),$$

where J_1 and J_R correspond to the water flux for the filtration of the HA solution and DI water during the final cycle, respectively.

3.3. Results and discussion

3.3.1. Characterization of ZIF-8 nanoparticles

ZIF-8 nanoparticles were synthesized by rapid coordination of Zn^{2+} and 2-methylimidazole at specified concentrations and temperature. The crystal structure of ZIF-8 is represented in Fig. 3.2. In Fig. 3.3a, the XRD patterns of the nanoparticles show characteristic peaks at 2θ = 7.3°, 10.4°, 12.7°, 14.7°, 16.5°, and 18.1°, which correspond to the (011), (002), (112), (022), (013), and (222) crystal faces of ZIF-8, respectively [33,34]. From the TEM image, the ZIF-8 nanoparticles possess a typical polyhedral shape with a diameter of 30–60 nm (Fig. 3.3b). The chemical structure of ZIF-8 was confirmed by FT-IR (Fig. 3.3c). The band at 421 cm^{-1} is the most important as it corresponds to the formation of Zn–N bonds [35]. The other bands mostly arise

from the presence of 2-methylimidazole: 3135 and 2929 cm^{-1} for the aromatic and aliphatic C–H stretching vibrations, 1580 cm^{-1} for the C=N stretching vibration, and 1460–600 cm^{-1} for the stretching and bending vibrations of the entire imidazole ring [36]. The successful synthesis of ZIF-8 nanoparticles was thus confirmed. Then, the ZIF-8 nanoparticles were subjected to PDA coating via self-polymerization of dopamine. The prepared sample, cZIF-8, showed an XRD pattern identical to that of ZIF-8 (Fig. 3.3a). The morphology of the nanoparticles did not change significantly before and after the coating (Fig. 3.3b). However, at an enlarged scale, the edges of the nanoparticles became rounder, and the nanoparticles were occasionally connected to each other by a neck-like structure. These changes were believed to correspond to the formation of the PDA layer. Consistent with the crystalline structure, the PDA coating did not alter the basic chemical structure of ZIF-8 (Fig. 3.3c). Meanwhile, the presence of PDA was confirmed by bands newly appearing in addition to those of ZIF-8: 3400–3500 cm^{-1} for the stretching vibration of catechol –OH [37], 1624 cm^{-1} for indole stretching, 1510 cm^{-1} for indoline stretching, and 1260 cm^{-1} for the phenolic C–O–H stretching [27]. TGA was conducted to estimate the amount of the PDA layer (Fig. 3.3d). The uncoated ZIF-8 exhibited a sharp weight loss at around 400 °C, which was ascribed to the decomposition of the organic ligand. In the case of cZIF-8, the weight loss started from a lower temperature due to the degradation of PDA [38]. The PDA amount was estimated to be around 14 wt% based on the difference in the weight loss between ZIF-8 and cZIF-8.

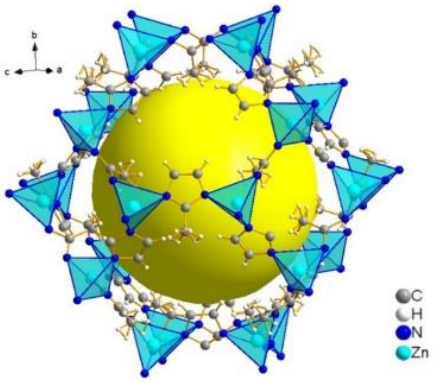

Fig. 3.2. Representation of ZIF-8 using Diamond software, where blue tetrahedra and the yellow sphere indicate ZnN4 and micropore, respectively. Crystal data from CCDC (The Cambridge Crystallographic Data Centre; CCDC-602542).

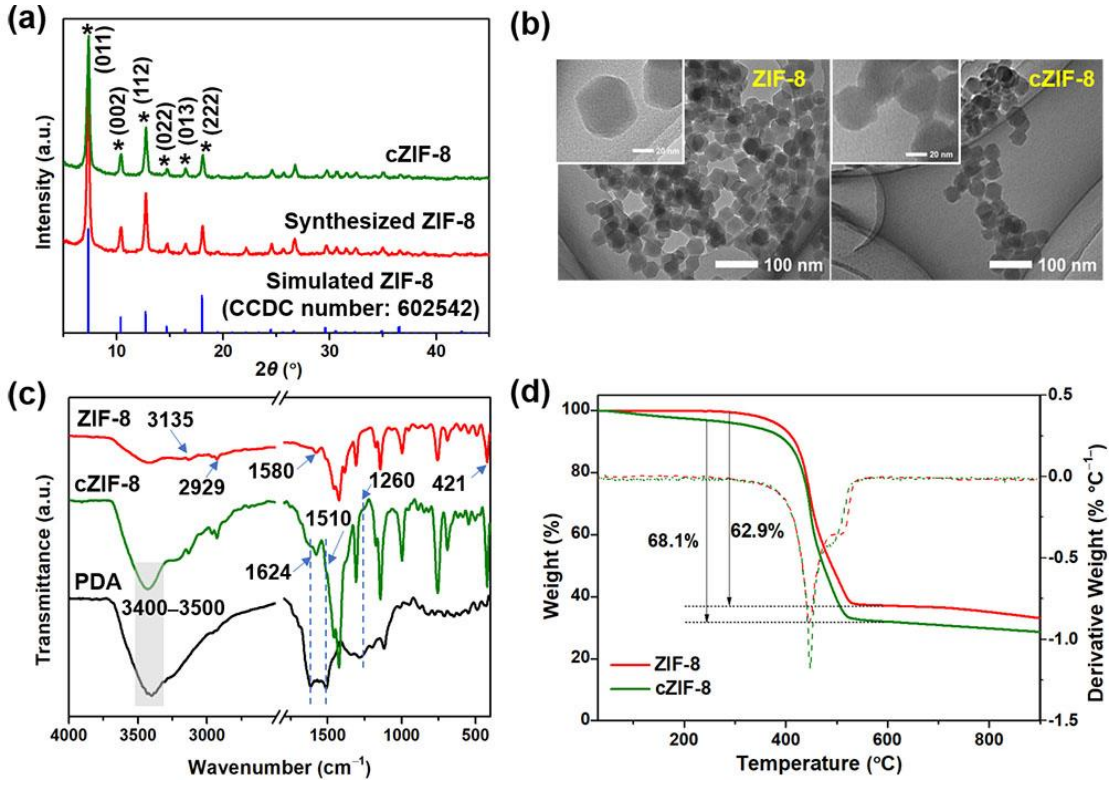

Fig. 3.3. Characterization of ZIF-8 and cZIF-8: a) XRD patterns, b) TEM images, c) FT-IR spectra, and d) TGA profiles. XRD pattern of simulated ZIF-8 taken from CCDC database (CCDC number:602542).

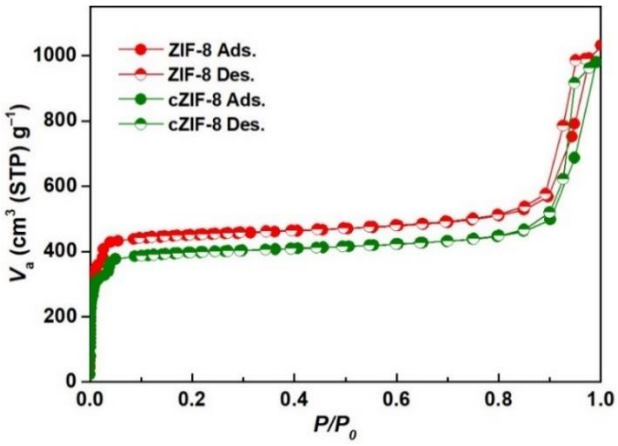

Fig. 3.4. Nitrogen adsorption/desorption isotherms of ZIF-8 and cZIF-8.

The nitrogen adsorption/desorption isotherms are shown in Fig. 3.4. The adsorption isotherms of ZIF-8 and cZIF-8 both showed features corresponding to micropores from the crystal structure of ZIF-8 and meso-to-macropores as interparticle voids of the nanoparticles. The specific surface area of ZIF-8 and cZIF-8 was respectively derived as 1800 and 1540 m^2 g^{-1}, while the micropore volume was 0.670 and 0.594 cm^3 g^{-1}. Subtracting the weight of the PDA, cZIF-8 showed no loss in the specific surface area and pore volume as compared to ZIF-8, which means that the PDA coating did not cause pore blockage.

The PDA coating hardly affected the crystal structure and the morphology of the ZIF-8 nanoparticles, while the location of the PDA on the nanoparticle surfaces significantly affected the surface properties. The WCA measurement was performed on a compressed disk of ZIF-8 and cZIF-8 nanoparticles. The WCA decreased from 50.2° for ZIF-8 to 0° for cZIF-8 (Fig. 3.5). In the preparation of a TFN membrane using interfacial polymerization, the dispersion of ZIF-8 nanoparticles in an aqueous phase

would be directly related to their dispersibility in the selective layer. Fig. 3.6 compares the dispersibility of ZIF-8 and cZIF-8 in water. Note that the PDA coating changed the color of the nanoparticles from white to black. Most of the ZIF-8 nanoparticles sedimented within 12 hours after the dispersion treatment, while the cZIF-8 nanoparticles were kept similarly dispersed. This fact indicated that the PDA coating was stable and effective in improving the dispersion.

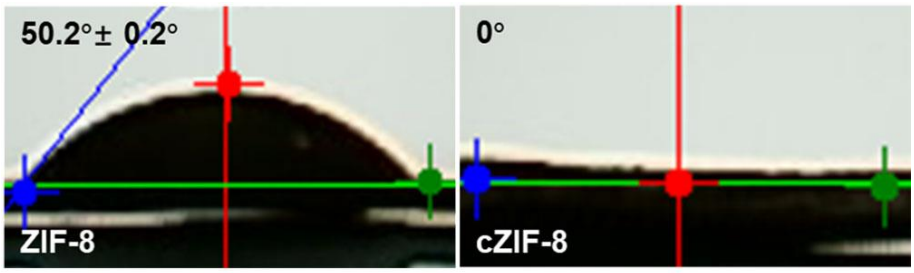

Fig. 3.5. WCAs of ZIF-8 and cZIF-8.

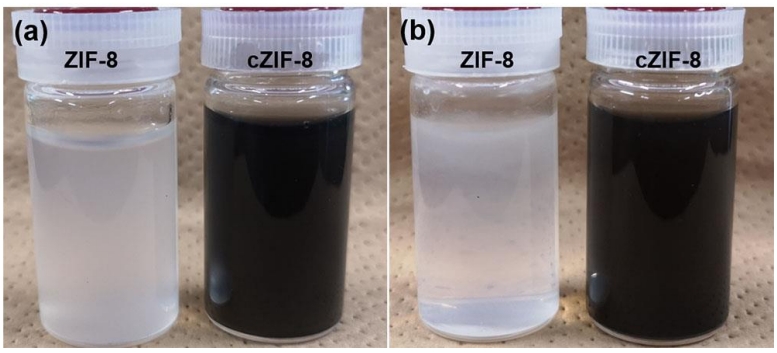

Fig 3.6. The appearance of the dispersion a) immediately after sonication and b) after 12 hours of standing.

3.3.2. Characterization of membranes

The TFC and TFN membranes were fabricated through interfacial polymerization of MPD and TMC to form the crosslinked aromatic PA selective layer

on the PES support. For the fabrication of TFN, ZIF-8 or cZIF-8 nanoparticles were added to the MPD solution to embed the nanoparticles into the selective layer. Fig. 3.7a presents the ATR-IR spectra of the PES substrate, PA-TFC, PA/ZIF-8-TFN (40 wt%), and PA/cZIF-8-TFN (40 wt%). As the penetration depth of IR for the employed diamond crystal (around 2 μm) is much greater than a typical thickness of the selective layer (around 100–200 nm), the IR spectra of the TFC and TFN membranes were dominated by the features of the PES substrate. However, the formation of the selective layer could be confirmed by the appearance of a band at 1663 cm^{-1} for the stretching vibration of C=O of the amide group [9,39]. Meanwhile, the characteristic peaks of ZIF-8 or cZIF-8 were not observed for the TFN membranes, plausibly due to an overlap with the intense peaks of the PES substrate.

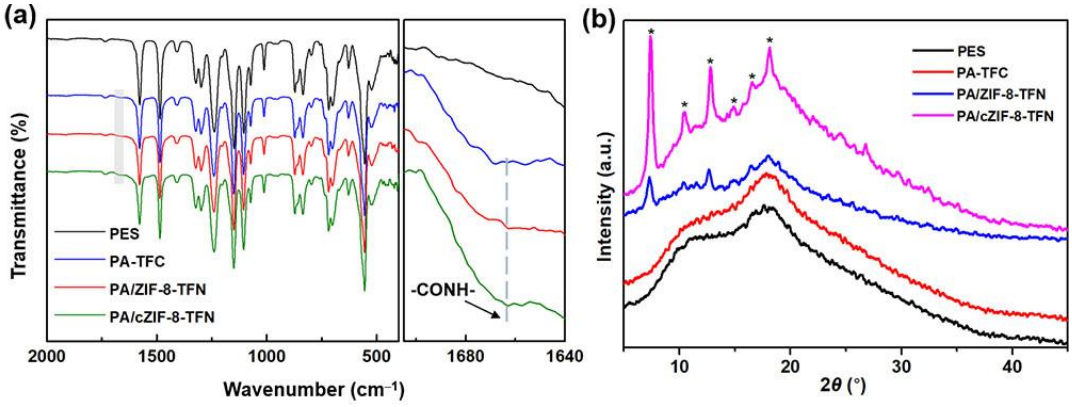

Fig. 3.7. a) ATR-IR spectra, and b) XRD patterns of the PES substrate, PA-TFC, PA/ZIF-8-TFN (40 wt%), and PA/cZIF-8-TFN (40 wt%).

The XRD patterns of the membranes are shown in Fig. 3.7b. To start, the PES substrate showed an amorphous halo typical for this material [40]. A similar pattern was observed for the TFC membrane, suggesting the non-orderliness of the PA layer. In the

PA/cZIF-8-TFN membrane, diffraction peaks consistent with the crystal structure of ZIF-8 nanoparticles were observed at 2θ = 7.3°, 10.4°, 12.7°, 14.7°, 16.5°, and 18.1°, indicating the retention of the crystal structure during the interfacial polymerization. The embedment of the nanoparticles was confirmed by TEM, where the selective layer was peeled off from the PES substrate for the observation (Fig. 3.8). In the case of the PA/ZIF-8-TFN membrane, the diffraction peaks of the ZIF-8 crystal became much less intense, and a new weak peak appeared at 2θ = 11.1°, which could be ascribed to $Zn(OH)_2$ or their hydrates together with some unknown phase [41,42]. The XRD result indicated that the crystal structure of unmodified ZIF-8 was deteriorated during the membrane preparation process.

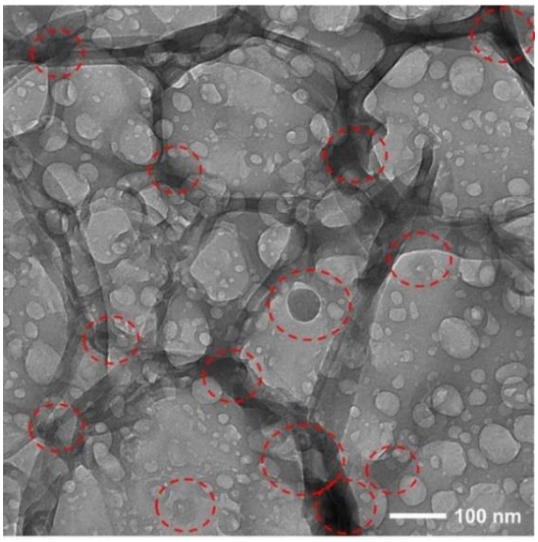

Fig. 3.8. TEM image of the crosslinked aromatic PA selective layer peeled off from PA/cZIF-8-TFN (40 wt%). cZIF-8 nanoparticles were marked with red circles.

In order to understand the stability of ZIF-8 during the interfacial polymerization, ZIF-8 and cZIF-8 nanoparticles were respectively immersed in solutions containing

different compounds that are used or produced in the interfacial polymerization at room temperature for 1 h. These solutions included pure H_2O, pure hexane, an aqueous solution of MPD (2% w/v), a hexane solution of TMC (0.15% w/v), an aqueous solution of TEA (4% w/v), and dilute HCl (0.2 mM). Fig. 3.9 shows XRD patterns of ZIF-8 particles after immersion. Clearly, all the solutions other than dilute HCl had no obvious effect on the crystallinity of ZIF-8 (Fig. 3.9a). The immersion in HCl led to the decrease in the original diffraction peaks together with the appearance of a new peak at 2θ = 11.1°, which was consistent with that observed in the PA/ZIF-8-TFN membrane. In fact, although ZIF-8 is chemically stable, it is known to degrade under acidic conditions [43]. Nevertheless, after the modification with PDA, the crystallinity of cZIF-8 kept stable even in dilute HCl (Fig. 3.9b), suggesting that the PDA coating was beneficial in improving the stability of ZIF-8 during the interfacial polymerization.

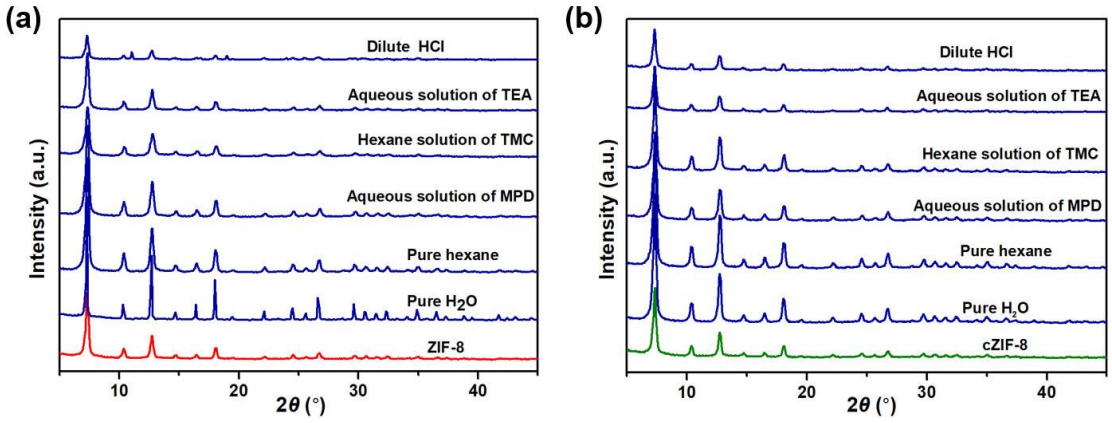

Fig. 3.9. XRD patterns of a) ZIF-8 and b) cZIF-8 nanoparticles after immersion in different solutions at room temperature for 1 h.

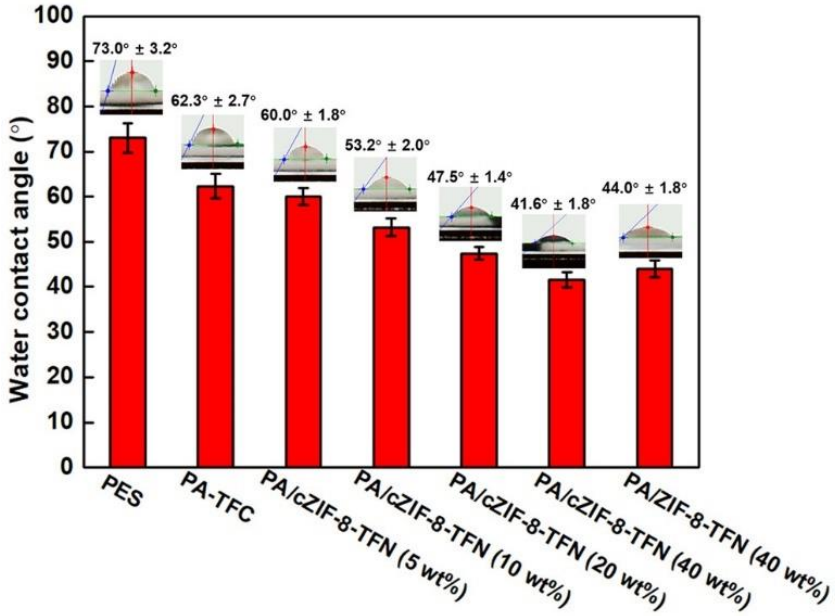

Fig. 3.10. WCAs of the PES substrate, PA-TFC, PA/cZIF-8-TFN, and PA/ZIF-8-TFN.

It is well acknowledged that the hydrophilicity of the membranes has certain influences on the water permeability and antifouling properties [44]. The hydrophilicity of the PES substrate, PA-TFC, and PA/cZIF-8-TFN was investigated (Fig. 3.10). The PES substrate exhibited a relatively hydrophobic property with the WCA of 73.0°, and the formation of the crosslinked aromatic PA layer decreased the WCA to 62.3°. The WCA monotonously decreased as the amount of the cZIF-8 nanoparticles was increased. In Fig. 3.5, the cZIF-8 nanoparticles showed much higher hydrophilicity than the ZIF-8 nanoparticles. However, the WCA of PA/ZIF-8-TFN was not only comparable to that of PA/cZIF-8-TFN, but also lower than that of the original nanoparticles (50.2°). This could be explained by the deterioration of unmodified ZIF-8 during the interfacial polymerization and/or by the smoother surface of the membrane (mentioned later).

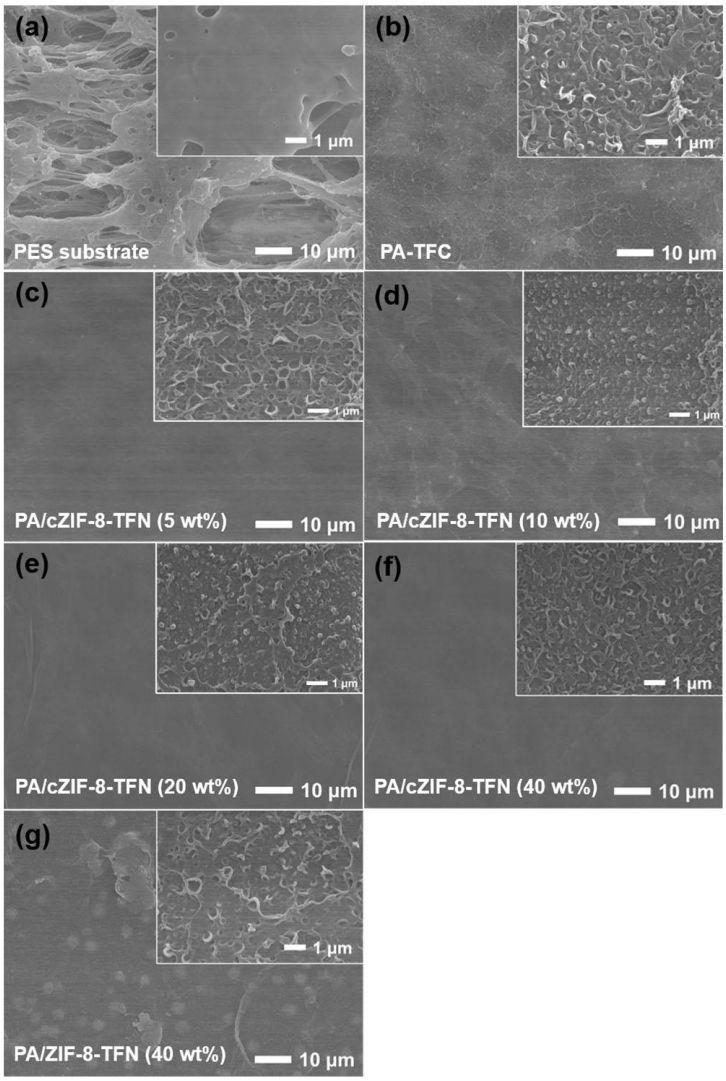

Fig. 3.11. Top-view SEM images of the membranes.

The surface and cross-sectional morphologies of the TFN membranes were studied by SEM (Figs 3.11 and 3.12). As shown in Fig. 3.11, the porous structure of the PES substrate (Fig. 3.11a) was no longer observed after the interfacial polymerization. In general, crosslinked aromatic PA forms a crumpled surface morphology with tufts extending in an outward direction from the PES surface as the MPD molecules diffuse into the hexane phase where the crosslinking takes place [45,46]. In a qualitative sense, all of the TFC and TFN membranes possessed the typical surface morphology (insets

in Fig. 3.11b–g). Meanwhile, the details were affected by the addition and the surface properties of the nanoparticles. In the absence of ZIF-8 nanoparticles (Fig. 3.11b, PA-TFC), the crumpled structure was relatively rougher, and the tufts were relatively long with the width of ca. 60 nm. The thickness of the selective layer was calculated from the cross-sectional SEM image (Fig. 3.12a). Along with the amount of cZIF-8, the tufts became shorter and narrower (width = ca. 45 nm at 40 wt%), which made the crumpled structure of the membrane smoother (Fig. 3.11b–f). A similar morphological change was also observed in HKUST-1-embedded PA-TFN membranes [48]. A potential explanation is that MPD molecules were adsorbed to the pre-deposited hydrophilic nanoparticles, and constrained the interfacial polymerization near the cZIF-8 nanoparticles [47,48].

In case of PA/ZIF-8-TFN, poor dispersibility of unmodified ZIF-8 in the MPD solution caused an obvious agglomeration of nanoparticles, resulting in an uneven distribution of the tufts (Fig. 3.11g). The agglomeration of nanoparticles can be clearly seen in the cross-sectional SEM image (Fig. 3.12f), which is not the case for the PA/cZIF-8-TFN (Fig. 3.12b–e).

The thickness of the crosslinked aromatic PA layer was not sensitive to the presence or absence of ZIF-8 and its modification, ranging from 75–100 nm for all the TFC and TFN membranes (Fig. 3.12).

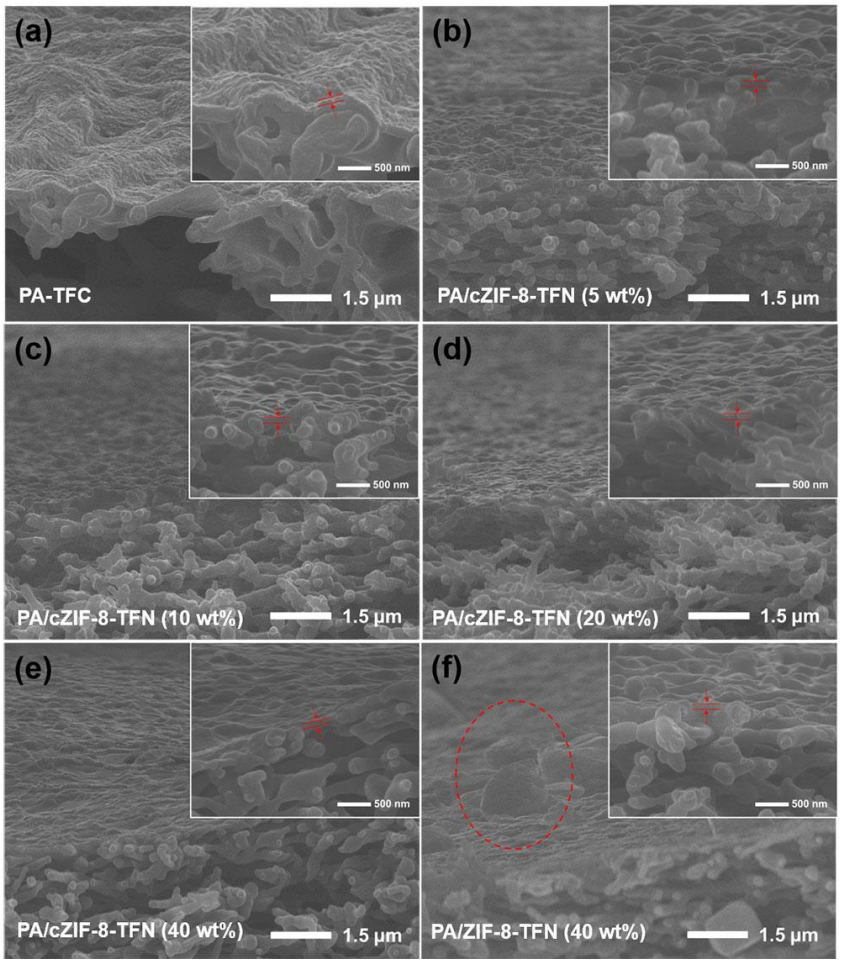

Fig. 3.12. Cross-sectional SEM images of the membranes.

3.3.3. Separation performance

The performance of the prepared membranes in brackish water desalination was evaluated. The filtration was performed using a home-made filtration system. First, pure water was supplied to stabilize the filtration, and the water flux was measured at different transmembrane pressures (Fig. 3.13). For all the membranes, the water flux increased proportionally to the differential pressure, encompassing the stable operation. A linear fit to the pressure dependence of the flux led to 6.4 ± 0.1 LMH bar^{-1} for PA-TFC. The introduction of cZIF-8 into the selective layer greatly improved the

permeability of the membranes. The permeability increased along with the addition amount of cZIF-8 added, and it reached 15.6 ± 0.3 LMH bar^{-1} at 40 wt%, which was more than twice that of PA-TFC. The enhanced permeability of the TFN membranes was attributed to the presence of cZIF-8, which would increase the water transport pathways and/or improve the membrane properties. The nano-sized cZIF-8 inclusions provide additional transport pathways as the intrinsic nanochannels and/or interfacial voids, plausibly causing lower migration resistance as well as faster transport of water molecules compared to the TFC membrane with a densely crosslinked aromatic PA layer [12,16]. The enhanced hydrophilicity of the membranes also improves the interaction of water molecules with the membranes [49]. Further, the ridge-and-valley surface morphologies with a finer crumpled structure increase the effective membrane area to facilitate the dissolution/diffusion of water molecules [50].

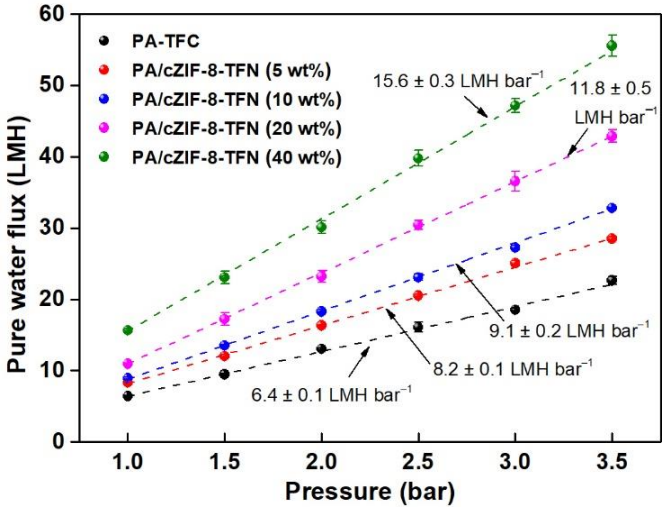

Fig. 3.13. Pure water flux of PA-TFC and PA/cZIF-8-TFN with different cZIF-8 loadings at different transmembrane pressures.

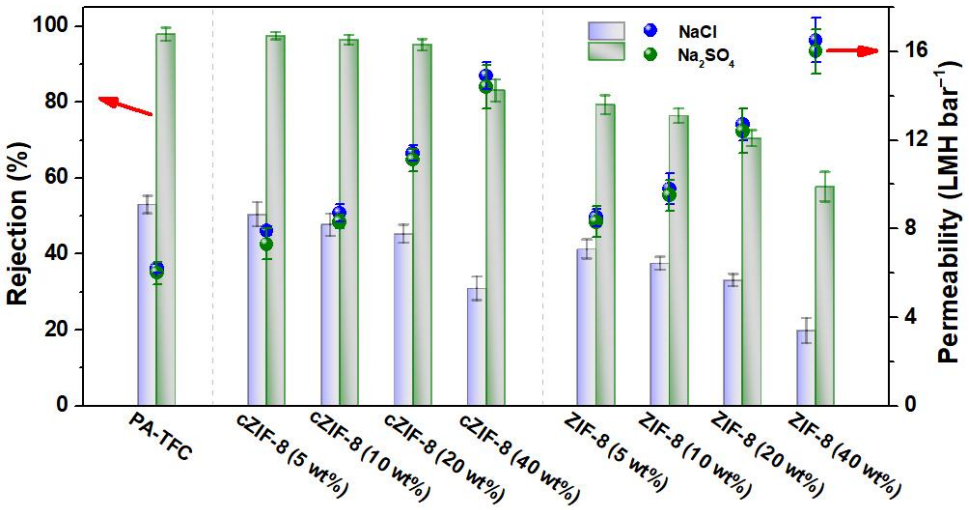

Fig. 3.14. Desalination performance of the TFC and TFN membranes with different ZIF-8 and cZIF-8 loadings. (Pressure: 2 bar, salt concentration: 1000 ppm).

Table 3.1. Summary of desalination performance of all the membranes.

Membrane	Permeability (LMH bar^{-1})		Rejection (%)	
	NaCl	Na_2SO_4	NaCl	Na_2SO_4
PA-TFC	6.2 ± 0.2	6.0 ± 0.5	53.0 ± 2.3	97.9 ± 1.7
PA/cZIF-8-TFN (5 wt%)	7.9 ± 0.2	7.3 ± 0.7	50.4 ± 3.2	97.5 ± 1.0
PA/cZIF-8-TFN (10 wt%)	8.7 ± 0.4	8.3 ± 0.3	47.7 ± 2.9	96.4 ± 1.3
PA/cZIF-8-TFN (20 wt%)	11.4 ± 0.4	11.1 ± 0.5	45.3 ± 2.4	95.1 ± 1.5
PA/cZIF-8-TFN (40 wt%)	14.9 ± 0.6	14.4 ± 1.0	30.9 ± 3.1	83.1 ± 2.9
PA/ZIF-8-TFN (5 wt%)	8.5 ± 0.4	8.3 ± 0.7	41.3 ± 2.5	79.3 ± 2.5
PA/ZIF-8-TFN (10 wt%)	9.8 ± 0.7	9.5 ± 0.7	37.5 ± 1.7	76.4 ± 1.9
PA/ZIF-8-TFN (20 wt%)	12.7 ± 0.7	12.4 ± 1.0	33.1 ± 1.6	70.5 ± 2.1
PA/ZIF-8-TFN (40 wt%)	16.5 ± 1.0	16 ± 1.0	19.8 ± 3.3	57.7 ± 3.9

Fig. 3.14 and Table 3.1 summarize the rejection efficiency and the permeability of the TFC and TFN membranes, which were acquired in filtration of an aqueous feed solution of NaCl or Na_2SO_4 (1000 ppm) at differential pressure of 2 bar. Compared to pure water, the permeability of each membrane reduced by ca. 5% due to the presence of hydrated salt ions [48]. In other words, the enhancement of the permeability by the

addition of ZIF-8 was also obtained in the desalination. Of all the membranes tested, PA-TFC gave the highest rejection: 97.9% for Na_2SO_4 while 53.0% for NaCl. In general, the rejection efficiency of a membrane is determined by the electrostatic charge repulsion called the Donnan effect and the diffusion rate [51,52]. The negatively charged PA layer [51] causes the repulsion of negatively charged ions, where the repulsion becomes more prominent for divalent SO_4^{2-} than monovalent Cl^{-1}. Besides, the smaller hydrated Cl^- ions (dia. = 6.6 Å) can diffuse faster than the larger hydrated SO_4^{2-} ions (dia. = 7.6 Å) [17,44]. These factors led to a lower rejection efficiency and higher permeability for NaCl as compared to Na_2SO_4.

The introduction of ZIF-8 nanoparticles into the selective layer more or less deteriorated the selectivity (in particular for NaCl) and instead enhanced the permeability. However, the extents of the deterioration and the enhancement were highly dependent on the amount of nanoparticles added and the presence of PDA coating. This is explained as follows, taking Na_2SO_4 as an example. In the case of cZIF-8 at 20 wt%, the rejection efficiency was only 2.8% lower than that of PA-TFC, while the permeability was 184% enhanced. These values were contrasted to −28% and 205% for unmodified ZIF-8 at the same loading, which allowed us to conclude that the PDA coating can alleviate the permeability-selectivity tradeoff to some extent. The enhanced permeability could be ascribed to combined effects of nanochannels for fast transport [16], the improved hydrophilicity [49], and the finer crumpled structure [50]. Meanwhile, the formation of non-selective defects caused by the particle agglomeration [47] and acid-aided structure deterioration were suppressed by the PDA coating, which

in addition improved interfacial adhesion [39]. This would explain the relatively good retention of the selectivity in PA/cZIF-8-TFN. Note that the agglomeration suppression was not achieved when an excessive loading, i.e., 40 wt%, was applied.

Long-term desalination performance was investigated for PA-TFC, PA/cZIF-8-TFN (20 wt%), and PA/ZIF-8-TFN (20 wt%). The filtration was performed for 72 h with the continuous feed of a Na_2SO_4 solution (1000 ppm). As shown in Fig. 3.15a, PA-TFC exhibited a stable separation performance throughout the whole period: The selectivity tended to be constant (−1.3%), while the concentration polarization effect [53] led to a slight decline in permeability (−4.8%). A similar behavior was observed for PA/cZIF-8-TFN (20 wt%): The performance deterioration after 72 h was 1.5% in selectivity and 5.6% in permeability. Conversely, PA/ZIF-8-TFN (20 wt%) displayed obvious decline in the selectivity (−15.3%). This is because ZIF-8 in the selective layer tended to deteriorate during the long-term filtration [47], giving rise to interfacial defects between PA and ZIF-8. The XRD patterns of the used membranes confirmed the loss of the ZIF-8 crystal in the absence of PDA coating (Fig. 3.16). These results further support the fact that the PDA coating can effectively preserve the ZIF-8 nanoparticles in the selective layer for high membrane stability.

Antifouling properties of PA-TFC, PA/ZIF-8-TFN (20 wt%), and PA/cZIF-8-TFN (20 wt%) were investigated using HA as a typical foulant which commonly exists in soils, sediments, and natural water. The experiments were performed by repeating three processes: Filtration of an aqueous solution of HA (200 ppm), washing with DI water, and filtration of DI water. The fluxes recorded along the cycles are normalized and

shown in Fig. 3.15b. The relevant values are calculated in Table 3.2. It can be seen that the flux value in the filtration of the HA solution is lower than that for the DI water, and that the flux in the DI water filtration is not completely restored by rinsing the membrane. The drop of the flux value during the filtration of the HA solution means the occurrence of membrane fouling, and the incomplete recovery of the flux indicates irreversible fouling. It was found that the extents of the fouling and the recovery after rinsing differed greatly among the three types of membranes. It is clear that the fouling resistance and recovery improved in the order of PA-TFC < PA/ZIF-8-TFN << PA/cZIF-8-TFN. The difference expanded as the cycle progressed. In general, membranes with more hydrophilic and smoother surfaces are more resistance to fouling due to the formation of a hydrated layer and/or the weakness of interaction with organic foulants [47]. As shown in Figs 3.10–3.12, PA/ZIF-8-TFN was more hydrophilic and smoother than PA-TFC, resulting in the improved fouling resistance. On the other hand, PA/cZIF-8-TFN was as hydrophilic as and rather rougher than PA/ZIF-8-TFN, while its fouling resistance was much better. This deviation would be explained by prevention of ZIF-8 from the direct interaction or reaction with HA due to the PDA coating.

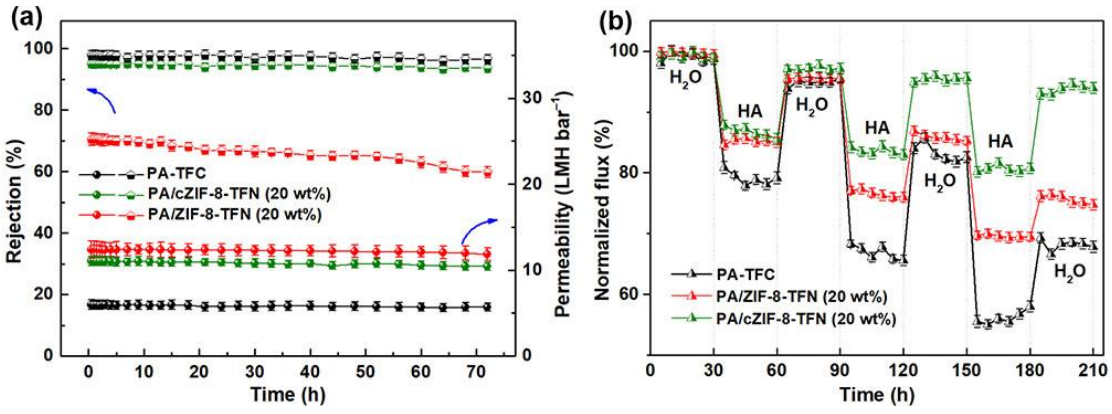

Fig. 3.15. a) Separation performance during a 72-h test (Pressure: 2 bar, salt: 1000 ppm of Na_2SO_4) and b) the antifouling properties (200 ppm of HA) of PA-TFC, PA/ZIF-8-TFN (20 wt%), and PA/cZIF-8-TFN (20 wt%).

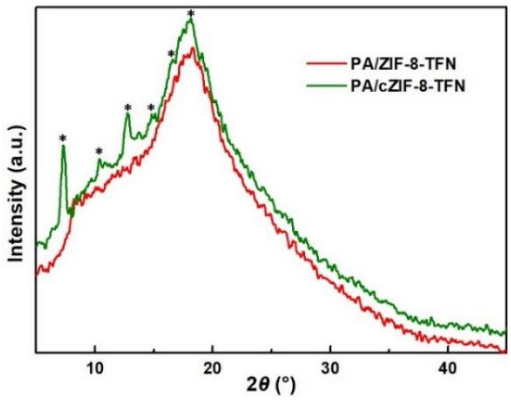

Fig. 3.16. XRD patterns of PA/ZIF-8-TFN (20 wt%) and PA/cZIF-8-TFN (20 wt%) after the filtration test for 72 h.

Table 3.2. Antifouling properties of PA-TFC, PA/ZIF-8-TFN (20 wt%), and PA/cZIF-8-TFN (20 wt%).[a]

Membrane	F_r (%)	F_{rr} (%)	R_r (%)	R_{ir} (%)
PA-TFC	43.5	68.9	12.4	31.1
PA/cZIF-8-TFN (20 wt%)	18.7	94.4	13.1	5.6
PA/ZIF-8-TFN (20 wt%)	30.3	76.2	6.5	23.8

[a] The antifouling properties were examined using an aqueous solution of HA (200 ppm). The total fouling ratio (F_r), the flux recovery ratio (F_{rr}), the reversible fouling ratio (R_r), and the irreversible fouling ratio (R_{ir}) are respectively as given in Eqs. (3.4–3.7).

3.4. Conclusions

Metal-organic framework (MOF)-based thin-film nanocomposite (TFN) membranes are promising for addressing the permeability-selectivity tradeoff in

desalination. Key challenges have been identified at the dispersion and stability of MOFs during interfacial polymerization/desalination as well as at the interfacial bonding with the polymeric matrix. In **Chapter 3**, I attempted to solve these problems by using polydopamine (PDA)-coated ZIF-8 nanoparticles. PDA significantly improved the dispersibility of ZIF-8 nanoparticles in the aqueous phase of interfacial polymerization without blocking the nanochannels of ZIF-8. The crystal structure of ZIF-8 is not stable against HCl generated during interfacial polymerization, where PDA coating significantly improved the chemical stability of ZIF-8. A TFN membrane with 20 wt% of PDA-coated ZIF-8 nanoparticles exhibited Na_2SO_4 rejection efficiency comparable to that of a MOF-free thin film composite membrane. In contrast, the rejection efficiency of a TFN membrane with uncoated ZIF-8 was significantly lower due to agglomeration, interfacial voids, and crystal deterioration. The PDA coating provided stability to ZIF-8 and ensured long-term filtration performance. Furthermore, the PDA coated ZIF-8 markedly improved the fouling resistance of the membrane likely as combined consequences of the hydrophilicity and the coating itself. In conclusion, this chapter clearly evidenced multiple important roles of surface modification of MOF in preparing performant and stable TFN membranes.

3.5. References

[1] R. Zhang, Y. Liu, M. He, Y. Su, X. Zhao, M. Elimelech, Z. Jiang, Antifouling membranes for sustainable water purification: strategies and mechanisms, Chem. Soc. Rev. 45 (2016) 5888–5924.

[2] C. Castel, E. Favre, Membrane separations and energy efficiency, J. Membr. Sci. 548 (2018) 345–357.

[3] K.P. Lee, T.C. Arnot, D. Mattia, A review of reverse osmosis membrane materials for desalination-development to date and future potential, J. Membr. Sci. 370 (2011) 1–22.

[4] J.E. Cadotte, R.J. Petersen, R.E. Larson, E.E. Erickson, A new thin-film composite seawater reverse osmosis membrane, Desalination 32 (1980) 25–31.

[5] J. Glater, M.R. Zachariah, S.B. McCray, J.W. McCutchan, Reverse osmosis membrane sensitivity to ozone and halogen disinfectants, Desalination 48 (1983) 1–16.

[6] Z. Jiang, S. Karan, A.G. Livingston, Water transport through ultrathin polyamide nanofilms used for reverse osmosis, Adv. Mater. 30 (2018) 1705973.

[7] N. Ma, J. Wei, R. Liao, C.Y. Tang, Zeolite-polyamide thin film nanocomposite membranes: towards enhanced performance for forward osmosis, J. Membr. Sci. 405 (2012) 149–157.

[8] H. Sun, P. Wu, Tuning the functional groups of carbon quantum dots in thin film nanocomposite membranes for nanofiltration, J. Membr. Sci. 564 (2018) 394–403.

[9] F. Xiao, X. Hu, Y. Chen, Y. Zhang, Porous Zr-based metal-organic frameworks (Zr-MOFs)-incorporated thin-film nanocomposite membrane toward enhanced desalination performance, ACS Appl. Mater. Interfaces 11 (2019) 47390–47403.

[10] X. Song, Y. Wang, C. Jiao, M. Huang, G.H. Wang, H. Jiang, Microstructure regulation of polyamide nanocomposite membrane by functional mesoporous polymer for high-efficiency desalination, J. Membr. Sci. 597 (2020) 117783.

[11] W.J. Lau, S. Gray, T. Matsuura, D. Emadzadeh, J.P. Chen, A.F. Ismail, A review on polyamide thin film nanocomposite (TFN) membranes: history, applications, challenges and approaches, Water Res. 80 (2015) 306–324.

[12] B.H. Jeong, E.M.V. Hoek, Y. Yan, A. Subramani, X. Huang, G. Hurwitz, A.K. Ghosh, A. Jawor, Interfacial polymerization of thin film nanocomposites: a new concept for reverse osmosis membranes, J. Membr. Sci. 294 (2007) 1–7.

[13] M.D. Firouzjaei, A.A. Shamsabadi, S.A. Aktij, S.F. Seyedpour, M. Sharifian Gh, A. Rahimpour, M.R. Esfahani, M. Ulbricht, M. Soroush, Exploiting synergetic effects of graphene oxide and a silver-based metal-organic framework to enhance antifouling and anti-biofouling properties of thin-film nanocomposite membranes, ACS Appl. Mater. Interfaces 10 (2018) 42967–42978.

[14] M. Amini, M. Jahanshahi, A. Rahimpour, Synthesis of novel thin film nanocomposite (TFN) forward osmosis membranes using functionalized multi-walled carbon nanotubes, J. Membr. Sci. 435 (2013) 233–241.

[15] C. Li, S. Li, L. Tian, J. Zhang, B. Su, M.Z. Hu, Covalent organic frameworks (COFs)-incorporated thin film nanocomposite (TFN) membranes for high-flux

organic solvent nanofiltration (OSN), J. Membr. Sci. 572 (2019) 520–531.

[16] J. Duan, Y. Pan, F. Pacheco, E. Litwiller, Z. Lai, I. Pinnau, High-performance polyamide thin-film nanocomposite reverse osmosis membranes containing hydrophobic zeolitic imidazolate framework-8, J. Membr. Sci. 476 (2015) 303–310.

[17] E. Nightingale Jr, Phenomenological theory of ion solvation. Effective radii of hydrated ions, J. Phys. Chem. 63 (1959) 1381–1387.

[18] J.W. Krumpfer, T. Schuster, M. Klapper, K. Müllen, Make it nano-keep it nano, Nano Today 8 (2013) 417–438.

[19] W. Li, Metal-organic framework membranes: production, modification, and applications, Prog. Mater. Sci. 100 (2019) 21–63.

[20] C.V. Goethem, R. Verbeke, M. Pfanmöller, T. Koschine, M. Dickmann, T. Timpel-Lindner, W. Egger, S. Bals, I.F.J. Vankelecom, The role of MOFs in thin-film nanocomposite (TFN) membranes, J. Membr. Sci. 563 (2018) 938–948.

[21] I.H. Aljundi, Desalination characteristics of TFN-RO membrane incorporated with ZIF-8 nanoparticles, Desalination 420 (2017) 12–20.

[22] H.M. Park, K.Y. Jee, Y.T. Lee, Preparation and characterization of a thin-film composite reverse osmosis membrane using a polysulfone membrane including metal-organic frameworks, J. Membr. Sci. 541 (2017) 510–518.

[23] M. Kadhom, W. Hu, B. Deng, Thin film nanocomposite membrane filled with metal-organic frameworks UiO-66 and MIL-125 nanoparticles for water

desalination, Membranes 7 (2017) 31.

[24] J.H. Ryu, P.B. Messersmith, H. Lee, Polydopamine surface chemistry: a decade of discovery, ACS Appl. Mater. Interfaces 10 (2018) 7523–7540.

[25] G. Fredi, F. Simom, D. Sychev, I. Melnyk, A. Janke, C. Scheffler, C. Zimmerer, Bioinspired polydopamine coating as an adhesion enhancer between paraffin microcapsules and an epoxy matrix, ACS Omega 5 (2020) 19639–19653.

[26] Q. Liu, N. Wang, J. Caro, A. Huang, Bio-inspired polydopamine: a versatile and powerful platform for covalent synthesis of molecular sieve membranes, J. Am. Chem. Soc. 135 (2013) 17679–17682.

[27] Z. Wang, D. Wang, S. Zhang, L. Hu, J. Jin, Interfacial design of mixed matrix membranes for improved gas separation performance, Adv. Mater. 28 (2016) 3399–3405.

[28] H. Lee, S.M. Dellatore, W.M. Miller, P.B. Messersmith, Mussel-inspired surface chemistry for multifunctional coatings, Science 318 (2007) 426–430.

[29] H. You, G.Y. Shangkum, P. Chammingkwan, T. Taniike, Surface wettability switching of a zeolitic imidazolate framework-deposited membrane for selective efficient oil/water emulsion separation, Colloids Surf., A 614 (2021) 126204.

[30] Z. Hu, Y. Chen, J. Jiang, Zeolitic imidazolate framework-8 as a reverse osmosis membrane for water desalination: insight from molecular simulation, J. Chem. Phys. 134 (2011) 134705.

[31] J. Cravillon, S. Münzer, S.J. Lohmeier, A. Feldhoff, K. Huber, M. Wiebcke, Rapid room-temperature synthesis and characterization of nanocrystals of a

prototypical zeolitic imidazolate framework, Chem. Mater. 21 (2009) 1410–1412.

[32] W. Yuan, A.L. Zydney, Humic acid fouling during ultrafiltration, Environ. Sci. Technol. 34 (2000) 5043–5050.

[33] J. Wang, Y. Wang, Y. Zhang, A. Uliana, J. Zhu, J. Liu, B. Van der Bruggen, Zeolitic imidazolate framework/graphene oxide hybrid nanosheets functionalized thin film nanocomposite membrane for enhanced antimicrobial performance, ACS Appl. Mater. Interfaces 8 (2016) 25508–25519.

[34] Y. Pan, Y. Liu, G. Zeng, L. Zhao, Z. Lai, Rapid synthesis of zeolitic imidazolate framework-8 (ZIF-8) nanocrystals in an aqueous system, Chem. Commun. 47 (2011) 2071–2073.

[35] M. He, J. Yao, Q. Liu, K. Wang, F. Chen, H. Wang, Facile synthesis of zeolitic imidazolate framework-8 from a concentrated aqueous solution, Microporous Mesoporous Mater. 184 (2014) 55–60.

[36] Y. Hu, H. Kazemian, S. Rohani, Y. Huang, Y. Song, In situ high pressure study of ZIF-8 by FTIR spectroscopy, Chem. Commun. 47 (2011) 12694–12696.

[37] Y. Wang, L. Liu, M. Li, S. Xu, F. Gao, Multifunctional carbon nanotubes for direct electrochemistry of glucose oxidase and glucose bioassay, Biosens. Bioelectron. 30 (2011) 107–111.

[38] R.A. Zangmeister, T.A. Morris, M.J. Tarlov, Characterization of polydopamine thin films deposited at short times by autoxidation of dopamine, Langmuir 29 (2013) 8619–8628.

[39] M. Qiu, C. He, Efficient removal of heavy metal ions by forward osmosis membrane with a polydopamine modified zeolitic imidazolate framework incorporated selective layer, J. Hazard. Mater. 367 (2019) 339–347.

[40] N.M. Chauke, R.M. Moutloali, J. Ramontja, Development of ZSM-22/polyethersulfone membrane for effective salt rejection, Polymers 12 (2020) 1446.

[41] B. Chen, F. Bai, Y. Zhu, Y. Xia, A cost-effective method for the synthesis of zeolitic imidazolate framework-8 materials from stoichiometric precursors via aqueous ammonia modulation at room temperature, Microporous Mesoporous Mater. 193 (2014) 7–14.

[42] K. Kida, M. Okita, K. Fujita, S. Tanaka, T. Miyake, Formation of high crystalline ZIF-8 in an aqueous solution, CrystEngComm 15 (2013) 1794–1801.

[43] S.H. Pang, C. Han, D.S. Sholl, C.W. Jones, R.P. Lively, Facet-specific stability of ZIF-8 in the presence of acid gases dissolved in aqueous solutions, Chem. Mater. 28 (2016) 6960–6967.

[44] Y. Zhao, Y. Liu, X. Wang, X. Huang, Y. Xie, Impacts of metal-organic frameworks on structure and performance of polyamide thin-film nanocomposite membranes, ACS Appl. Mater. Interfaces 11 (2019) 13724–13734.

[45] Y. Song, P. Sun, L.L. Henry, B. Sun, Mechanisms of structure and performance controlled thin film composite membrane formation via interfacial polymerization process, J. Membr. Sci. 251 (2005) 67–79.

[46] M.F.J. Solomon, Y. Bhole, A.G. Livingston, High flux membranes for organic solvent nanofiltration (OSN)-interfacial polymerization with solvent activation, J. Membr. Sci. 423 (2012) 371–382.

[47] Y. Lin, Y. Chen, R. Wang, Thin film nanocomposite hollow fiber membranes incorporated with surface functionalized HKUST-1 for highly-efficient reverse osmosis desalination process, J. Membr. Sci. 589 (2019) 117249.

[48] J. Zhu, L. Qin, A. Uliana, J. Hou, J. Wang, Y. Zhang, X. Li, S. Yuan, J. Li, M. Tian, J. Lin, B. Van der Bruggen, Elevated performance of thin film nanocomposite membranes enabled by modified hydrophilic MOFs for nanofiltration, ACS Appl. Mater. Interfaces 9 (2017) 1975–1986.

[49] M. Qasim, M. Badrelzaman, N.N. Darwish, N.A. Darwish, N. Hilal, Reverse osmosis desalination: a state-of-the-art review, Desalination 459 (2019) 59–104.

[50] Z. Tan, S. Chen, X. Peng, L. Zhang, C. Gao, Polyamide membranes with nanoscale turing structures for water purification, Science 360 (2018) 518–521.

[51] Y. He, Y.P. Tang, D. Ma, T.S. Chung, UiO-66 incorporated thin-film nanocomposite membranes for efficient selenium and arsenic removal, J. Membr. Sci. 541 (2017) 262–270.

[52] C. Hu, Z. Liu, X. Lu, J. Sun, H. Liu, J. Qu, Enhancement of the Donnan effect through capacitive ion increase using an electroconductive rGO-CNT nanofiltration membrane, J. Mater. Chem. A 6 (2018) 4737–4745.

[53] Y. Kang, J. Jang, S. Kim, J. Lim, Y. Lee, I.S. Kim, PIP/TMC interfacial polymerization with electrospray: novel loose nanofiltration membrane for dye

wastewater treatment, ACS Appl. Mater. Interfaces 12 (2020) 36148–36158.

Chapter 4

Preparation of ZIF-8-matrix nanocomposite membranes for high-flux desalination

Abstract

Hybrid polymer-metal organic framework (MOF) membranes are promising for addressing the permeability-selectivity tradeoff in membrane application. Key challenges for achieving high efficiency separation performance have been identified as improving MOF loading as well as interfacial compatibility with polymeric matrices. Herein, a novel designed (zeolitic imidazolate framework-8) ZIF-8-matrix nanocomposite membrane was prepared by forming a selective layer via interfacial polymerization on a PES substrate for desalination. Selective functionalization of the external surface of ZIF-8 has been conducted for the purpose of membrane preparation. Thereafter, a polymer-grafted ZIF-8 was crosslinked into the selective layer using trimesoyl chloride as a crosslinker. The mechanism and structure of selective layer formation, as well as the membrane's ZIF-8 loading, were investigated. The membrane exhibited ultrahigh ZIF-8 loading (ca. 70 wt%) in the selective layer, which led to a superior permeability (ca. 43.6 LMH bar^{-1}) with a Na_2SO_4 rejection above 95%. These ZIF-8-matrix nanocomposite membranes represent a significant advancement in achieving high-efficient separation in desalination with a high ZIF-8 loading.

4.1. Introduction

Metal-organic frameworks (MOFs), a class of emerging crystalline porous materials that are made of coordination of metal ions/clusters and organic ligands, have been regarded as promising materials for separation applications due to their special features, such as highly tunable pore structure and chemical versatility as well as functionalities [1–5], which are much preferred over conventional porous materials, such as zeolites [6]. As one of the engineered forms, MOF-based membranes are being intensively investigated for desalination.

Desalination is a separation process that reduces the concentration of dissolved salt in saline water to a usable level [7]. A recent concept is the incorporation of MOF nanoparticles into a crosslinked aromatic polyamide layer to produce a MOF-based thin-film nanocomposite (TFN) structure for desalination [8,9]. In MOF-based TFN membranes, MOFs are used as nanofillers, which primarily play a role in providing additional molecular sieving transport channels as well as facilitating hydrophilicity and membrane roughness for the purpose of enhancing their permeability as compared to polymeric membranes [10]. A series of relatively hydro-stable MOFs, such as MIL-53 (Al) [11], ZIF-8 [12,13], UiO-66 [14], NH_2-UiO-66 [15], and HKUST-1 [16], have been utilized in MOF-based TFN membranes for desalination. For example, Xiao et al. reported a MOF-based TFN membrane prepared by dispersing zeolitic imidazolate framework-8 (ZIF-8) nanoparticles into piperazine aqueous solution, followed by incorporating them into the polyamide selective layer via interfacial polymerization with TMC [13]. With increasing ZIF-8 loading from 0 to 0.02 (w/v%), water

permeability for the separation of a Na_2SO_4 aqueous solution increased from 5.4 to 7.3 L m^{-2} h^{-1} bar^{-1}, while maintaining almost the same selectivity. However, when further increasing the ZIF-8 loading, the selectivity showed a significant decline because non-selective voids were formed by ZIF-8 agglomeration.

Ideally, MOFs with suitable pores provide molecular sieving separation pathways for higher permeability, which should not affect the selectivity of the composite membranes [10]. However, the separation performance of MOF-based TFN membranes is not just an average of the two components, and usually becomes far below theoretical expectations [17]. One of the limitations is the poor interfacial compatibility between MOFs and polymers [18]. To data, strategies have been proposed to improve interfacial compatibility by modifying the surface of MOFs [8,16]. For example, in **Chapter 3**, I investigated the effect of a polydopamine (PDA) coating on the surface of ZIF-8 nanoparticles on the desalination performance of MOF-based TFN membranes [8]. The water permeability of the TFN membrane with 0.1 w/v% of PDA-coated ZIF-8 nanoparticles was 184% higher than that of the ZIF-8-free membrane for the separation of Na_2SO_4 aqueous solution, while the selectivity was slightly reduced (2.8%). These values were contrasted to 205% and –28% for the membrane with the raw ZIF-8 nanoparticles, allowing me to conclude that the PDA modification can alleviate the tradeoff between permeability and selectivity to some extent by improving the dispersibility and compatibility of ZIF-8. Although significant improvements in desalination performance have been achieved by engineering the surface MOFs, most reported MOF-based TFN membranes exhibit at most a twofold increase in

permeability under comparable selectivity [16,19,20]. This is partly due to the weak interaction between the MOF surface and polymer side chains [21]. Meanwhile, the high surface energy of MOF nanoparticles as well as the phase segregation tendency between MOF particles and polymers still lead to void defects due to agglomerations of MOF nanoparticles in the membranes, which makes an upper limit of the MOF loading in the selective layer, i.e., upper limit of the performance improvement [22]. Given all the above, an advanced MOF-based membrane that both maximizes MOF loading and addresses MOF-polymer interfacial compatibility is highly desired for desalination.

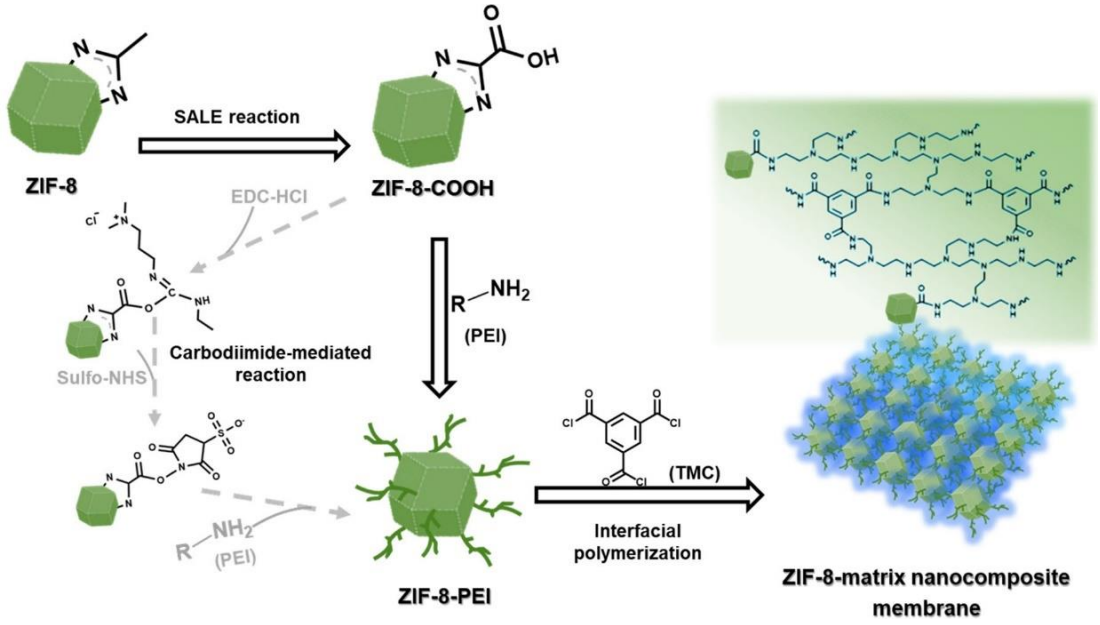

Scheme 4.1. Stepwise approach for preparation of ZIF-8-matrix nanocomposite membranes.

In **Chapter 4**, a novel strategy was proposed to prepare a MOF-matrix nanocomposite membrane (as shown in Scheme 4.1) for desalination, in which a polymer with film-forming ability was grafted onto the MOF surface to eliminate

interfacial defects, and the polymer-grafted MOFs were used as building blocks to form a selective layer with a high MOF loading by crosslinking on a substrate membrane. As a result, the as-prepared membranes exhibited several times higher permeability as compared to the traditional MOF-based TFN membranes while maintaining a comparable selectivity for desalination.

4.2. Experimental section

4.2.1. Materials

All reagents and solvents are commercially available. They were used as received without further purification. 2-Methylimidazole (MIm, > 98%), 2-imidazolecarboxylic acid (Im-COOH, > 98%), 1-(3-dimethylaminopropyl)-3-ethylcarbodiimide hydrochloride (EDC-HCl, > 98.0%), N-hydroxysulfosuccinimide sodium salt (sulfo-NHS, > 98%), and trimesoyl chloride (TMC, > 98%) were purchased from Tokyo Chemical Industry Co., Ltd. Zinc nitrate hexahydrate ($Zn(NO_3)_2 \cdot 6H_2O$, > 98%) polyethyleneimine, branched (PEI, M_n ~ 10,000, > 99%), and acetic acid-d_4 (≥ 99.5%, with 0.03 vol% of trimethoxysilane) were obtained from Sigma-Aldrich. Sodium sulfate (Na_2SO_4, > 99%), methanol, dimethylformamide (DMF), and *n*-hexane were purchased from Wako Pure Chemical Industries Ltd. A polyethersulfone (PES) membrane (47mm dia., 0.22 μm pore size, Merck Millipore) was chosen as a support membrane. An anodized aluminum oxide (AAO) membrane (47 mm dia., 0.1 μm pore size, Whatman®) was used as a support in characterizing freestanding ZIF-8-PEI films. Deionized (DI) water was used throughout the experiments.

4.2.2. Synthesis of polymer-grafted ZIF-8 nanoparticles

ZIF-8 nanoparticles

ZIF-8 nanoparticles were synthesized at room temperature according to literature [23]. Briefly, a solution of MIm (79.04 mmol in 200 mL of methanol) was rapidly mixed with a solution of $Zn(NO_3)_2 \cdot 6H_2O$ (9.87 mmol in 200 mL of methanol) and vigorously stirred for 1 h. The formed nanoparticles were collected by centrifugation, and then repetitively washed with methanol for 5 times. Finally, the wet ZIF-8 nanoparticles were re-dispersed in methanol for subsequent reactions.

Carboxyl-functionalized ZIF-8

Carboxyl-functionalized ZIF-8 nanoparticles were prepared via a SALE reaction [24]. 5.0 mmol of Im-COOH was dissolved in 50 mL of DMF at 60 °C, and then, 50 mL of a ZIF-8 nanoparticles suspension in methanol (10 mg/mL) was added to the solution under stirring. The mixture was then sonicated for 30 min, followed by refluxing at 60 °C for 24 h. The nanoparticles were collected by centrifugation, repetitively washed with methanol for 5 times, and redispersed into methanol. The carboxy-functionalized ZIF-8 nanoparticles are denoted as ZIF-8-COOH.

PEI-grafted ZIF-8 nanoparticles

PEI-grafted ZIF-8 nanoparticles were prepared by covalently grafting PEI onto the surface of ZIF-8-COOH via a carbodiimide-mediated reaction. Briefly, EDC-HCl (0.5 mmol) and sulfo-NHS (5 μmol) were added to 10 mL of a ZIF-8-COOH nanoparticle suspension in methanol (10 mg/mL), and stirred for 5 min at room temperature. Subsequently, 2.0 mL of a PEI solution in methanol (1 μmol/mL) was added to the

mixture, and stirred for 30 min. The product was collected by centrifugation, repetitively rinsed with methanol for 5 times, and then dried at 40 °C under a vacuum for 24 h. The PEI-grafted ZIF-8 nanoparticles are donated as ZIF-8-PEI.

4.2.3. Membrane preparation

ZIF-8-matrix nanocomposite membranes were fabricated via interfacial polymerization to form a selective layer made of ZIF-8-PEI crosslinked with TMC on a PES substrate. In detail, a suspension of ZIF-8-PEI nanoparticles in water (10 mg/mL) was prepared by dispersing 100 mg in 10 mL of DI water, followed by sonication for 5 min. 1.0 mL of the suspension (i.e. 10 mg of ZIF-8-PEI) was gently dropped onto the PES substrate, which was then dried in a ventilated environment, and its surface was fully covered by 1.0 mL of a TMC solution in hexane with a varying TMC concentration of 1.0-20.0 mg/mL. The interfacial polymerization was performed at room temperature for 30 min, followed by rinsing with hexane and drying at 60 °C for 30 min.

A freestanding film of ZIF-8-PEI was prepared for characterization purposes. Appropriate amounts of the ZIF-8-PEI suspension and a hexane solution of TMC (7.5 mg/mL) were contacted in the absence of a support membrane at room temperature. After a certain period of time, the film was collected on an AAO substrate and rinsed with hexane to terminate the reaction.

4.2.4. Characterization

X-ray diffraction (XRD) patterns were obtained using a Rigaku SmartLab diffractometer (Cu Kα radiation) at a scan speed of 0.5° per min in the range of 5–45°.

Fourier transform infrared (FTIR) spectra were recorded on a FTIR spectrometer (spectrum 100, Perkin-Elmer) with a resolution of 4 cm^{-1}. The KBr method was used to acquire transmission spectra of nanoparticle samples, while the attenuated total reflection mode was adopted for membrane samples. Morphological characterizations were performed by transmission electron microscopy (TEM, Hitachi H-7650, 100 kV) and scanning electron microscopy (SEM, Hitachi S-4500, 20 kV). The particle size was obtained by analyzing TEM images with ImageJ software. Elemental mapping was carried out on an energy dispersive X-ray analyzer (EDX, Hitachi 3030Plus) equipped with SEM. Proton nuclear magnetic resonance (^{1}H NMR) spectra were acquired on a Bruker 400 MHz spectrometer. Approximately 3 mg of the nanoparticles were fully digested in a solution of acetic acid-d_4. Thermogravimetric analysis (TGA, Thermo plus evo, Rigaku) was carried out under dry air flow (100 mL/min) at a heating rate of 10 °C/min from 30 °C to 800 °C. Nitrogen adsorption/desorption experiments were performed at 77 K using a BELSORP-mini II instrument (BEL JAPAN, Inc.). The specific surface area and the pre volume were calculated by the Brunauer-Emmet-Teller (BET) and Horvath-Kawazoe methods, respectively. Water contact angles (WCAs) were measured at room temperature using a contact angle goniometer (SImage AUTO 100, Excimer, Japan).

4.2.5. Membrane performance evaluation

The performance of the ZIF-8-matrix nanocomposite membranes was evaluated for desalination using a dead-end filtration setup with an effective area of 7.1 cm^2. The detail was described in **Chapter 3**. A membrane was appropriately cut and fixed on the

membrane holder. To ensure stable filtration, the membrane was pre-pressurized at a differential pressure of 4 bar for 1 h, and the pure water flux was measured at different transmembrane pressures (0.5, 1, 1.5, 2, 2.5, and 3 bar). Then, desalination was performed using an aqueous solution of Na_2SO_4 (1000 ppm), where the differential pressure was varied in a range of 1.0−3.0 bar.

The flux (J, L m^{-2} h^{-1}, abbreviated as LMH) was calculated as $J = V/A \cdot \Delta t$, where V (L) is the permeated volume, A (m^2) is the effective membrane area, and Δt (h) is the filtration time. The permeability (P, LMH bar^{-1}) was calculated as $P = J/\Delta p$, where Δp (bar) is the applied transmembrane pressure. The salt rejection (R, %) was calculated as $R = (1\text{-}C_P/C_0) \times 100$, where C_P and C_0 are the solute concentrations in the permeate and feed, respectively. The concentration of the solutes was measured by an electrical conductivity meter (FEP30, Mettler Toledo).

4.3. Results and discussion

4.3.1. Characterization of ZIF-8-based nanoparticles

As illustrated in Scheme 4.1, ZIF-8 nanoparticles were first synthesized by a rapid coordination of Zn^{2+} and 2-methylimidazole [23], followed by surface functionalization with a carboxyl group via the SALE reaction, and grafting of PEI via a carbodiimide-mediated reaction. During the PEI grafting process, EDC-HCl first reacts with the carboxyl group on ZIF-8-COOH. The carbodiimide intermediate can react with the amino group on PEI to form a stable amide bond, where the addition of sulfo-NHS increases the efficiency of the reaction [25]. Their characterization results are shown in Fig. 4.1. To start, pristine ZIF-8 nanoparticles (Fig. 4.1a) exhibited an XRD pattern

typical for the sodalite structure of ZIF-8 [2,8]. The FTIR spectrum of ZIF-8 (Fig. 4.1b) was consistent with literature [26,27]. The nanoparticles possessed a typical polyhedral morphology with a particle size of 35 ± 3 nm (Fig. 4.1c). The ligand exchange and the subsequent PEI grafting hardly affected the crystal structure and the morphology of ZIF-8 (Fig. 4.1a,c). Fig. 4.1b shows changes in the FTIR spectra due to the ligand exchange and grafting. Besides the main bands of ZIF-8, ZIF-8-COOH displayed an additional band at 1607 cm^{-1}, assigned to the C=O stretching vibration, indicating the successful carboxyl functionalization of ZIF-8 [28]. After the PEI grafting, a new characteristic peak was observed at 3231 cm^{-1}, which was attributed to the N–H stretching vibration of primary and secondary amino groups, suggesting that the PEI was grafted onto ZIF-8 [29].

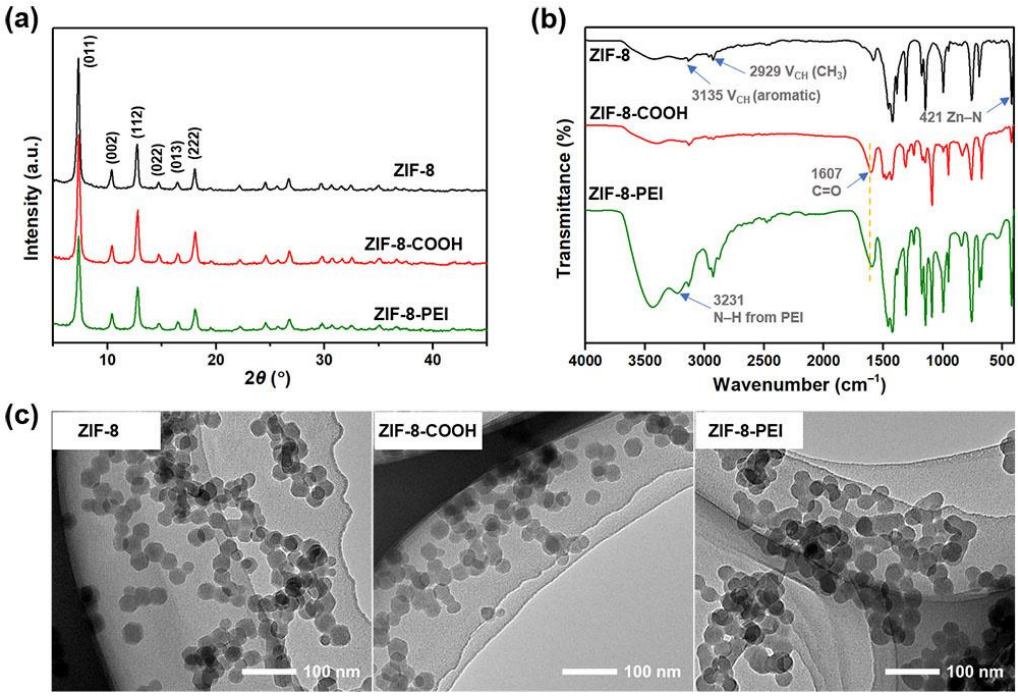

Fig. 4.1. Characterization of ZIF-8, ZIF-8-COOH, and ZIF-8-PEI: a) XRD patterns, b) FTIR spectra, and c) TEM images.

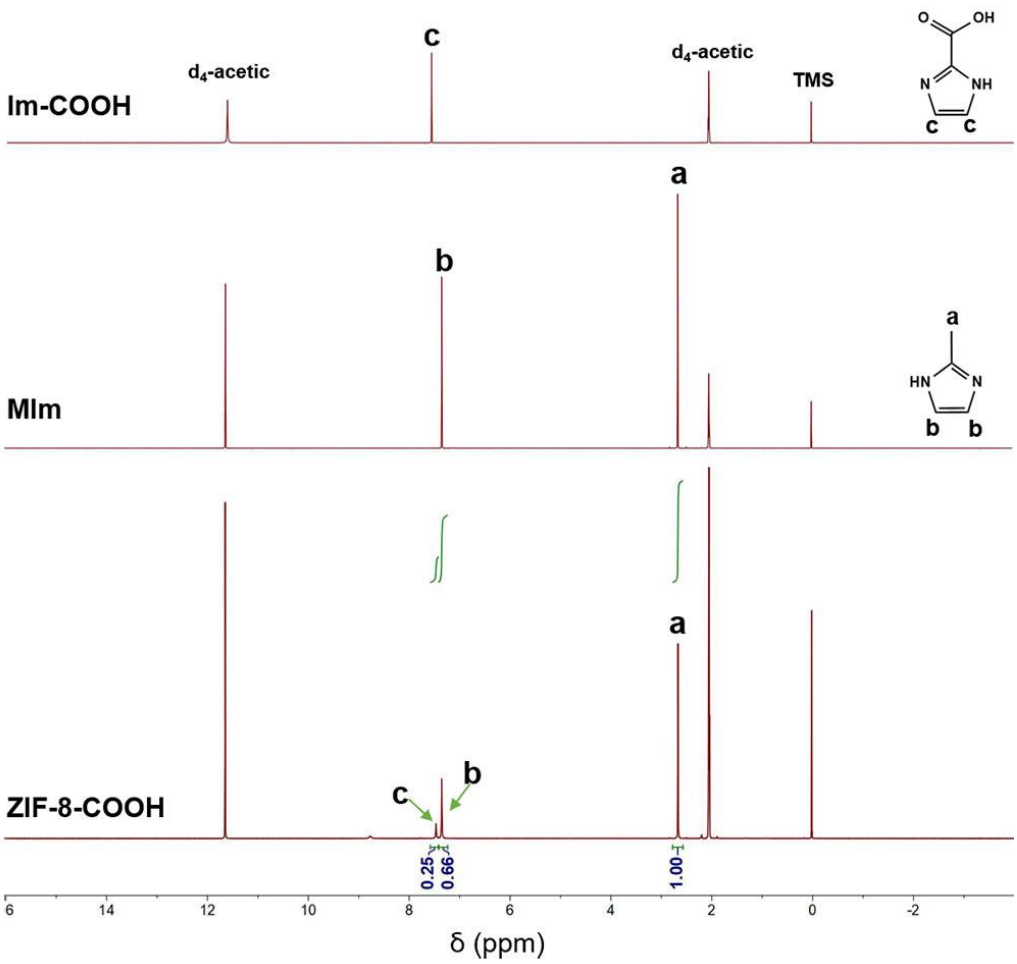

Fig. 4.2. [1]HNMR spectra of Im-COOH, MIm, and ZIF-8-COOH. The ligand exchange molar ratio in ZIF-8-COOH was calculated to 27% from the peak areas of aromatic protons for MIm (**b**, 7.36 ppm) and Im-COOH (**c**, 7.47 ppm) [30].

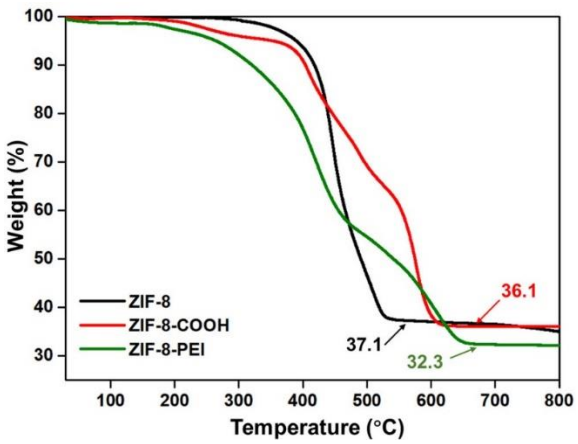

Fig. 4.3. TGA profiles of ZIF-8, ZIF-8-COOH, and ZIF-8-PEI.

Table 4.1. Weight loss, specific surface area, micropore volume, and WCA of ZIF-8 nanoparticles.

Samples	Weight loss[a] (%)	Specific surface area[b] (m^2 g^{-1})	Micropore volume[c] (cm^3 g^{-1})	WCA
ZIF-8	62.9	1800	0.67	50.0 ± 0.2
ZIF-8-COOH	63.9	1380	0.53	114.9 ± 3.5
ZIF-8-PEI	67.7	1260	0.45	0

[a] Obtained by TGA.

[b] Determined by the BET method

[c] Determined by the Horvath-Kawazoe method.

^{1}HNMR was performed to quantify the amount of Im-COOH in the ZIF-8-COOH particles (Fig. 4.2). The ligand exchange molar ratio of Im-COOH in ZIF-8-COOH is calculated to be 27%. TGA measurements (Fig. 4.3 and Table 4.1) were conducted to estimate the amount of PEI in ZIF-8-PEI. The original ZIF-8 displayed a sharp weight loss at around 400 °C, which was attributed to the decomposition of the MIm ligand [8]. In the case of ZIF-8-COOH, the weight loss started at 210 °C due to the degradation of Im-COOH linkers, while the ZnO residual did not show a significant difference as compared to that of ZIF-8. After grafting with the PEI, the weight loss started from a lower temperature due to the decomposition of the PEI. In general, ZIF-8 is converted to ZnO by combustion. From the weight after the combustion, the amounts of Zn and the ligands were respectively calculated as 32 and 68 wt% for ZIF-8-COOH. In ZIF-8-PEI, the amount of Zn was 28 wt%, and the amount of the ligands for this was estimated

to be 59 wt% based on the results for ZIF-8-COOH. The remaining 13 wt% was the estimated amount of grafted PEI. Assuming the molecular mass of PEI as 1.0×10^4 and the number of ZIF-8 nanoparticles as 4.31×10^{16} per gram, 13 wt% corresponded to ca. 220 chains per particle. Combining this with an estimated external surface area of 3.8 $\times 10^3$ nm^2/particle, the area assigned to each macromolecule is estimated as 17 nm^2 (cf. Calculation of the PEI density on the surface of ZIF-8 nanoparticles). In a general sense, this corresponds to a coverage for a semi-dilute brush.

Calculation of the PEI density on the surface of ZIF-8 nanoparticles

Mass% of PEI on ZIF-8 nanoparticles was estimated to compare with the value that calculated by TGA. Using a molecular mass of 10000 g mol^{-1} for PEI and assuming PEI (2.0×10^{-8} mol) was fully grafted to ZIF-8 nanoparticles (1.0×10^{-3} g), the mass% was:

$$\frac{2.0 \times 10^{-8}\ \text{mol} \times 10000\ \text{g mol}^{-1}}{2.0 \times 10^{-8}\ \text{mol} \times 10000\ \text{g·mol}^{-1} + 1.0 \times 10^{-3}\ \text{g}} = 16.7\ \%,$$

Considering the mass% of actual grafted PEI on ZIF-8 particles calculated from TGA data was 13 % (see Fig. 4.3), the molar amount of PEI used per milligram of ZIF-8 nanoparticles should be 1.6×10^{-8} mol.

The mass density of ZIF-8 nanoparticles is $\rho = 0.95$ g·mL^{-1}, which is determined by the structure refinement of the XRD pattern [31]. Considering a mean radius of ZIF-8 nanoparticles ($r = 1.75 \times 10^{-5}$ mm) taken from TEM-analysis (see Fig. 4.1), a number of particles per milligram (n) was calculated to be:

$$n = \frac{V_{\text{overall}}}{V_{\text{NP}}} = 4.31 \times 10^{13},$$

where $V_{\text{overall}} = \frac{m}{\rho} = 1.053\ \text{mm}^3$ *per milligram of ZIF-8 nanoparticles*, and $V_{\text{NP}} = \frac{4}{3}\pi$

$r^3 = \frac{4}{3}\,\pi\,(1.75 \times 10^{-5}\ mm)^3 = 2.445 \times 10^{-14}\ mm^3$, as *the volume of a sphere with the size of one ZIF-8 nanoparticle*.

The amount of PEI used per milligram ZIF-8 nanoparticles calculated above was 1.6×10^{-8} mol. With the Avogardro constant (N_A), the respective number of PEI chains (N_{PEI}) was:

$$N_{PEI} = 1.6 \times 10^{-8}\ \text{mol} \times 6.022 \times 10^{23}\ \text{mol}^{-1} = 9.635 \times 10^{15},$$

So, the number of PEI chains per ZIF-8 nanoparticle was: $= \frac{9.635 \times 10^{15}}{4.31 \times 10^{13}} = 224,$

To calculate the mean area occupied by one PEI chain on the surface of one ZIF-8 nanoparticle, the surface area one ZIF-8 nanoparticle was evaluated:

$$S = 4\,\pi\,r^2 = 4\,\pi\,(1.75 \times 10^{-5}\ mm)^2 = 3.848 \times 10^3\ nm^2,$$

Surface space occupied by one PEI chain on one ZIF-8 nanoparticle:

$$\frac{3.848 \times 10^3\ nm^2}{224} = 17.2\ nm^2.$$

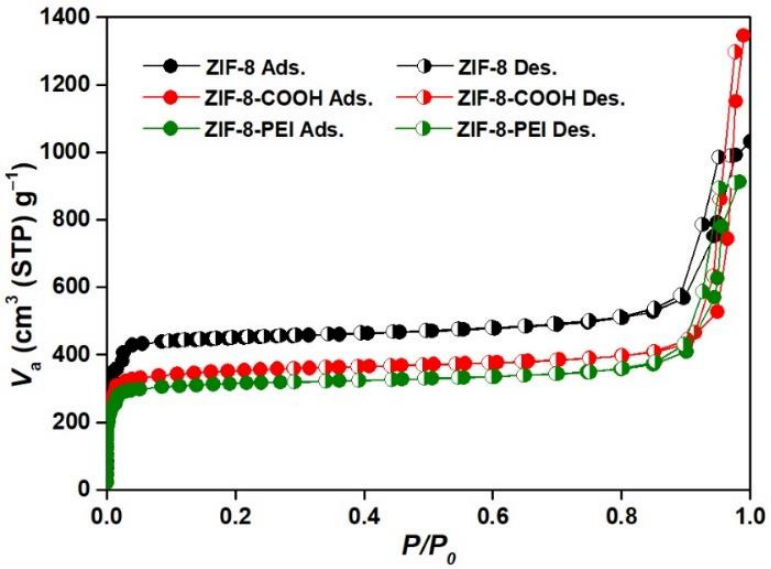

Fig. 4.4. Nitrogen adsorption/desorption isotherms of ZIF-8, ZIF-8-COOH, and ZIF-8-PEI nanoparticles.

Nitrogen adsorption/desorption isotherms of ZIF-8, ZIF-8-COOH, and ZIF-8-PEI are shown in Fig. 4.4. All of them exhibited the Type I isotherm, which is characteristic of microporous materials [2]. The specific surface area and the micropore volume for pristine ZIF-8 nanoparticles were calculated to be 1800 m^2 g^{-1} and 0.67 cm^3 g^{-1}, respectively (Table 4.1). After carboxyl functionalization, the values for ZIF-8-COOH decreased to 1380 m^2 g^{-1} and 0.53 cm^3 g^{-1} (Table 4.1). This is probably due to partial degradation or etching during the introduction of Im-COOH. Moreover, the ligand exchange ratio of 27% suggests that the ligand exchange proceeded not only on the external surfaces but also, to some extent, deep into the bulk, and the presence of COOH groups could explain the reduced surface area and pore volume. In the case of ZIF-8-PEI, the specific surface area and micropore volume were 1260 m^2 g^{-1} and 0.45 cm^3 g^{-1}, respectively. Assuming that PEI occupies 13 wt% in ZIF-8-PEI and that the contribution of PEI to the surface area and pore volume is negligible, the surface area and pore volume of ZIF-8-PEI can be estimated as 1200 m^2 g^{-1} and 0.46 cm^3 g^{-1}, respectively, from those of ZIF-8-COOH. The agreement between the measured and estimated values suggests that the grafting of PEI, unlike the ligand exchange, did not affect the crystal structure of ZIF-8, proceeded only on the external surfaces due to its bulkiness, and did not lead to pore blocking. WCAs measurements were conducted to determine the hydrophilicity of the particles. The WCAs of ZIF-8, ZIF-8-COOH, and ZIF-8-PEI were found to be 50.0°, 114.9°, and 0°, respectively (Table 4.1 and Fig. 4.5). The larger WCA in ZIF-8-COOH was ascribed to the introduction of the carboxylic groups near the external surfaces. The PEI grafting made the ZIF-8 surface

superhydrophilic, as a result of which ZIF-8-PEI nanoparticles stayed dispersed well in water over 72 h (not the case for ZIF-8 and ZIF-8-COOH, as shown in Fig. 4.5.

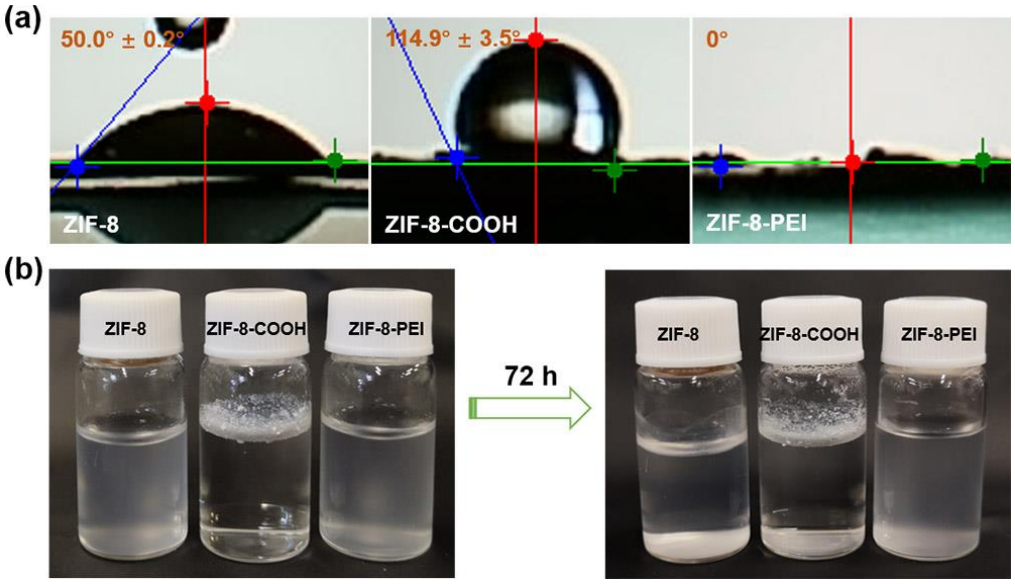

Fig. 4.5. a) WCAs of ZIF-8, ZIF-8-COOH, and ZIF-8-PEI, b) Particle dispersion of modified and unmodified ZIF-8 nanoparticles before and after 72 h in water.

4.3.2. Characterization of the membranes

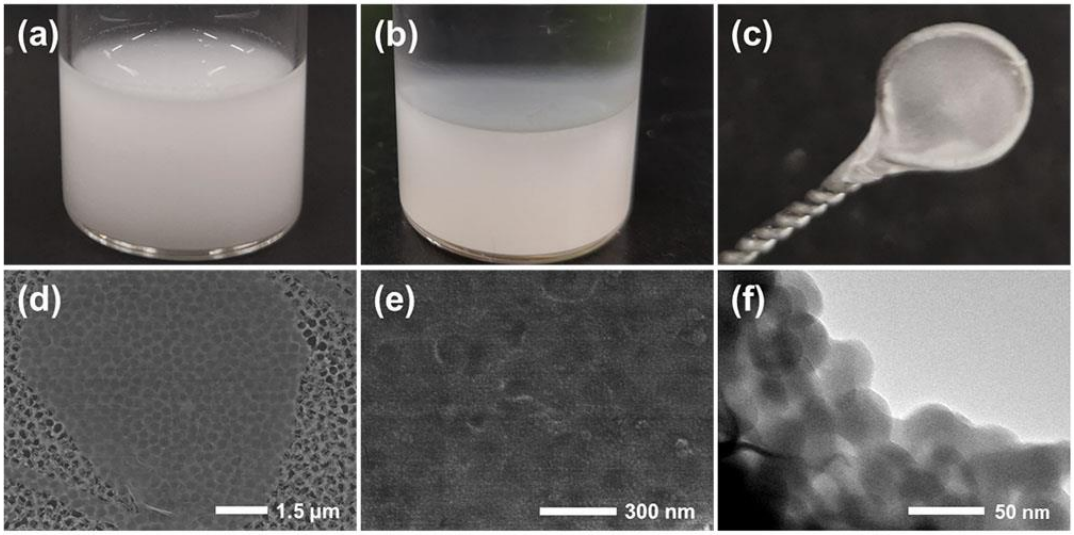

Fig. 4.6. Photographs of a) a ZIF-8-PEI suspension, and b) interfacial polymerization, where a free-standing film of crosslinked ZIF-8-PEI was formed at the hexane-water

interface. The freestanding film made in b) was c) taken out by an iron wire loop, d,e) transferred onto a AAO substrate for SEM measurements at different magnifications, and f) a TEM image of the film.

It is known that PEI has an ability to afford a selective layer by crosslinking its abundant amino groups with TMC [32]. I hypothesized that PEI chains grafted onto ZIF-8 were crosslinked by TMC across the nanoparticles to form a film in which the matrix was ZIF-8 due to its size, and the interparticle voids were filled with crosslinked polyamide. However, the film-forming ability of ZIF-8-PEI nanoparticles at the hexane-water interface was unknown. Hence, I tried to prepare a free-standing film of crosslinked ZIF-8-PEI at a hexane-water interface via interfacial polymerization. As shown in Fig. 4.6a–c, a dispersion of ZIF-8-PEI nanoparticles in water was contacted with a TMC solution in hexane for 10 min at room temperature. The formation of a large-area film at the hexane-water interface proved a film-forming ability of ZIF-8-PEI. It is worth noting that a film-like product was formed even in the absence of TMC due to the insolubility of PEI in hexane, but such a product did not show integrity and fractured into small pieces in the collection, contrary to the film formed in the presence of TMC. The free-standing film of crosslinked ZIF-8-PEI was then transferred to an AAO substrate for SEM observations (Fig. 4.6d,e), which indicated the film was thinner than the electron penetration depth and did not contain obvious pinholes at the observed scales. A TEM image of the film (an edge part) clearly displays that the film was formed by the assembly of ZIF-8-PEI nanoparticles, where a polymer phase acted as a link

among the nanoparticles (Fig. 4.6f).

In order to understand the film-forming process, free-standing films were prepared at different time intervals (1, 2, 5, and 10 min) of the reaction. Each film was transferred onto the AAO substrate, and rinsed with hexane to terminate the reaction. SEM images of these films are summarized in Fig. 4.7a. Up to 2 min, the product consisted of fragments and did not form a continuous film. A continuous but cracked film was obtained at 5 min, and it fully became intact at 10 min by curing the cracks. The film-forming process is sketched in Fig. 4.7b. When ZIF-8-PEI nanoparticles suspended in the water phase come into contact with the hexane phase, the PEI grafted on the surface of the particles crosslinks with TMC. As the reaction proceeds, more and more particles are accumulated at the hexane-water interface via crosslinking, finally forming a continuous film.

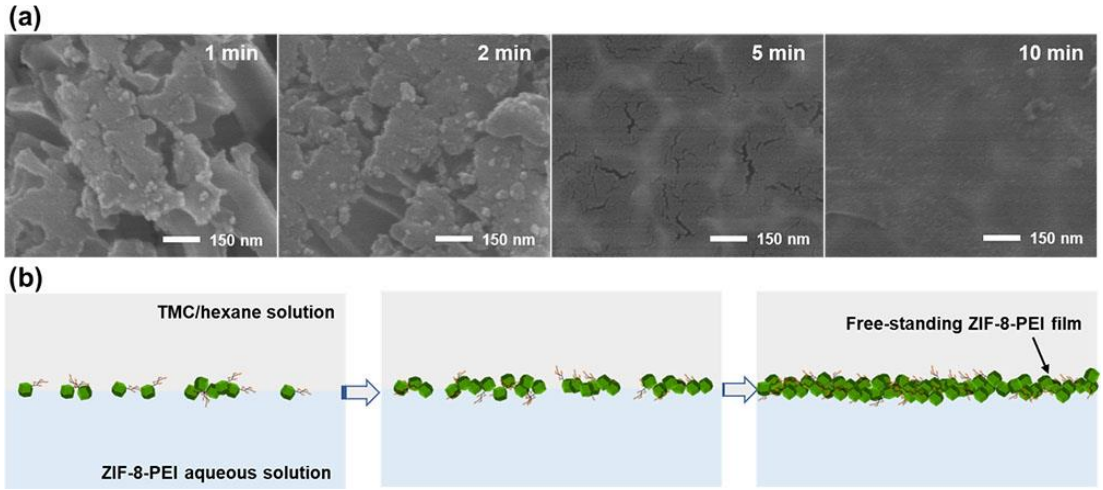

Fig. 4.7. a) SEM images of free-standing ZIF-8-PEI film obtained after different reaction intervals and b) schematic of the film-formation process.

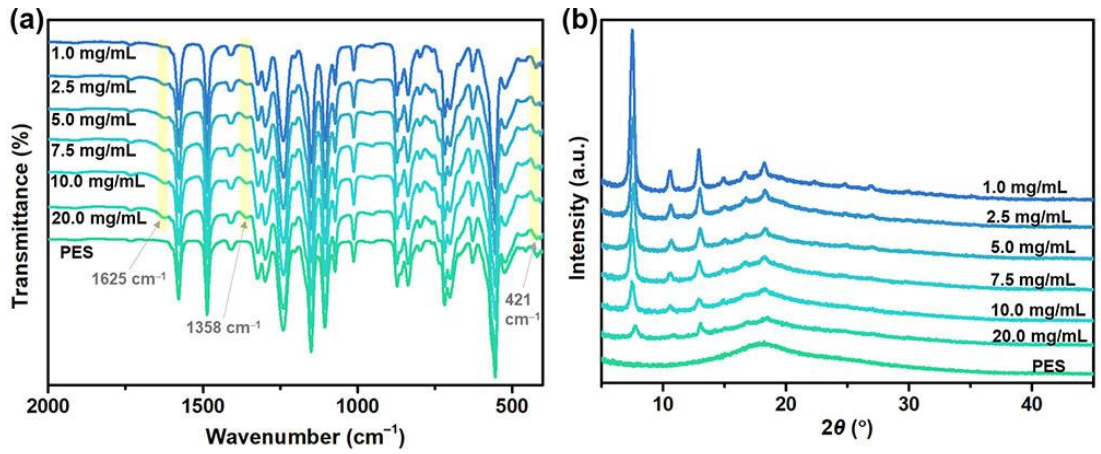

Fig. 4.8. The formation of a crosslinked ZIF-8-PEI selective layer on the PES substrate studied by a) ATR-IR spectra and b) XRD patterns. The nanocomposite membranes were prepared with different concentrations of TMC in hexane (1.0–20.0 mg/mL).

After confirming the film-forming ability of ZIF-8-PEI in the presence of TMC, nanocomposite membranes were prepared for desalination using a PES membrane as a substrate. In the interfacial polymerization, the use of the appropriate amount of TMC is important to increase the crosslinking degree [33]. Hence, the effect of the TMC concentration was examined on the structure and performance of the selective layer. Fig. 4.8 summarizes the ATR-IR spectra and XRD patterns of the nanocomposite membranes prepared by varying the TMC concentration from 1.0 to 20.0 mg/mL. In Fig. 4.8a, apart from the characteristic peaks of the PES substrate, two new peaks were observed at 1358 and 1625 cm^{-1} for all the nanocomposite membranes, which correspond to the stretching vibration of C–N and C=O of amide groups [34], and thus proved the occurrence of the crosslinking reaction between PEI and TMC. Since the penetration depth of IR for the employed diamond crystal is around 2 μm, which is much greater than the thickness of the selective layer, the IR spectra of the

nanocomposite membranes were dominated by the features of the PES substrate, making the characteristic peaks of ZIF-8 nanoparticles less obvious: only visible was a shoulder at 421 cm^{-1} corresponding to the Zn–N bonds of ZIF-8. The XRD patterns of the nanocomposite membranes consist of the overlay of the ZIF-8 reflections and the PES amorphous halo [8]. The shrinking contribution of the ZIF-8 reflections was plausibly attributed to the partial decomposition of ZIF-8 crystals by HCl emission and its dissolution in the water phase where ZIF-8 existed.

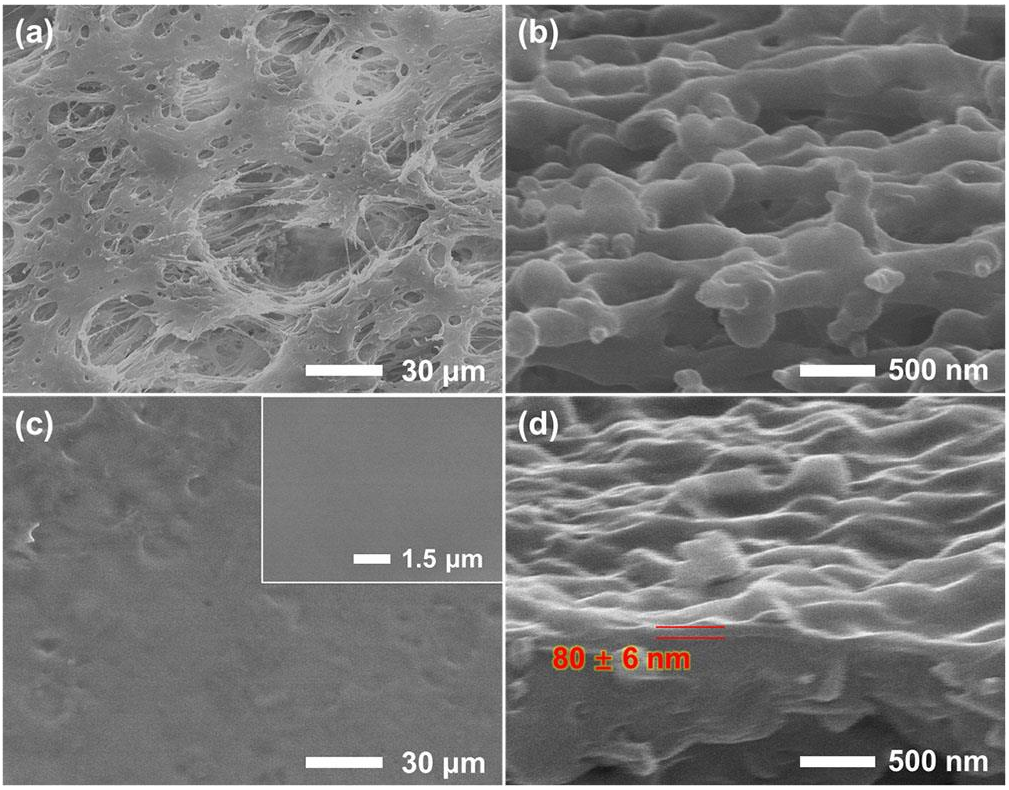

Fig. 4.9. Top-view and cross-sectional SEM images of: a,b) the PES substrate and c) a nanocomposite membrane prepared with a TMC concentration of 7.5 mg/mL. The images in the left column are top view, while those in the right column are cross-sectional side view.

SEM images of the PES substrate and a nanocomposite membrane prepared with a

TMC concentration of 7.5 mg/mL are shown in Fig. 4.9. In top view (Fig. 4.9a,c), the porous structure of the PES substrate was no longer observed after forming a selective layer. The selective layer was relatively smooth, and did not show a crumple structure typical for the conventional fully crosslinked aromatic polyamide [8]. This is due to the use of the solid building block instead of the molecular amine, which diffuses to the polymerization front and creates the crumple structure. Furthermore, the nanocomposite membrane revealed a defect-free surface in a high-magnification SEM image (insert in Fig. 4.9c). EDX mapping analysis confirmed a uniform distribution of Zn, suggesting that the ZIF-8-PEI nanoparticles were uniformly distributed in the selective layer (Fig. 4.10). In cross-sectional side view, the selective layer presented a ridge-and-valley structure (Fig. 4.9d) because it was supported by a PES substrate with such a structure (Fig. 4.9b). The thickness of the selective layer was measured to be 80 ± 6 nm. Considering the size of the nanoparticles around 30 nm, the 80 nm-thick selective layer was composed of 2–3 nanoparticles in the transmembrane direction.

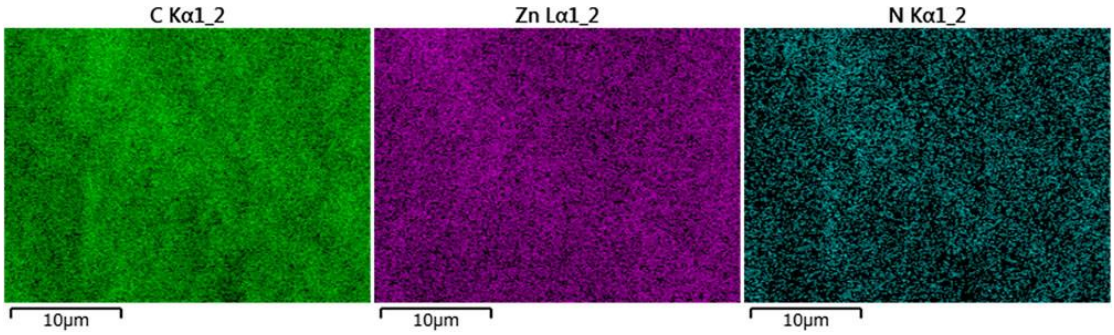

Fig. 4.10. EDX-mapping on the surface of the nanocomposite membrane prepared with a TMC concentration of 7.5 mg/mL.

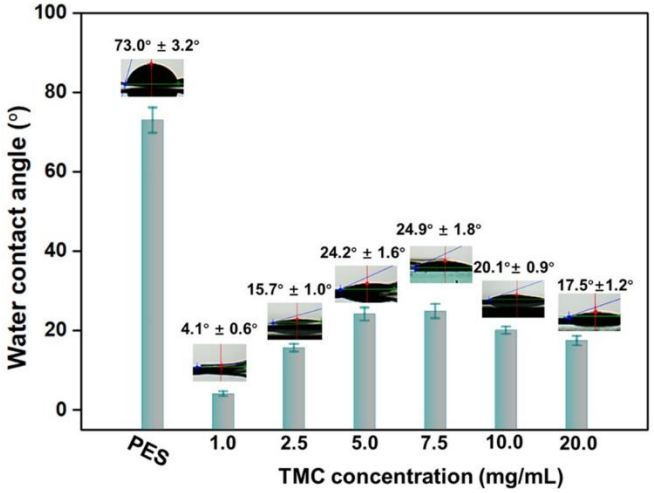

Fig. 4.11. WCAs of the PES substrate and nanocomposite membranes prepared with different concentrations of TMC in hexane.

The loading of ZIF-8 nanoparticles in the selective layer was estimated in two ways. One way was based on gravimetric analysis, where the ZIF-8 loading (not including PEI) was estimated at ca. 70 wt% by using weight gains before and after the nanoparticle deposition and the interfacial polymerization. The other way is based on the thermogravimetric analysis, where the entire membrane was combusted. By subtracting the contribution of the PES combustion, the ZIF-8 loading was derived from the ZnO residual weight as ca. 68 wt%, similar to 70 wt% from the gravimetric analysis. To the best of our knowledge, this loading was far the highest compared with those of MOF-based TFN membranes in literature.

It is well acknowledged that hydrophilicity plays an important role in improving permeability in desalination [8]. Hence, the WCA measurements were performed on the nanocomposite membranes (Fig. 4.11). The PES substrate was relatively hydrophobic with a WCA of 73.0°. After the formation of a selective layer, the

hydrophilicity of the membranes was largely enhanced due to the hydrophilic nature of the PEI layer. When the TMC concentration was increased from 1.0 mg/mL, the WCA increased from 4.1° to 24.9° up to 7.5 mg/mL, and then turned to decrease after that. The former is attributed to the replacement of the amino groups by amide groups with an aromatic moiety, while the latter is possibly explained by the residual carboxylic acid arising from excessive grafting of TMC [35].

4.3.3. Separation performance of the membranes

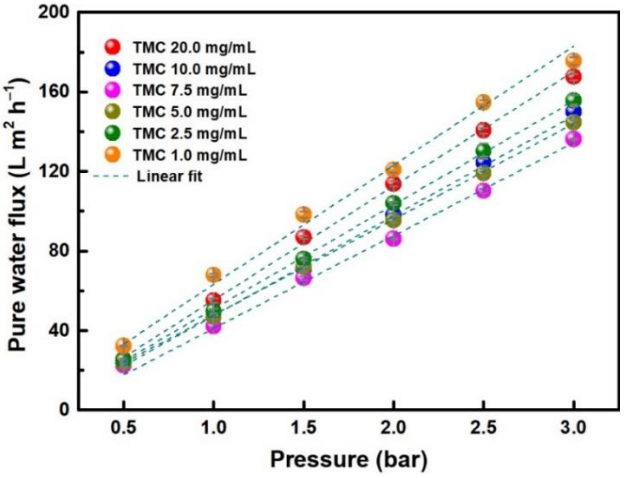

Fig. 4.12. Pure water flux of the membranes at different transmembrane pressures.

The as-prepared ZIF-8-matrix nanocomposite membranes were used for brackish water desalination in a low-pressure nanofiltration process, and the separation performance was evaluated in terms of the permeability and salt rejection. First, the filtration of pure water was conducted, where the water flux increased proportionally to the differential pressure irrespective of the TMC concentration (as shown in Fig. 4.12), confirming the stable operation. Then, the membranes were performed in separating an aqueous solution of Na_2SO_4 (1000 ppm) under 2 bar, which exhibited a

superior permeability of 43.6 LMH bar^{-1} with a selectivity of > 95% when the membranes were prepared with a TMC concentration of 7.5 mg/mL. The desalination performance in terms of permeability and rejection for Na_2SO_4 of the as-prepared ZIF-8-matrix nanocomposite membrane was compared with those of the reported membranes, including the ZIF-8-based TFN membrane presented in **Chapter 3** [8,13,14,19,33,36–48]. As shown in Fig. 4.13, the comparison suggests that the desalination performance of the ZIF-8-matrix nanocomposite membrane is somehow superior to most other membranes developed by others, including polyamide thin-film composite membranes [33,39], MOF-incorporated TFN membranes [8,13,14,19], TFN membranes incorporated with other nanomaterials [38,40–42], continuous MOF membranes [43,44], MOF-based mixed matrix membranes [45,46], membranes with a ultrathin selective layer [36], and 2D nanomaterials-assembled membranes [47,48], which show several folds of enhancement in permeability as compared to most others, while maintaining a high Na_2SO_4 rejection.

In general, two efficient strategies have been proven to be promising alternatives for the improvement of membrane permeability: reducing selective layer thickness and hybridizing nanofillers [34]. Selective layers with a thickness of ~10 nm have been reported, which showed excellent performance for desalination (as shown in Fig. 4.13) [36,37]. I have tried to increase the nanofiller (ZIF-8 nanoparticles) loading in **Chapter 3** for the improvement of permeability while maintaining selectivity. When the concentration of ZIF-8 nanoparticles in the selective layer was increased from 0 to 20 wt%, the permeability doubled (11.1 LMH bar^{-1}) while the selectivity remained greater

than 95%. However, at 40 wt% of ZIF-8 loadings in the selective layer, there was a very significant decrease in the selectivity (83%) due to the non-selective defects caused by particle agglomeration [8]. In this chapter, the concentration of ZIF-8 nanoparticles in the selective layer was increased to ca. 70 wt%, which provides more channels for water transportation, resulting in such high permeability. Meanwhile, the good compatibility of ZIF-8-PEI nanoparticles introduced by the grafted polymer maintained a comparable selectivity for the membranes.

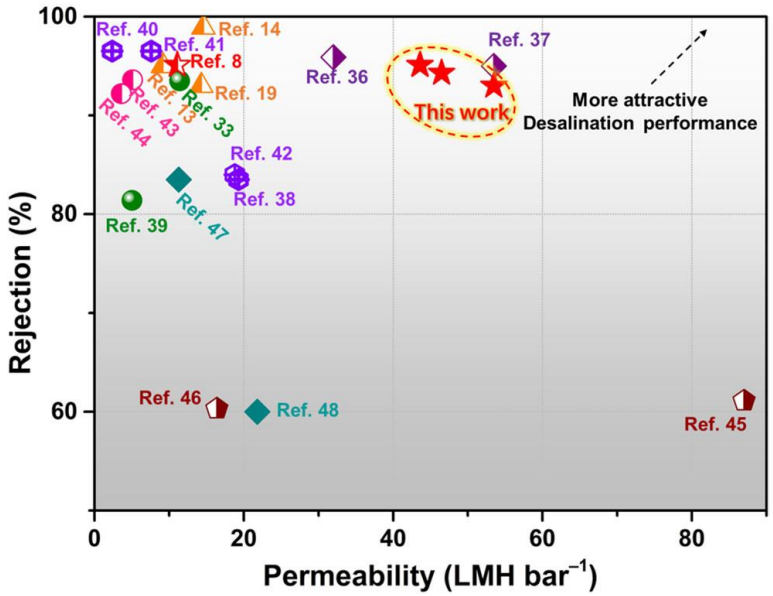

Fig. 4.13. Comparisons of desalination performance of the nanocomposite membrane with various reported membranes in consideration of permeability and rejection for Na_2SO_4.

The impact of the TMC concentration on the desalination performance of the membranes was investigated using 1000 ppm of Na_2SO_4 at a differential pressure of 2 bar. As illustrated in Fig. 4.14, as the TMC concentration increased from 1.0 to 7.5 mg/mL, the rejection of Na_2SO_4 increased accordingly from 89.7% to 95.1%.

Consequently, the permeability decreased from 62.1 to 43.6 LMH bar^{-1}. This is due to the fact that the low concentration of TMC was not enough to react with the PEI grafted on the surface of ZIF-8, leading to a loose crosslinked elective layer. The selective layer was gradually well formed as the TMC concentration increased [49]. However, the further increase in TMC concentration led to a negative effect on the rejection, in which the rejection of Na_2SO_4 slightly decreased from 95.1% to 93.0% when the concentration increased from 7.5 to 20.0 mg/mL. Because the molar ratio between the amines of PEI and the –COCl groups of TMC was reduced, which resulted in reduced crosslinking, leading to a decrease in rejection [50]. Moreover, when the TMC concentration was higher than that of the optimum, the excess of unreacted –COCl groups from TMC were hydrolyzed to –COOH groups, resulting in a higher hydrophilicity of the membranes [35]. Consequently, the permeability increased from 43.6 to 53.5 LMH bar^{-1}. The influence of operation pressure on the salt rejection and permeate flux for the membrane (7.5 mg/mL) was also studied at the differential pressure of 1.0–3.0 bar using 1000 ppm of Na_2SO_4. The separation performance was shown in Fig. 4.14. The water permeating fluxes increased linearly with the applied pressure from 1 to 2.5 bar, while only a slight decline was observed in the salt rejection (–1.1%). When the applied pressure was up to 3 bar, the increase in the water permeating flux tended to level off due to concentration polarization [37], thus the salt rejection decreased to 92.1%.

To evaluate the operational stability of the nanocomposite membranes (7.5 mg/mL), a 72-h filtration was performed with the continuous feed of 1000 ppm of Na_2SO_4 under a differential pressure of 2 bar. As shown in Fig. 4.15, except for a slight fluctuation at

the beginning, the permeability and Na_2SO_4 rejection remained almost constant until 50 h. For the whole period, the membranes exhibited a negligible reduction in rejection (–1.1%), while the concentration polarization effect gave rise to a slight decline in permeability (–8.2%). This indicated high membrane stability, which is probably attributed to the covalent connection of ZIF-8 with polymeric matrices.

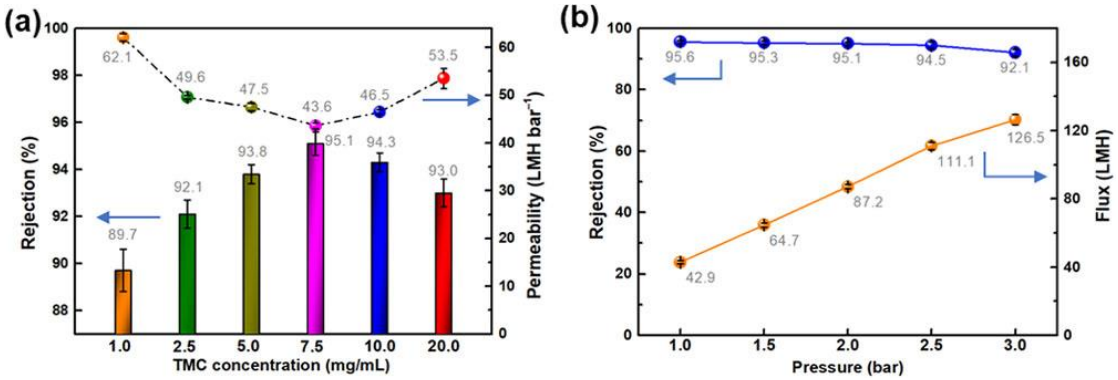

Fig. 4.14. Desalination performance of the nanocomposite membranes. a) TMC concentration effect on desalination performance (Salt: 1000 ppm Na_2SO_4; applied transmembrane pressure: 2 bar); b) separation performance as a function of applied transmembrane pressure for the membrane prepared with a TMC concentration of 7.5 mg/mL (Salt: 1000 ppm Na_2SO_4).

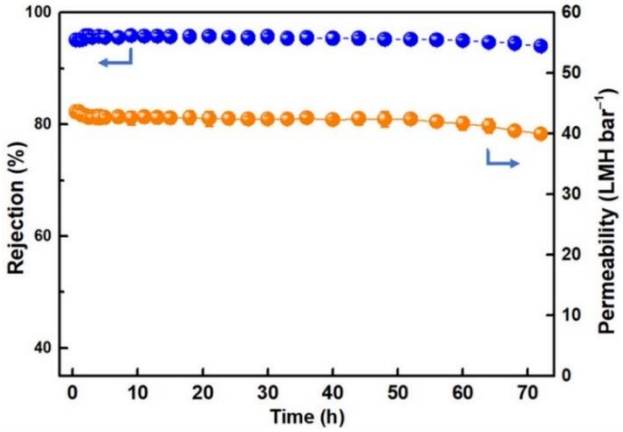

Fig. 4.15. Separation performance of the membrane prepared with a TMC concentration

of 7.5 mg/mL during a 72-h test (Salt: 1000 ppm of Na_2SO_4; applied transmembrane pressure: 2 bar).

4.4. Conclusions

In consideration of the theoretically excellent separation performance of porous MOF nanoparticles and the easy processability of polymeric membranes, a novel designed ZIF-8-matrix nanocomposite membrane with high ZIF-8 loading was developed for desalination separation. In this chapter, carboxyl-functionalized ZIF-8 nanoparticles prepared by ligand exchange reaction were first proposed for the purpose of polymer grafting. Following that, a PEI was successfully grafted on the external surface of ZIF-8 via a simple carbodiimide-mediated reaction in the presence of –COOH groups. I have also shown synthetic control of the ZIF-8-matrix nanocomposite membranes by forming a selective layer using PEI-grafted ZIF-8 nanoparticles as building blocks via interfacial polymerization on a PES substrate for desalination. The tailored PEI-grafted ZIF-8 nanoparticles were crosslinked into a crosslinked ZIF-8-PEI selective layer using TMC as a crosslinker. Owing to the absence of free amine in such a process, a very high ZIF-8 loading in the selective layer has been achieved (ca. 70wt%), facilitating an outstanding permeability (> 43.6 LMH bar^{-1}) of the membranes in the desalination separation, which was several folds as compared to most of the reported membranes, while maintaining a reasonably high Na_2SO_4 rejection (95.1%). Overall, such a strategy paves the way for the design of newly MOF-matrix nanocomposite membranes for more attractive desalination performance.

4.5. References

[1] M.S. Denny Jr., J.C. Moreton, L. Benz, S.M. Cohen, Metal-organic frameworks for membrane-based separations, Nat. Rev. Mater. 1 (2016) 1–17.

[2] H. You, G.Y. Shangkum, P. Chammingkwan, T. Taniike, Surface wettability switching of a zeolitic imidazolate framework-deposited membrane for selective efficient oil/water emulsion separation, Colloids Surf., A 614 (2021) 126204.

[3] G.Y. Shangkum, P. Chammingkwan, D.X. Trinh, T. Taniike, Design of a semi-continuous selective layer based on deposition of UiO-66 nanoparticles for nanofiltration, membranes 8 (2018) 129.

[4] D.X. Trinh, T.P. Tran, T. Taniike, Fabrication of new composite membrane filled with UiO-66 nanoparticles and its application to nanofiltration, Sep. Purif. Technol. 177 (2017) 249–256.

[5] P. Chammingkwan, G.Y. Shangkum, P. Mohan, A. Thakur, T. Wada, T. Taniike, Modulator-free approach towards missing-cluster defect formation in Zr-based UiO-66, RSC Adv. 10 (2020) 28180–28185.

[6] J. Dechnik, J. Gascon, C.J. Doonan, C. Janiak, C.J. Sumby, Mixed-matrix membranes, Angew. Chem. Int. Ed. 56 (2017) 9292–9310.

[7] H.T. El-Dessouky, H.M. Ettouney, Fundamentals of salt water desalination, Elsevier, 2002.

[8] H. You, X. Zhang, D. Zhu, C. Yang, P. Chammingkwan, T. Taniike, Advantages of polydopamine coating in the design of ZIF-8-filled thin-film nanocomposite (TFN) membranes for desalination, Colloids Surf., A 629 (2021) 127492.

[9] X. Li, Y. Liu, J. Wang, J. Gascon, J. Li, B. Van der Bruggen, Metal-organic frameworks based membranes for liquid separation, Chem. Soc. Rev. 46 (2017) 7124–7144.

[10] W.J. Koros, C. Zhang, Materials for next-generation molecularly selective synthetic membranes, Nat. Mater. 16 (2017) 289–297.

[11] Y. Zhao, Y. Liu, X. Wang, X. Huang, Y. Xie, Impacts of metal-organic frameworks on structure and performance of polyamide thin-film nanocomposite membranes, ACS Appl. Mater. Interfaces 11 (2019) 13724–13734.

[12] I.H. Aljundi, Desalination characteristics of TFN-RO membrane incorporated with ZIF-8 nanoparticles, Desalination 420 (2017) 12–20.

[13] F. Xiao, B. Wang, X. Hu, S. Nair, Y. Chen, Thin film nanocomposite membrane containing zeolitic imidazolate framework-8 via interfacial polymerization for highly permeable nanofiltration, J. Taiwan Inst. Chem. Eng. 83 (2018) 159–167.

[14] F. Xiao, X. Hu, Y. Chen, Y. Zhang, Porous Zr-based metal-organic frameworks (Zr-MOFs)-incorporated thin-film nanocomposite membrane toward enhanced desalination performance, ACS Appl. Mater. Interfaces 11 (2019) 47390–47403.

[15] Y. Gong, S. Gao, Y. Tian, Y. Zhu, W. Fang, Z. Wang, J. Jin, Thin-film nanocomposite nanofiltration membrane with an ultrathin polyamide/UiO-66-NH_2 active layer for high-performance desalination, J. Membr. Sci. 600 (2020) 117874.

[16] Y. Lin, Y. Chen, R. Wang, Thin film nanocomposite hollow fiber membranes

incorporated with surface functionalized HKUST-1 for highly-efficient reverses osmosis desalination process, J. Membr. Sci. 589 (2019) 117249.

[17] H.B. Park, J. Kamcev, L.M. Robeson, M. Elimelech, B.D. Freeman, Maximizing the right stuff: The trade-off between membrane permeability and selectivity, Science 356 (2017) eaab0530.

[18] T.T. Moore, W.J. Koros, Non-ideal effects in organic-inorganic materials for gas separation membranes, J. Mol. Struct. 739 (2005) 87–98.

[19] J. Zhu, L. Qin, A. Uliana, J. Hou, J. Wang, Y. Zhang, X. Li, S. Yuan, J. Li, M. Tian, J. Lin, B. Van der Bruggen, Elevated performance of thin film nanocomposite membranes enabled by modified hydrophilic MOFs for nanofiltration, ACS Appl. Mater. Interfaces 9 (2017) 1975–1986.

[20] H. Liu, M. Zhang, H. Zhao, Y. Jiang, G. Liu, J. Gao, Enhanced dispersibility of metal-organic frameworks (MOFs) in the organic phase via surface modification for TFN nanofiltration membrane preparation, RSC Adv. 10 (2020) 4045–4057.

[21] T. Liu, H. Yuan, Y. Liu, D. Ren, Y. Su, X. Wang, Metal-organic framework nanocomposite thin films with interfacial bindings and self-standing robustness for high water flux and enhanced ion selectivity, ACS Nano 12 (2018) 9253–9265.

[22] W. Li, Y. Zhang, Q. Li, G. Zhang, Metal-organic framework composite membranes: Synthesis and separation applications, Chem. Eng. Sci. 135 (2015) 232–257.

[23] J. Cravillon, S. Münzer, S. Lohmeier, A. Feldhoff, K. Huber, M. Wiebcke, Rapid

room-temperature synthesis and characterization of nanocrystals of a prototypical zeolitic imidazolate framework, Chem. Mater. 21 (2009) 1410–1412.

[24] K.C. Jayachandrababu, D.S. Sholl, S. Nair, Structural and mechanistic differences in mixed-linker zeolitic imidazolate framework synthesis by solvent assisted linker exchange and *de novo* routes, J. Am. Chem. Soc. 139 (2017) 5906–5915.

[25] J. Bart, R. Tiggelaar, M. Yang, S. Schlautmann, H. Zuilhof, H. Gardeniers, Room-temperature intermediate layer bonding for microfluidic devices, Lab Chip 9 (2009) 3481–3488.

[26] M. He, J. Yao, Q. Liu, K. Wang, F. Chen, H. Wang, Facile synthesis of zeolitic imidazolate framework-8 from a concentrated aqueous solution, Microporous Mesoporous Mater. 184 (2014) 55–60.

[27] Y. Hu, H. Kazemian, S. Rohani, Y. Huang, Y. Song, In situ high pressure study of ZIF-8 by FTIR spectroscopy, Chem. Commun. 47 (2011) 12694–12696.

[28] F. Yang, W. Li, Y. Zhang, B. Tang, Realizing uniform dispersion of MnO_2 with the post-synthetic modification of metal-organic frameworks (MOFs) for advanced lithium ion battery anodes, Dalton Trans. 47 (2018) 13657–13667.

[29] Y. Gao, Z. Qiao, S. Zhao, Z. Wang, J. Wang, In situ synthesis of polymer grafted ZIFs and application in mixed matrix membrane for CO_2 separation, J. Mater. Chem. A 6 (2018) 3151–3161.

[30] Y. Katayama, M. Kalaj, K.S. Barcus, S.M. Cohen, Self-assembly of metal-

organic framework (MOF) nanoparticle monolayers and free-standing multilayers, J. Am. Chem. Soc. 141 (2019) 20000–20003.

[31] J.C. Tan, T.D. Bennett, A.K. Cheetham, Chemical structure, network topology, and porosity effects on the mechanical properties of zeolitic imidazolate frameworks, Proc. Natl. Acad. Sci. U.S.A. 107 (2010) 9938–9943.

[32] J. Wang, J. Zhu, M.T. Tsehaye, J. Li, G. Dong, S. Yuan, X. Li, Y. Zhang, J. Liu, B. Van der Bruggen, High flux electroneutral loose nanofiltration membranes based on rapid deposition of polydopamine/polyethyleneimine, J. Mater. Chem. A 5 (2017) 14847–14857.

[33] P. Xu, W. Wang, X. Qian, H. Wang, C. Guo, N. Li, Z. Xu, K. Teng, Z. Wang, Positive charged PEI-TMC composite nanofiltration membrane for separation of Li^+ and Mg^{2+} from brine with high Mg^{2+}/Li^+ ratio, Desalination 449 (2019) 57–68.

[34] X. Wu, G. Zhou, X. Cui, Y. Li, J. Wang, X. Cao, P. Zhang, Nanoparticle-assembled thin film with amphipathic nanopores for organic solvent nanofiltration, ACS Appl. Mater. Interfaces 11 (2019) 17804–17813.

[35] C. Li, S. Li, L. Tian, J. Zhang, B. Su, M.Z. Hu, Covalent organic frameworks (COFs)-incorporated thin film nanocomposite (TFN) membranes for high-flux organic solvent nanofiltration (OSN), J. Membr. Sci. 572 (2019) 520–531.

[36] Y. Zhu, W. Xie, S. Gao, F. Zhang, W. Zhang, Z. Liu, J. Jin, Single-walled carbon nanotube film supported nanofiltration membrane with a nearly 10 nm thick polyamide selective layer for high-flux and high-rejection desalination, Small

12 (2016) 5034–5041.

[37] Z. Wang, Z. Wang, S. Lin, H. Jin, S. Gao, Y. Zhu, J. Jin, Nanoparticle-templated nanofiltration membranes for ultrahigh performance desalination, Nat. Commun. 9 (2018) 1–9.

[38] C. Wang, Z. Li, J. Chen, Z. Li, Y. Yin, L. Cao, Y. Zhong, H. Wu, Covalent organic framework modified polyamide nanofiltration membrane with enhanced performance for desalination, J. Membr. Sci. 523 (2017) 273–281.

[39] Y. Li, Y. Su, J. Li, X. Zhao, R. Zhang, X. Fan, J. Zhu, Y. Ma, Y. Liu, Z. Jiang, Preparation of thin film composite nanofiltration membrane with improved structural stability through the mediation of polydopamine, J. Membr. Sci. 476 (2015) 10–19.

[40] Y. Kang, M. Obaid, J. Jang, I.S. Kim, Sulfonated graphene oxide incorporated thin film nanocomposite nanofiltration membrane to enhance permeation and antifouling properties, Desalination 470 (2019) 114125.

[41] H. Zhang, X. Gong, W. Li, X. Ma, C.Y. Tang, Z. Xu, Thin-film nanocomposite membranes containing tannic acid-Fe^{3+} modified MoS_2 nanosheets with enhanced nanofiltration performance, J. Membr. Sci. 616 (2020) 118605.

[42] J. Chen, Z. Li, C. Wang, H. Wu, G. Liu, Synthesis and characterization of gC_3N_4 nanosheet modified polyamide nanofiltration membranes with good permeation and antifouling properties, RSC Adv. 6 (2016) 112148–112157.

[43] Y. Xiao, W. Zhang, Y. Jiao, Y. Xu, H. Lin, Metal-phenolic network as precursor for fabrication of metal-organic framework (MOF) nanofiltration membrane for

efficient desalination, J. Membr. Sci. 624 (2021) 119101.

[44] Y. Xu, Y. Xiao, W. Zhang, H. Lin, L. Shen, R. Li, Y. Jiao, B. Liao, Plant polyphenol intermediated metal-organic framework (MOF) membranes for efficient desalination, J. Membr. Sci. 618 (2021) 118726.

[45] L. Shu, L.-H. Xie, Y. Meng, T. Liu, C. Zhao, J. Li, A thin and high loading two-dimensional MOF nanosheet based mixed-matrix membrane for high permeance nanofiltration, J. Membr. Sci. 603 (2020) 118049.

[46] Y. Meng, L. Shu, L.-H. Xie, M. Zhao, T. Liu, J. Li, High performance nanofiltration in BUT-8 (A)/PDDA mixed matrix membrane fabricated by spin-assisted layer-by-layer assembly, J. Taiwan Inst. Chem. Eng. 115 (2020) 331–338.

[47] Y. Han, Y. Jiang, C. Gao, High-flux graphene oxide nanofiltration membrane intercalated by carbon nanotubes, ACS Appl. Mater. Interfaces 7 (2015) 8147–8155.

[48] Y. Han, Z. Xu, C. Gao, Ultrathin graphene nanofiltration membrane for water purification, Adv. Funct. Mater. 23 (2013) 3693–3700.

[49] W. Fang, L. Shi, R. Wang, Mixed polyamide-based composite nanofiltration hollow fiber membranes with improved low-pressure water softening capability, J. Membr. Sci. 468 (2014) 52–61.

[50] M.B.M.Y. Ang, Z. Luo, J.A.D. Marquez, H. Tsai, S. Huang, W. Hung, C. Hu, K. Lee, J. Lai, Merits of using cellulose triacetate as a substrate in producing thin-film composite nanofiltration polyamide membranes with ultra-high

performance, J. Taiwan Inst. Chem. Eng. 112 (2020) 251–258.

Chapter 5

General Conclusion

5.1. General conclusions

The thesis begins in **Chapter 1** with a description of the advantages of membrane technologies in liquid separation. Separation mechanisms and types of membranes are also explained. MOFs have been mentioned in this chapter as appealing candidates for liquid membrane separations due to their advantages of well-fined pore structures, flexibility, chemical functionality, and so on. In order to achieve high-performance MOF-based membranes for liquid separation, key issues are proposed in this chapter, which include the stability, hydrophilicity/hydrophobicity, as well as dispersibility of MOFs. Due to the presence of organic ligands, MOFs exhibit a rich selection of functionality, which enable to address the issues through goal-directed surface engineering. In this thesis, ZIF-8, one of the most stable MOFs, was employed to prepare ZIF-8-based membranes for liquid separation applications. Goal-directed designs were performed by tailoring the external surface of ZIF-8 in various ways, for oil/water emulsion separation and desalination purposes. The main conclusions are as follows:

In **Chapter 2**, a solvent-assisted ligand exchange reaction was performed on the surface of ZIF-8 micro- as well as nanoparticles to switch the surface wettability from relatively hydrophilic to hydrophobic (ZIF-8-DMBIM). Novel ZIF-8 composite membranes were prepared by separately depositing ZIF-8 or ZIF-8-DMBIM particles onto a regenerated cellulose substrate. To facilely optimize the selective layer, a simple, a scalable sequential deposition method was performed for balancing the permeability and selectivity. The impact of the particle size distribution on separation performance

was also examined. The relatively hydrophilic ZIF-8-deposited membranes were used for oil-in-water emulsion separation, while the hydrophobic ZIF-8-DMBIM-deposited membranes were applied for separating water-in-oil emulsions. These membranes exhibited excellent permeability (1411.8–1643.1 L m^{-2} h^{-1} bar^{-1}) and a separation efficiency of more than 99.9% in both of oil-in-water and water-in-oil emulsion separation. This chapter successfully proposes a facile way to prepare MOF-based membranes for nanofiltration, with a particular attention in balancing the permeability-selectivity tradeoff.

To separate species of a smaller size, ZIF-8-based thin-film nanocomposite (TFN) membranes were designed in **Chapter 3**. For the ZIF-8-based TFN membranes, ZIF-8 nanoparticles were incorporated into the polyamide selective layer as nanofillers to introduce additional transport channels for the purpose of enhancing permeability in desalination. The interface between ZIF-8 nanoparticles and the polymeric matrix was managed to avoid particle agglomeration, which was based on coating a polydopamine (PDA) layer on the surface of ZIF-8. The PDA coating facilitated the dispersion of ZIF-8 nanoparticles in the aqueous phase of interfacial polymerization and significantly improved the chemical stability of ZIF-8. As a result, the TFN membrane with PDA-coated ZIF-8 nanoparticles showed a two-fold enhancement in permeability as compared to ZIF-8-free thin-film composite (TFC) membranes, while maintaining comparable selectivity in the separation of Na_2SO_4 aqueous solution. This chapter evidences the significant roles of surface modification of ZIF-8 in preparing stable and performant ZIF-8-based TFN membranes.

In **Chapter 4**, to further increase the ZIF-8 loading in ZIF-8-based composite membranes for desalination, amine groups were introduced on the external surface of ZIF-8 nanoparticles by grafting polyethylenimine (PEI). The precisely tailored ZIF-8 nanoparticles were in-situ crosslinked with trimesoyl chloride (TMC) to form an ultrathin selective layer with superhigh ZIF-8 loading (>70 wt%). Such membranes facilitated an outstanding permeability in separation of Na_2SO_4 aqueous solution, which was several folds as compared to most of the reported membranes for desalination, while maintaining a relatively high Na_2SO_4 rejection (95.1%). In summary, the strategy in this chapter paves a way to develop a new type of MOF-based membranes for more attractive desalination performance.

To summarize, MOF-based membranes have shown great potential for liquid separation. The surface engineering of MOF nanoparticles has provided a smart strategy to maximize the advantage of MOFs' nanochannels and alleviate their interfacial failure in designing MOF-based membranes for liquid separation. I believe that the surface design of MOF nanoparticles for the preparation of high-performance MOF-based membranes for liquid separation in this thesis has shown good sights and broad thinking.

5.2. Perspectives

Many efforts and explorations have been made in this thesis to improve separation performance in liquid separation by modulating the ZIF-8 surface within ZIF-8-based membranes. The following describe issues that were not directly addressed in this thesis but are worth studying in future research.

(1) Theoretically, ultrathin MOF nanomaterials can provide higher membrane

permeability in liquid separation due to the low transport resistance. The majority of the ZIF-8-based membranes described in this thesis, as well as the majority of those described in the literature, used 3-dimensional ZIF-8 nanocrystals. Therefore, the design and synthesis of ZIF-8 nanosheets with the thickness of several nanometers for ZIF-8-based membranes are thus very appealing.

(2) In this thesis, the prepared ZIF-8-based membranes have been applied for oil-water emulsion separation and desalination. However, considering the excellent chemical stability of ZIF-8 nanoparticles, they are also promising in the usage of organic solvent nanofiltration, where the designs and strategies proposed in this thesis must be useful.

List of publications and other achievements

Publications

Thesis related:

1. **H. You**, G.Y. Shangkum, P. Chammingkwan, T. Taniike, Surface wettability switching of a zeolitic imidazolate framework-deposited membrane for selective efficient oil/water emulsion separation, Colloids Surf., A 614 (2021) 126204. (Chapter 2)
2. **H. You**, X. Zhang, D. Zhu, C. Yang, P. Chammingkwan, T. Taniike, Advantages of polydopamine coating in the design of ZIF-8-filled thin-film nanocomposite (TFN) membranes for desalination, Colloids Surf., A 629 (2021) 127492. (Chapter 3)
3. **H. You**, P. Chammingkwan, T. Taniike, Preparation of ZIF-8-matrix nanocomposite membranes for high-flux desalination, In preparation. (Chapter 4)

Others:

4. S. Reghu, **H. You**, K. Seenivasan, S. Nishimura, T. Taniike, E. Miyako Design and Control of Bioinspired Millibots, Advanced Intelligent Systems, 2 (2020) 2000059.
5. X. Zhang, X. Xia, **H. You**, T. Wada, P. Chammingkwan, A. Thakur, T. Taniike, Design of continuous segregated polypropylene/Al_2O_3 nanocomposites and impact of controlled Al_2O_3 distribution on thermal conductivity, Composites, Part A 131 (2020) 105825.

Conferences

Domestic Conference

1. **H. You**, G.Y. Shangkum, T. Toshiaki, High-flux membranes based on zeolitic imidazolate framework for organic solvent nanofiltration, 64th SPSJ Annual Meeting, Fukuoka, Japan, May 27–29, 2020.

International Conferences

2. **H. You**, G.Y Shangkum, P. Chammingkwan, T. Taniike, Surface wettability switching of a zeolitic imidazolate framework membrane for efficient oil/water emulsion separation, the 48th World polymer Congress (IUPAC-MACRO2020+), Jeju, Korea, May 16–20, 2021.